Variations and Sources of Atmospheric CO_2 Measured at East Trout Lake, Canada

by

Myung Gwang Kim

A thesis
presented to the University of Waterloo
in fulfillment of the
thesis requirement for the degree of
Doctor of Philosophy
in
Earth Sciences

Waterloo, Ontario, Canada, 2015

AUTHOR'S DECLARATION

I hereby declare that I am the sole author of this thesis. This is a true copy of the thesis, including any required final revisions, as accepted by my examiners.

I understand that my thesis may be made electronically available to the public.

Abstract

Reducing uncertainties in projections of surface emissions of major greenhouse gases (GHGs) including CO_2 relies on continuously improving our scientific understanding of the exchange processes between the atmosphere and land at regional scales. In order to enhance our understanding in emission processes and atmospheric transports, an integrated framework that addresses individual natural and anthropogenic factors in a complementary way proves to be invaluable. This study presents an example of top-down inverse modeling that utilizes high precision measurement data collected at a Canadian greenhouse gas monitoring site. The measurements include multiple tracers encompassing standard greenhouse gas species, stable isotopes of CO_2, and combustion-related species. The potential for the proposed analysis framework is demonstrated using Stochastic Time-Inverted Lagrangian Transport (STILT) model runs to yield a unique regional-scale constraint that can be used to relate the observed changes of tracer concentrations to the processes in their upwind source regions. The uncertainties in emission estimates are assessed using different transport fields and background concentrations coupled with the STILT model. Also, methods to further reduce uncertainties in the retrieved emissions by incorporating additional constraints including tracer-to-tracer correlations and satellite measurements are briefly discussed. The inversion approach both reproduces source areas in a spatially explicit way through sophisticated Lagrangian transport modeling and infers emission processes that leave imprints on atmospheric tracers. The results indicate that the changes in greenhouse gas concentration are strongly influenced by regional sources, including significant contributions from fossil fuel emissions, and that the integrated approach can be used for regulatory regimes to verify reported emissions of the greenhouse gas from oilsands developments.

Acknowledgements

Sincere thanks to my teachers, colleagues, friends, and beloved family to all of whom I have been deeply indebted in the way to coming this far.

Dedication

To EJ for all you have done for me.

Table of Contents

List of Figures

List of Tables

Chapter 1
Introduction

Atmospheric CO_2 is fundamental to primary productions in ecosystems that support lives on Earth, and it is important to well characterize variations of atmospheric CO_2 with its relation to responsible fluxes. Such knowledge can provide the key ingredient to reliably predict future behaviors of Earth's environmental system. Atmospheric measurements have played key roles in assessing growth rates of global CO_2, and sources and sinks on various spatial scales are derived from these long term observation results of atmospheric CO_2 [*Keeling and Whorf*, 1994; *Conway et al*., 1994]. One of the greatest challenges when attributing certain atmospheric species to its sources and sinks comes naturally from the fact that atmospheric flows integrate physical and chemical properties of substances that make contact with the fluid. A common method to infer sources and sinks from atmospheric measurements is to use a transport model to estimate the relationship between fluxes and tracer distributions, and then to derive source estimates using inversions. The techniques of inversion have been widely used for carbon cycle studies using trace gas concentrations. For an inverse problem, quantities that one wants to know is not given directly, rather information is on linear combination of related quantities. For example, the spatial distribution of trace gas concentrations represents a combination of the effect of spatially varying sources and sinks and the effect of atmospheric transport. In other words, the source/sink distributions can be deduced from observed concentration of a trace gas given atmospheric transport is known.

In recent decades, research communities have experienced of progresses in constraining uncertainties in the atmospheric carbon cycle by making combined use of high precision measurements with sophisticated atmospheric transport modeling techniques. Since isotopic composition of CO_2 contains information about its sources and sinks, use of isotopic composition of the GHG has been growing after the pioneering works [*Keeling et al.*, 1989; *Pataki et al.*, 2003a].

Notably, the carbon isotopes have proven to add significant information to synthesis inversion studies of global atmospheric CO_2 budgets [*Rayner et al.*, 1999; *Rayner et al.*, 2009]. Utilizing isotope measurements for CO2 cycle studies can provide multiple advantages including i) fossil fuels contain no radiocarbon because of their originating age, ii) depending on local plant water availability, the oxygen isotope composition of CO_2 is generally distinct for respiration versus anthropogenic CO_2, and iii) CO_2 derived from natural gas combustion is more isotopically depleted in ^{13}C than CO_2 from gasoline combustion. Thorough reviews on principles of the methods and key considerations of utilizing stable isotopes in terrestrial carbon cycle studies are found in published literature [*Sheppard*, 1981; *Flanagan and Ehleringer*, 1998; *Yakir and Sternberg*, 2000]. For regional scale applications, *Pataki et al.* [2003b; 2006] demonstrated benefits of utilizing multiple isotopes (i.e., ^{13}C, ^{18}O, and ^{14}C) of CO_2 when tracing urban sources of atmospheric CO_2 using ground measurements data.

The focus of this thesis will be given to understanding variations and contributing sources of atmospheric CO_2 measured at a Canadian GHG monitoring network site located in the province of Saskatchewan, Canada. This thesis starts by presenting total atmospheric CO_2 mixing ratios [*part per million volume*, ppm] measured in vertical profiles up to about 7 km above ground level. Its isotopic compositions are also examined to investigate seasonal cycles of the greenhouse gas. In addition, the Keeling plot method is applied to the CO_2 mixing ratio data collected at the same measurement locations in an effort to determine influences from various local sources to regional scale carbon cycles captured at the Canadian boreal landscape.

Data and measurement site information are introduced in Chapter 2, and principles and recent advances the application to interpreting the exchange of CO_2 between the atmosphere and different reservoirs (i.e., sources and sinks of the atmospheric CO_2) in the process of biogeochemical cycles are briefed at the beginning of Chapter 3. Discussions on important considerations underlying the Keeling plot method are followed before a linear mixing model of CO_2 using mass balance of isotopic

components is utilized in the way to complement a top-down inversion approach using the STILT model.

1.1 Preliminary outcomes

Preliminary outcomes relevant to this study have been presented in the following scientific conferences and meetings.

Kim, M. G., J. C Lin, L Huang, T. W. D Edwards, D. Worthy, D. Wang, C. Sweeney, J. White, L. Bruhwiler, A. Andrews, T. Oda, and F. Deng (2013), Assessing uncertainties in GHG emission estimates from Canada's oil sands developments, *American Geophysical Union Fall meeting 2013*, San Francisco, USA.

Kim, M. G., J. C. Lin, L. Huang, and D. Worthy (2013), Quantifying CO_2 emissions from Canada's oil sands developments-results from a multi-tracer atmospheric observational/modeling approach, *9th International Carbon Dioxide Conference*, Beijing, China.

Kim, M. G. (2013), Effects of boundary condition to CO_2 emission estimates, *2nd Environment Canada-Carbon Assilmilation System Workshop*, Toronto, Canada.

Kim, M. G., J. C. Lin, L. Huang, D. Worthy, D. B. Jones, and S. Polavarapu (2013), Quantifying CO_2 emissions from Canada's oil sands developments – a multi-tracer atmospheric monitoring approach, *4th NACP All-Investigators Meeting*(Feb. 4~7th, 2013), Albuquerque, NM, USA.

Kim M. G., J. C. Lin, L. Huang, T. W. D. Edwards, J. P. Jones, S. Polavarapu, and R. Nassar (2012), Assessing CO_2 emissions from Canada's oil sands developments - an inversion approach combined with stable isotope data*, *2012 American Geophysical Union Fall Meeting.*

***winner of Outstanding Student Paper Awards (OSPA) in the Atmospheric Sciences section; information about the award can be found at http://atmospheres.agu.org/sectionawards/studentawards.shtml/.**

Kim, M. G. (2012), Estimating GHG emissions from Canada's oil sands: initial results, *1st Environment Canada-Carbon Assilmilation System Workshop*, Toronto, Canada.

Polavarapu, S., M. Neish, S. Ren, R. Nassar, D. Chan, D. Jones, J. C. Lin, F. Deng, and M. G. Kim (2012), Development of the Environment Canada Carbon Assimilation System, *Atmospheric Tracer Transport Model Intercomparison (TransCom) Project meeting*, June 4-8, Nanjing, China.

Nassar, R., S. Polavarapu, M. Neish, S. Ren, D. Chan, A. Kabbekke, D.B.A. Jones, J.C. Lin, and M. Kim (2012), Progress toward assimilation of GOSAT CO_2 in the Environment Canada Carbon Assimilation System (EC-CAS) and complementary systems, Pasadena, California, June 20-22, *GOSAT RA PI meeting* at CalTech, CA, USA.

Nassar, R., S. Polavarapu, M. Neish, S. Ren, D. Jones, F. Deng, J. C. Lin, and M. G. Kim (2012), Progress toward the assimilation of GOSAT observations in the Environment Canada Carbon Assimilation System (EC-CAS) and complementary systems, 8th *International Workshop on Greenhouse Gas Measurements from Space*, CA, USA.

Lin, C. J., D. Wen, and M. G. Kim (2012), Overview of regional scale modelling: making the link between GHG and air quality, *Environment Canada-Carbon Assimilation Workshop,* Toronto, Canada.

Lin, C. J., M. G. Kim, and D. Wen (2011), Interpreting regional scale signals of global change from atmospheric concentrations, *Environment Canada-Carbon Assimilation System (EC-CAS) meeting*, Toronto, Canada.

Chapter 2

Variability of CO_2 measured at East Trout Lake, Canada

Knowledge about greenhouse gases (GHG) accumulating in the atmosphere can provide a key ingredient to reliable prediction of future changes in the global environmental system. In particular, rapidly accumulating long-lived GHG such as carbon dioxide (CO_2) is known to be the dominant factor in the warming of the global climate in recent decades [*Solomon et al.*, 2007] and expected to continue to be so [*Zickfeld et al.,* 2012]. Various types of measurements have thus expanded to assist in assessing its status in the atmosphere on various temporal and spatial scales. For example, careful long term measurements have proved that growth rates of CO_2 mixing ratio over the global atmosphere have been increasing [*Keeling and Whorf*, 1994; *Conway et al.*, 1994; *Keeling et al.*, 1995].

More recently, space-born instruments have started adding extra dimensions to surface observation networks by providing column measurements of CO_2. These satellite instruments, such as OCO-2, GOSAT, or SCIAMACHY, measure latitudinal variations in vertical profiles of CO_2 concentration with improved accuracy and precision over broad swaths of regions in oceans and remote areas of continents where ground measurements were limited [*Hungershoefer et al.,* 2010*; Miyamoto et al.,* 2013]. These multi-dimensional direct measurements of atmospheric CO_2 have been used with state-of-the-art atmospheric transport models in order to infer relationships between the variations in GHG concentration and changes of surface fluxes using inverse modeling frameworks [*Patra et al.,* 2005; *Stephens et al.*, 2007*; Peters et al.*, 2007; *Rayner et al.*, 2010; *Nassar et al.*, 2011]. The observational and modeling evidences strongly support that anthropogenic sources have contributed to the acceleration of GHG growth in the global atmosphere.

Usefulness of stable isotopes in addressing a range of questions in CO_2 cycles has well been recognized. In parallel with increases in attention to emphasis of utilizing stable isotopes in ecological

studies which focus on interpreting plant carbon-water relations [*Farquhar and Lloyd,* 1993; *Flanagan and Ehleringer*, 1998; *Yakir and Sternberg*, 2000; *Bowling et al.*, 2008; *Flanagan et al.*, 2012], values of using stable isotopes have been introduced to interpret CO_2 exchanges between the atmosphere and land surfaces in order to refine the understanding of biogeochemical cycles of the GHG over larger spatial scales [*Keeling et al.*, 1989; *Ciais et al.*, 1995; *Bakwin et al.,* 1998; *Rayner et al.*, 1999; *Randerson et al.*, 2002; *Ballantyne et al.*, 2012].

These studies showed that isotopic values of atmospheric CO_2 can be used to reveal its sources as well as processes of which the isotopes must have gone through before it ends up being in the

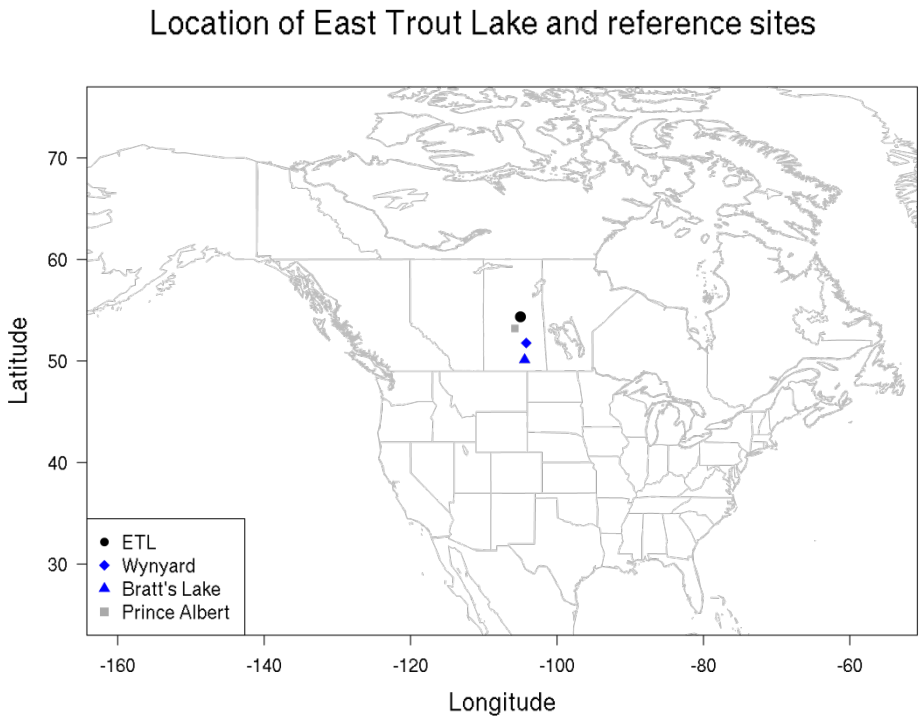

Figure 1 Location of the East Trout Lake measurement site (ETL, in black dot) which is also the receptor location of the transport model is presented in a map. The other two measurement

sites referenced are Wynyard (in blue diamond) and Bratt's Lake (in blue triangle). These two sites measured the oxygen isotope of ^{18}O in precipitation that provides information of understanding interactions of the oxygen isotope of ^{18}O in CO_2.

atmosphere since such isotopic "signatures" are mostly unique to certain processes and mixing status. For instance, $^{13}C/^{12}C$ ratio of CO_2 can be used to disclose photosynthetic pathways, and to distinguish plant and soil respiration as well as consumption of different fossil fuel types. Also, $^{18}O/^{16}O$ records phase changes of water in processes taking place over various scales, for example, evaporation, condensation, biomass burning, or combustion of fossil fuels. As such, careful observations of the isotopic composition of CO_2 in relationship with concentration changes can provide information on its origin, transport and mixing of CO_2 in the atmosphere [*Keeling,* 1958; *Keeling,* 1984; *Pataki et al.,* 2005].

This study seeks to serve as an expository investigation on atmospheric CO_2 and its isotopic values from direct measurements from data collected at a remote boreal forest of central Canada. The CO_2 and its isotopic data are made from a long-term measurement effort at East Trout Lake (ETL; 54.35^0N, 104.98^0W) site located in northern Saskatchewan, Canada (Figure 1). The ETL site used in this study derive from the Canadian Greenhouse Gas Measurement Program [*Puckett and Worthy*, 2010], and Environment Canada conducted air sampling approximately weekly through two-liter flasks at the site. In addition, Earth System Research Laboratory of National Oceanic and Atmospheric Administration (NOAA ESRL) administered aircraft sampling directly above the ETL site in coordinated efforts to construct profiles of measurements using air samples.

In a previous study, *Higuchi et al*. [2003] examined time-series of in-situ observations combined with aircraft measurements of CO_2 made at a different Canadian boreal forest site, but those authors focused on influences of vegetation productivity on observed variations of CO_2 concentration and their aircraft data was independent of surface measurements. Several years later, *Shashkov et al.* [2007] also investigated vertical profiles of atmospheric CO_2 at another Canadian

boreal forest site using an aircraft to suggest importance of considering directional transport of CO_2 over horizontal distances in determining surface fluxes from a stationary measurement. They analyzed measurement results using data collected over a four-day period.

The purpose of this study is to present and discuss measurement results of CO_2 and its stable isotopes collected through synchronized, long-term collaborations that were carried out by both Environment Canada and NOAA ESRL. To the best knowledge, this study is the first presentation to the date of writing of such comprehensive, long-term measurements CO_2 and its isotopic values in a remote Canadian boreal forest through the collaborative efforts by multiple research institutes. The overarching research question for the current study concerns changes in observed concentration levels and the isotopic ratios of CO_2 collectively measured at a comprehensive GHG monitoring site at the prime period of its operation from October 2005 until the end of calendar year 2010 during which the richest suite of data was produced. The main focus of this paper is in two folds: i) to present variability of CO_2 and its isotopic values and ii) to discuss source values of CO_2 isotopes derived with a statistical approach for isotopic analysis techniques.

Principles of data analysis adopted for this study are summarized in Section 2.1. In addition, the best estimate of variability of CO_2 and its isotopic values with confidence intervals is presented and discussed in Section 2.2, followed by the conclusion and suggestions for future studies.

2.1 Data and Methods

2.1.1 Site and measurement systems

This study utilizes molar ratios and isotopic compositions of CO_2 sampled at a Canadian Greenhouse Gas Monitoring Program station (ETL; shown in Figure 1) located in a boreal forest ecosystem. The boreal forest surrounding ETL is slightly rising and falling as gentle slopes, and its dominant vegetation type is needle-leaf trees including black spruce and jack pine with a small portion of

deciduous-like larch. The average height of these trees is approximately 15 meters and last known major disturbances such as timber harvests in the region took place 70~120 years ago. Short tree species grow understory, and the depth of organic matter on the surface ranges from a few to several ten centimeters depending on surface geology, soil wetness, and other environmental conditions [*Kljun et al.*, 2006; *Chen et al.*, 2008]. The ETL site is about 150 km north from Prince Albert, which is the nearest urbanized area with population of more than 35,000 (Figure 1).

A suit of standard greenhouse gas species including CO_2, CH_4, CO, N_2O, SF_6, and ^{13}C and ^{18}O of CO_2 are sampled nearly weekly through intake lines installed at two separate heights (22 and 100 meter above ground level) on a 105-meter-tall tower. The air samples are filled in two-liter flasks twice a sampling day at 09 and 21 UTC (or 03 and 15 Local Time) by an automated sampler located in a ground station, subject to instrument maintenance needs and weather conditions. These flasks are then shipped to an Environment Canada's laboratory located in Toronto, Canada for intended analysis of the greenhouse gas species and the stable isotopes [*Huang and Worthy*, 2005]. The same GHG species, but not the stable isotopes of CO_2, are measured continuously in-situ using a non-dispersive infrared methodology [*Worthy et al.*, 1998], and these gas measurements for the same species are used to complement one another as well as to serve as a cross-check on quality of the data for the site. Isotopic measurements of CO_2 by Environment Canada are meticulously carried out, thus comparable with independent measurements of equivalent element species from leading isotope laboratories [*Huang et al.*, 2013].

NOAA ESRL takes aircraft sampling of the same greenhouse gas species over ETL through collaborative efforts with Environment Canada. The flights of the research aircraft have been synchronized to collect air sample at multiple altitudes, which can be combined to line up with the tower measurements as a profile since October 2005. The air samples are filled in a programmable flask package (PFP; http://www.esrl.noaa.gov/gmd/ccgg/aircraft/packages.html) that consists of 12-

pack 0.7-liter flasks. Each of these flasks collects air samples at a different altitude during a flight routine where the aircraft flies to change its navigating altitudes from about 600 meter to 7,800 meter above the ground. The 12-pack flask packages are then delivered to Global Monitoring Division of NOAA ESRL in Boulder, Colorado for analysis of numerous gas species in addtion to the stable isotopes laboratory at the Institute of Arctic and Alpine Research in University of Colorado at Boulder for the stable isotopes analysis of CO_2.

The isotopic ratios of CO_2 for both $^{13}C/^{12}C$ and $^{18}O/^{16}O$ used throughout in this paper are expressed in δ notation relative to VPDB-CO2 (Vienna PeeDee Belemnite-carbon dioxide):

Equation 1

$$\delta = \left(R_{sample} / R_{stnd} - 1\right) \times 1000 \, {}^{O}/_{OO}$$

where R is a ratio of rare to abundant isotopic species, and subscripts $_{sample}$ and $_{stnd}$ respectively stand for the ratio of sample and the ratio of standard. The VPDB-CO2 scale uses the CO_2 evolved from the VPDB carbonate ($CaCO_3$) through the acid digestion by pure H_3PO_4 [*Brand et al.*, 2009]. During this reaction, there is no fractionation between CO_2 gas and the carbonate, thus the ratio of carbon isotopes ($^{13}C/^{12}C$) in CO_2 is the same as that in the carbonate. Therefore, for $\delta^{13}C$, the scale of VPDB-CO2 is the same as the VPDB scale which is more commonly used internationally. However, as for $\delta^{18}O$, the scale of VPDB-CO2 is different from that of VPDB because the oxygen isotope ratio ($^{18}O/^{16}O$) in CO_2 has changed from that of the carbonate through the reaction. Rigorous technical details of the isotope analysis system including its uncertainty and traceability are found in *Huang et al.* [2013] as well as in *Trolier et al*. [1996], and interested readers of VPDB-CO2 scale are invited to references therein.

2.2 Derivation of isotope values

2.2.1 Keeling plot methods

The measured CO_2 values represent the net result of mixing between advected background and emissions from local sources:

Equation 2

$$c_T = c_B + c_S$$

where subscript $_T$, $_B$, and $_S$ respectively stand for measured total, advected background, and local sources of CO_2. Treatments of background parameters are found usually in two ways, either by employing a meticulous experimental design to ensure constant background conditions or by prescribing reasonable references as background conditions. Although theories behind mixing model approaches are well understood, these kinds of treatments of backgrounds for mixing model parameters still require caution in various practical applications. This is mainly both because i) constant background values for any given mixing in the atmosphere can rarely be established due to dynamic nature of the mixing medium, and because ii) variability of CO_2 and its isotopic composition are strongly influenced not only by atmospheric transport and mixing but also by changes in surface fluxes, which can themselves be highly variable (Appendix F). Equation 2 can be combined with isotopic compositions to be re-written, given a single source causes changes to CO_2 concentration and to its isotopic composition relative to the background:

Equation 3

$$\delta_T c_T = \delta_B c_B + \delta_S c_S$$

Equation 3 is an approximation form of the exact expression, where the discrepancy between the two formations is very small [*Tans et al.*, 1993; *Bakwin et al.*, 1998]. When Equation 2 is plugged into Equation 3, the isotopic mass balance of a two-end-member mixing system can be derived since the product of CO_2 concentration and its isotopic composition is known to be nearly conserved [*Tans*, 1980; *Ballantyne et al.*, 2010]:

Equation 4

$$\delta_T = (\delta_B - \delta_S)(c_B / c_T) + \delta_S$$

A number of studies took advantage of this approach widely known as Keeling plot method [*Keeling*, 1958; *Keeling*, 1961] as expressed in Equation 4. This form of Keeling plot method describes the relationship between measured CO_2 concentration and CO_2 being added from a source with a simple linear relationship of $y = mx + b$. In Eq.4, the isotopic value of a source being added to the atmosphere is found by the y-intercept from relating inverse of measured CO_2 concentration to its isotopic ratios. One great benefit of using Eq.4 is that one does not need to know about background concentration nor its isotopic composition, but it requires assuming constant backgrounds during sampling periods [*Flanagan et al.*, 1997; *Bakwin et al.*, 1998; *Pataki et al.,* 2003b; *Bowling et al.*, 2005].

Permutations to the Keeling method were proposed by *Bakwin et al.* [1998, in their equation (11)] and by *Miller and Tans* [2003, in their equation (5)] to provide the isotopic source values of CO_2 using:

Equation 5

$$\delta_T c_T = \delta_S c_T + c_B(\delta_B - \delta_S)$$

In fact, Equation 5 is mathematically equivalent to Eq.4 except that δ_s is found with 'm' instead of 'b' in the linear expression $y = mx + b$. These authors argued that advantage of using Eq.5 over Eq.4 is that the background mixing ratio and its isotopic composition can remain unknown but do not need to be constant. In addition, in Equation 5 the isotopic source values are obtained from the slope of a linear relation between measured CO_2 mixing ratio and the product of measured CO_2 and its δ value. Consequently, δ_s in Equation 5 is derived with the slope of a regression line that best approximates actual measurements rather than being represented by an extrapolation (i.e., y-intercept) that can be sensitive to uncertainties embedded in each data point that the line goes through.

2.2.2 Uncertainties in isotopic source values

Methods to examine uncertainties in derived isotopic source values from Keeling-like mixing models are found in several previous studies [*Veldkamp and Weitz*, 1994; *Phillips and Gregg*, 2001; *Zobitz et al.*, 2006; *Kayler et al.*, 2009]. These studies committed to probing errors inherent in linear mixing models using statistical approaches for multiple samples of different mixtures (e.g., soil organic matters, food webs, or the atmosphere) to find that simple mass balance approaches are useful in general, but uncertainties need to be reported along with the best estimate of isotopic source values contributing to variability of a mixture.

This study presents derived Keeling plot values with its statistical sensitivity. The sensitivity of linear regression methods to obtain the y-intercept and slope for Eq.4 or Eq.5 is tested by comparing results from "Type I" and "Type II" regression models, following *Flanagan et al.* [1996], *Pataki et al*. [2003b], *Zobitz et al*. [2006], and *Kayler et al*. [2009]. "Type I" regressions are known to be an appropriate prediction, for example, when errors of response variable (y) are expected to be much larger than errors of the predictor (x), and "Type II" regression models assume equal accuracies of x and y and are appropriate when the relationship is bivariate normal. Since the y-intercept of linear

regressions is essentially an extrapolation from actual measurements and the linear mixing is based on two end-members, both types of regression models should be appropriate choices to Keeling plot approaches and inter-comparisons of sensitivity test could reveal valuable information that potentially helps quantify the uncertainties in the linear mixing approaches. This study adopts Ordinary Least Square (OLS) for Type I regression, and Geometric Mean Regression (GMR) is adopted for Type II regression. The OLS method finds the minimal sum of residuals from a hypothetical best-fit line to each data point, and the GMR method offers optimal residuals from trigonometric functions of the slope of a regression line to each data point [*Zobitz et al.*, 2006]. In addition to testing sensitivity of the Keeling plot methods towards different regression approaches, the significance tests are also applied to each linear regression to constrain upper and lower bounds of coefficients at 95% confidence intervals.

Keeling plot values are derived from each measurement profile sampled at up-to fourteen different altitudes incorporating typically two flasks sampled at two different altitudes on a tower and twelve PFP collected during a coordinated flight routine. Since complete sampling of one profile is implemented within a two-hour time period, we postulate that one profile represents air samples from a reasonably homogenous blob of mixed gases in the atmosphere. We then recall that the Keeling plot method works for a mixture of gases which reflects additions of a source to background while conserving mass. Further, if any hypothetical blob of air is reasonably well-mixed and not freely exchanging its chemical properties with external systems, high correlations between CO_2 and its isotope ratios are expected. Hence, it is prudent to hypothesize a reasonably uniform system of atmospheric mix when strong correlation between CO_2 and its isotopic values is indeed found in data obtained from a measurement profile despite of varying altitudes where samples are respectively taken. Pearson correlation coefficients are chosen as a statistical measure in order to test if the well-mixedness is met for each profile of measurements.

This study constructed linear regressions to derive the isotopic source values using selected data that shows coefficient of determination that are greater than 0.9 ($R^2 > 0.90$) for $\delta^{13}C$ and CO_2 concentration. A slightly relaxed selection criterion of $R^2 > 0.70$ is used for $\delta^{18}O$ and CO_2 concentration. Because of its active involvements in water cycles, the oxygen isotope typically shows a less strong correlation with CO_2 concentration. Consequently, correlation between $\delta^{18}O$ and CO_2 concentration is barred at a lower cut-off for evaporation and condensation of atmospheric water strongly affects the isotopic values of oxygen in CO_2 through equilibrium processes [*Gat*, 1980]. When the correlation between CO_2 and its isotopes are found unsatisfactory to the criteria the entire profile is unused for Keeling plots. In order for observed variability of $\delta^{18}O$ of CO_2 to be properly presented in a broader context, this study examines $\delta^{18}O$ of precipitation measured at nearest Canadian Network for Isotopes in Precipitation (CNIP; [*Birks et al.*, 2003; *Gibson et al.*, 2005]) stations shown as Wynyard and Bratt's Lake in Figure 1. Amount-weighted averages of $\delta^{18}O$ values in monthly precipitation were calculated at the two individual sites, and the values are expressed in δ notation relative to Vienna Standard Mean Ocean Water (VSMOW) following conventions used previously by *Birks and Edwards* [2009] and *Birks and Gibson* [2009].

2.3 Variability of atmospheric CO_2 and its isotopic composition

This section presents variations in mixing ratio of CO_2 and its stable isotopic compositions measured at ETL from October 2005 to December 2010 during which a tall tower data is available in combination with the aircraft sampling program. The ground measurements at ETL are conducted using both a weekly flask program and a continuous in-situ technique (Section 2.1). The differences in concentration values between weekly flasks sampled at 100 meter above ground and in-situ data are statistically significant, but the mean discrepancy is within acceptable measurement errors (< 0.11 ppm, unpublished in-situ measurement data). Furthermore, the $\delta^{13}C$ and $\delta^{18}O$ of CO_2 are analyzed in the Environment Canada's laboratory together with its mixing ratio from each sample collected using

a flask. Hence, this study focuses presentation of CO_2 measurement results using values from flask samples in order to be compatible with its isotopic values of $\delta^{13}C$ and $\delta^{18}O$. Each measurement profile may consist of fourteen flask samples from which CO_2 concentration as well as $\delta^{13}C$ and $\delta^{18}O$ at maximum of fourteen different altitudes can be obtained. The variability of $\delta^{13}C$ and $\delta^{18}O$ of CO_2 is examined in Section 2.3.1, followed by discussions on its sources derived with Keeling plot analysis in the subsequent sections.

2.3.1 Observed variability in $\delta^{13}C$ and $\delta^{18}O$ of CO_2: a link to hydrologic cycles

The atmospheric CO_2 concentration measured at ETL reveals dynamic seasonal variations as following the trend of global average shown in dark grey line, as shown in Figure 2. The peak value of CO_2 mixing ratio during the entire time period is measured at 403.56 ppm in November 2010, the lowest being at 365.08 ppm in July 2008. Lower concentration values are found in general during summer months when the vegetation surrounding the measurement site is actively sequestering CO_2 for productions, while higher values are in winter when the vegetation is mostly dormant, resulting in the accumulation of the greenhouse gas in the atmosphere. Indeed, the seasonal average of vertical profiles of CO_2 presented in Figure 3 shows active vegetation during warm months uptakes CO_2 as indicated by concentration levels below 1 km altitude is lower than that of background atmosphere aloft. The vertical profile of CO_2 concentration levels for cold months is shown as if it is flipped to the opposite side, higher concentration of CO_2 is found predominantly at lower altitudes during the winter seasons.

The $\delta^{13}C$ values shown in red circles with cross symbols in the top panel of Figure 2 vertically mirror CO_2 concentrations in general; more depleted in heavy isotopes when concentration levels are elevated during winter and vice versa during growing seasons. For example, the highest individual value in $\delta^{13}C$ of CO_2 is in July 2008 when CO_2 concentration is found low, and the lowest $\delta^{13}C$ value corresponds to the incident when highest CO_2 concentration is measured in November 2010. The

same pattern applies true for the mean vertical profiles shown in Figure 3. During warm months, when atmospheric CO_2 near surface is being utilized by plants, $\delta^{13}C$ values are less depleted. On the other hand, when CO_2 accumulates near the surface during winter months, the carbon isotope ratio at lower altitudes shifts toward more negative values likely due to influences from combustion of fossil fuels. In addition, the Pearson correlation coefficient between CO_2 mixing ratio and $\delta^{13}C$ for the entire measurement sample is found around -0.91. This negative correlation between CO_2 concentration and $^{13}C/^{12}C$ is known to be due primarily to preferential uptake of lighter carbon (^{12}C) during photosynthesis by vegetation types growing in the boreal forest [*Farquhar et al.,* 1989]. The discrimination against the heavier isotope in atmospheric CO_2 during photosynthesis occurs because enzymes preferentially assimilate the lighter carbon [*Lloyd and Farquhar*, 1994]. On the other hand, when CO_2 concentration increases during winter seasons as vegetation is less active, additional CO_2 from combustion of fossil fuels lowers $\delta^{13}C$ of atmospheric CO_2 because most types of fossil fuels are composed of ancient vegetation thus depleted in ^{13}C. It is noted that the carbon isotope ratio of ambient CO_2 are affected not only by contributions from respiratory flux from ecosystem but in concert with the rate of mixing in atmospheric pools of CO_2 [*Yakir and Sternberg*, 2000]. Consideration of these effects that determine degrees of the imprint by these processes on carbon isotope ratios is an actively evolving area of ecosystem research concerning plant-atmosphere interactions.

The $\delta^{18}O$ values shown by blue circles with cross symbols in the lower panel of Figure 2 are scattered to a wider extent than $\delta^{13}C$ is. Individual values range from -30.33 ‰ to 0.98 ‰ VPDB-CO2 (note that -30.33 ‰ is off the scale shown in the figure), while the majority of daily mean values is found between -2 ‰ and 0 ‰. The mean of entire measurement is found at -0.84 ‰. The highest value is measured in October 2008 and the lowest being in July 2008. To a first degree, the

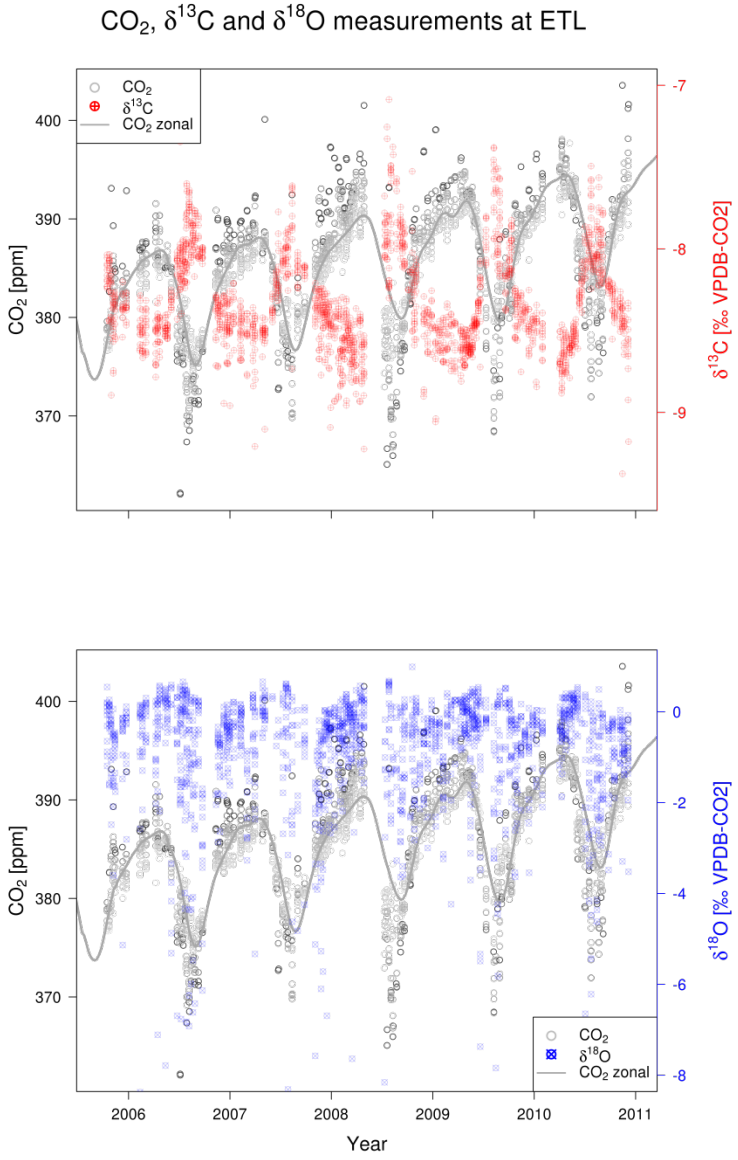

Figure 2 Time-series plots showing changes in measured CO_2 mixing ratios and $\delta^{13}C$ of CO_2 at the upper panel and $\delta^{18}O$ of CO_2 at the bottom panel, respectively. Black and grey circles represent daily CO_2 values measured at all altitudes of profile measurements. The darker the color of circles, the lower the measurement altitude it represents. The grey solid line represents zonal average of CO_2 values, which is a composite of measurement-based data for which the latitudes where the ETL exists. Colored circles with cross symbols inside represent individual isotopic values for $\delta^{13}C$ of CO_2 in red and $\delta^{13}C$ of CO_2 in blue. The same color-coding is used for representing different measurement altitudes of the isotopes: darker colors represent lower measurements.

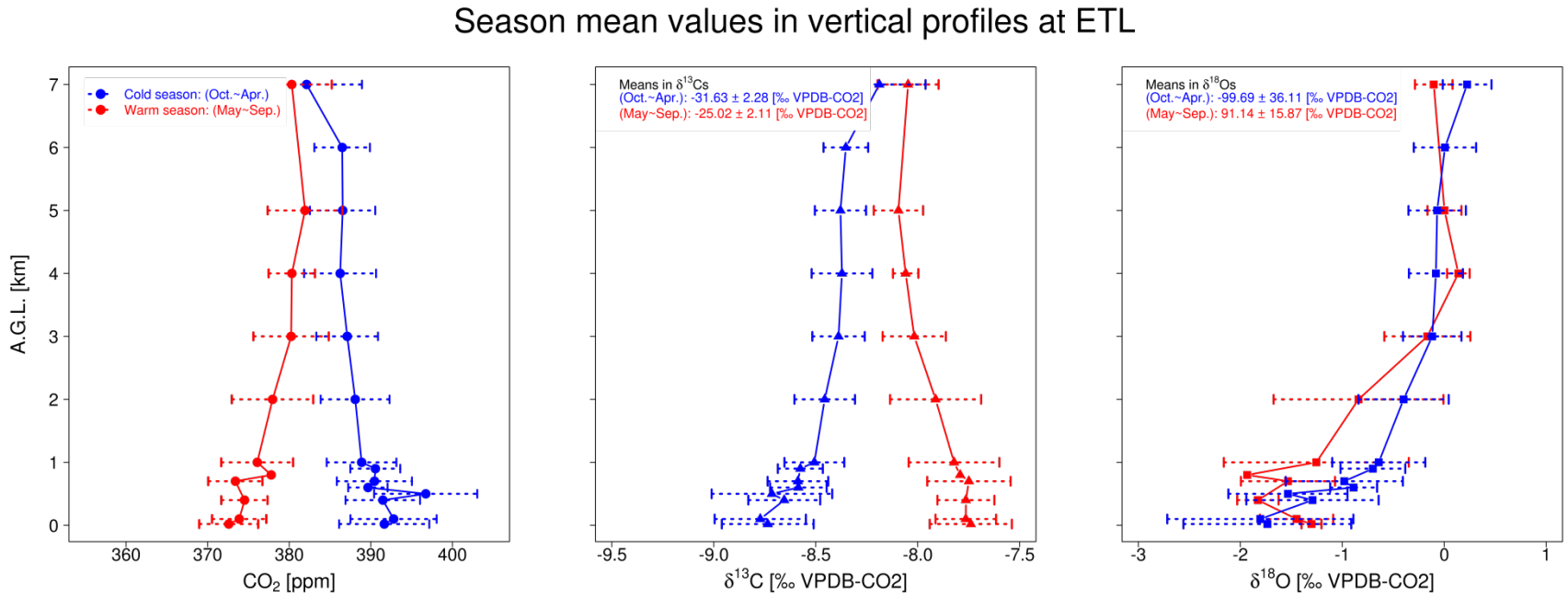

Figure 3 Average vertical profiles of measurements. Seasonal mean vertical profiles of CO_2 mixing ratio (left), $\delta^{13}C$ (center), and $\delta^{18}O$ (right), are plotted. Average values are plotted in solid symbols at corresponding altitudes, and standard deviations are presented with horizontal dotted-lines at each mean value. Mean values and standard deviations are calculated for two different groups of months depending on monthly mean air temperature; months of May to September are considered as warm months, and the rest of months are cold months.

relationship between $\delta^{18}O$ and CO_2 concentration is relatively less obvious, and the correlation coefficient is found positive at 0.25. Daily measurement time-series in general, except for 2 days residing off the scale, indicate a course of variation that less depleted values correspond to higher CO_2 concentrations during winter, and more depleted values commonly seem to be found during summer seasons. This relationship for $\delta^{18}O$ and CO_2 concentration is also found in the mean vertical profiles. During vegetation is active when CO_2 level is relatively lower near surface, $\delta^{18}O$ is found generally more depleted because of transpirations. This agrees with a prevailing tendency reported in previous studies that examined ecosystem gas exchanges in boreal forests using stable isotopes [*Flanagan et al.*, 1997; *Flanagan and Ehleringer*, 1998]. What is intriguing to observe is the relationship between CO_2 levels and $\delta^{18}O$ during cold months. While exhaust from combustion of fossil fuels is being added to lower atmosphere, when the vegetation is dormant and evapotranspiration is much limited during cold months, CO_2 concentration stays relatively higher near the surface and $\delta^{18}O$ values at lower altitudes tend to be more depleted than background atmosphere at higher altitudes (refer to Figure 3).

Derived source values of the oxygen isotope are significantly more depleted than what is expected for the oxygen isotope ratios deriving from ecosystem respirations. This study seeks to investigate for a plausible explanation for the much depleted oxygen isotope source values, based on a chain of classic theories relating oxygen isotope exchanges between CO_2 and H_2O. A possible explanation stems from the fact that major changes in $\delta^{18}O$ also occur in the part of H_2O cycles [*Yurtsever and Gat*, 1981] which are exposed to atmospheric CO_2 [*Brenninkmeijer*, 1983; *Criss*, 1999; *Yakir and Sternberg*, 2000]. This fact constitutes to a considerable hypothesis that significantly depleted ^{18}O in CO_2 may be due to isotopic equilibrium between CO_2 and liquid-phase water before samples are taken in the ambient atmosphere. The first part of the hypothesis involves possibilities of sample contamination by water inclusion to flasks, despite of industrious efforts to keep PFP flasks dry throughout sample collection procedures. Several of anomalous $\delta^{18}O$ values that could be due to

such artifacts, caused by formation of water in flasks due to condensation processes for example, are flagged by meticulous adherence to technicality during sample analysis stages. All of the flagged samples are then manually examined by principal investigators. Furthermore this study inspected correlations between CO_2 and $\delta^{18}O$ for each day in order to examine whether the well-mixedness are met between samples used to derive a source value (Section 2.2.2). Almost all of the sampling days (99.98%) with distinctively low $\delta^{18}O$ of CO_2 shown in Figure 2 has persisted in these data screening steps, which disapproves likelihood of $\delta^{18}O$ of CO_2 being much depleted because of contaminations by liquid water inclusions in flasks. Second possibility for the hypothesis to be tested arises from respired CO_2 having been in contact with ecosystem water such as in plants, soils, or lakes. This study focuses on isotopic composition of ecosystem waters in plants and soils since about 70% of seasonal evapotranspiration observed in a boreal forest near ETL takes place through transpiration by the forest canopy [*Blanken and Black*, 2004].

Most of terrestrial vegetation utilizes soil waters for photosynthetic activities. Once the source water forms a freely evaporating surface in the site of evaporation in stomata, atmospheric CO_2 that enters into stomatal pores during photosynthesis equilibrates with the leaf-water. A portion of CO_2 that is isotopically altered subsequently diffuses (or is respired) back to the atmosphere [*Yakir and Sternberg*, 2000]. This equilibration between the leaf-water and CO_2 diffusing into and out of leaves is responsible for the observed seasonal and latitudinal distributions of $\delta^{18}O$ values over large scales [*Francey and Tans*, 1987; *Flanagan and Ehleringer*, 1998; *Pendall et al., 2005*]. These authors further suggest that relatively lower values in $\delta^{18}O$ of CO_2 are likely associated with soil-respired CO_2 which equilibrated with soil-water rather than leaf-water. The soil-respired CO_2 is derived by microbial activities or by root respiration [*Cerling et al.*, 1991], and the effective depth that influences $\delta^{18}O$ of soil-respired CO_2 is experimentally suggested at 5~15 cm [*Miller et al.*, 1999]. Isotopic compositions of water in this depth of unsaturated soil zone are fed directly from precipitation or

from fresh surface waters such as melting snow [*Gat*, 1981]. Thus, $\delta^{18}O$ of soil-respired CO_2 reflects isotopic composition of the meteoric source waters which correspond to that of local precipitation.

The isotopic compositions in precipitation collected at two CNIP sites closest to ETL are analyzed for $\delta^{18}O$ of H_2O as shown with grey dots in Figure 4. The isotopic values in precipitation measured at the two sites are plotted near the Global Meteoric Water Line (GMWL; [*Craig*, 1961]),

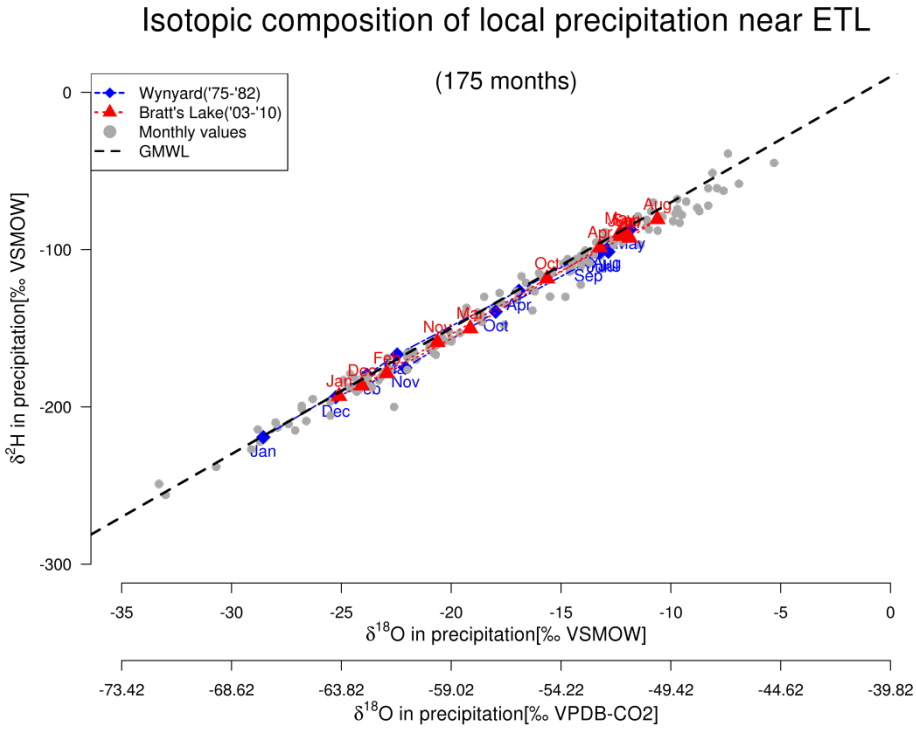

Figure 4 . Local meteoric water lines from two Canadian Network for Isotopes in Precipitation sites near ETL. Locations of Wynyard and Bratt's lake are depicted in the map (Figure 1). Grey dots represent amount-weighted isotopic values in precipitation for individual months from both Wynyard and Bratt's Lake stations, and blue squares indicate monthly averages for Wynyard while red triangle represents those of Bratt's Lake. Wynyard data is plotted using samples collected from August 1975 until July 1982, and Bratt's Lake uses data from May 2003 to November 2010. The black dashed-line indicates the Global Meteoric Water Line described by $\delta^2H=8*\delta^{18}O+10$.

which is shown as the black-dashed line in the figure. The GMWL closely approximates coupling of $\delta^{18}O$ and $\delta^{2}H$ in global precipitation, and deviations of precipitation isotopes from GMWL reflect spatial variability in the relationship of $\delta^{2}H=8*\delta^{18}O+10$, owing to changes in temperature, altitude, latitude, continentality, or any combination of them [*Edwards et al.*, 2004].

Despite of discrepancies in their sampling periods and distances, Wynyard and Bratt's Lake share a remarkably similar pattern in isotopic compositions of precipitation. Firstly, $\delta^{18}O$ from the both sites fall below GMWL because of their locations in relatively high latitudes. Secondly, changes in monthly averages of isotopic ratios observed at the both sites presented with colored symbols in Figure 4 can be summarized as cyclic changes in water isotopes, which loop two hydrologic regimes over years.

Isotopic composition of precipitations during cold months clusters in lower-left corner of the plot, and isotopic values in summer precipitation are shown in the upper-right corner. Namely, the $\delta^{2}H$ and $\delta^{18}O$ values start to progress diagonally toward a less depleted regime in the upper-right corner as temperature increases then loops back to where it started. Given that $\delta^{18}O$ values of soil-respired CO_2 is a strong function of isotopic contents of the source water in soils [*Miller et al.*, 1999; *Flanagan et al.*, 1999; *Mortazavi et al.*, 2004], the $\delta^{18}O$ of atmospheric CO_2 must reflect its source values to the $\delta^{18}O$ values in precipitation presented in Figure 4. In order to examine possibilities of influences from $\delta^{18}O$ of soil waters to respired CO_2, here we derive isotopic source values of atmospheric CO_2, following Keeling plot techniques.

2.3.2 Isotopic source values for the observed atmospheric CO_2 at ETL

The Keeling plot method is a form of linear mixing model which are applied to trace the source of an element in a mixture based on its isotopic mass balance. We adopt the traditional Keeling plot approach as well as its modification described in Section 2.2.1. Assuming a pseudo-closed system for the mass in a mixture such as an air parcel, the source value derived with Keeling plots indicates an

end member (i.e., δ_s) of the product of mixing. The derived source values presented here are from each set of measurements as long as the correlation between CO_2 and isotopic ratios for an individual profile is found stronger than a chosen threshold for respective isotope ratios ($R^2 > 0.90$ for $\delta^{13}C$; $R^2 > 0.70$ for $\delta^{18}O$). Also, as discussed in Section 2.2.2, differences in derived source values resulting from a particular approach of Keeling plot methods, for instance, when constructed with different linear regression techniques, are described.

The isotopic source values derived with four different configurations of Keeling plots are summarized in Table 1. It is noted that discrepancy between source values derived with different type of regressions (Type I and Type II) is larger than the discrepancy due to different formulations of the Keeling plot method (Eq.4 versus Eq.5). For example, the mean value of $\delta^{13}Cs$ derived using Type I regression is found at -29.35 ‰ regardless of formulations of Keeling plot equations, but Type II regression results in about 0.07 ‰ differences in the mean value of $\delta^{13}Cs$ depending on formulation

Table 1 The best estimate and its variances of isotope source values derived with different forms of the Keeling plot method. Pearson correlation coefficient between CO_2 concentration and the isotope values are calculated for each day, and samples with very strong correlations ($R^2 > 0.95$) were used to derive the source values.

[a]: number of sampling days with $R^2 > 0.95$ for both $\delta^{13}C$ and $\delta^{18}O$

Isotope species	Parameters	Traditional Keeling (Eq.4) [‰ VPDB-CO2]		Modified Keeling (Eq.5) [‰ VPDB-CO2]	
		Type I	Type II	Type I	Type II
$\delta^{13}C_s$ ($n^a = 77$)	Max.	-23.18	-23.28	-23.16	-23.23
	Mean	-29.35	-29.59	-29.35	-29.52
	Min.	-38.72	-38.91	-38.77	-38.91
	S.D.	3.13	3.20	3.14	3.19
$\delta^{18}O_s$ ($n^a = 7$)	Max.	-57.95	-59.30	-57.98	-59.33
	Mean	-78.12	-79.44	-78.14	-79.44
	Min.	-105.10	-106.60	-105.20	-106.70
	S.D.	15.81	16.13	15.82	16.13

of Keeling plot equations. Provided the basic assumptions for Keeling plot methods are met, deviation of the slope, hence the y-intercept, should converge to a minimum especially when the correlation is close to the unity [*Pataki et al.*, 2003b]. Since the traditional Keeling method (Eq.4) with Type I regression generates the minimal standard deviation of regression results for the given data. We further examine uncertainties in the y-intercept values by the ordinary least squares for each linear regression following *Sokal and Rohlf* [1995] and *Legendre and Legendre* [1998]. The traditional Keeling plot constructed with Type I regression is also advocated by previous ecosystem gas exchange studies [*Flanagan et al.*, 1997; *Pataki et al.*, 2003a; *Zobitz et al.*, 2006].

The isotopic source values of CO_2 for the available data are shown as dots in Figure 5, and each derived source value is accompanied with its uncertainty range as shown by vertical bars. Apparently, wintertime data in general has stronger correlations between CO_2 concentration and isotope ratios as expected. The ETL site normally undergoes five months of cold climate from November through next year March when the monthly mean air temperature falls below freezing [*Meteorological Service of Canada*, 2013]. The correlations during wintertime are stronger because influences from biospheric activities minimizes as vegetation goes dormant thus source signals related to ecosystem photosynthesis or transpiration [*Sternberg*, 1997] becomes minimal, particularly while snow cover and frozen grounds limits surface emissions being added to the atmosephere. These suggest atmospheric CO_2 observed at ETL during winter months is more likely originated from a lesser number of source processes that influence its isotopic compositions. Hence, relatively better suited for applying Keeling plot methods with the assumptions of two end-members being well-mixed in the atmosphere. In addition, it seems noteworthy that the number of sampling days that were used to successfully derive the δ^{18}Os values is far less than the number of derived for δ^{13}Cs despite of lower threshold values of correlation applied to the oxygen isotope and CO_2, and all of the stronger

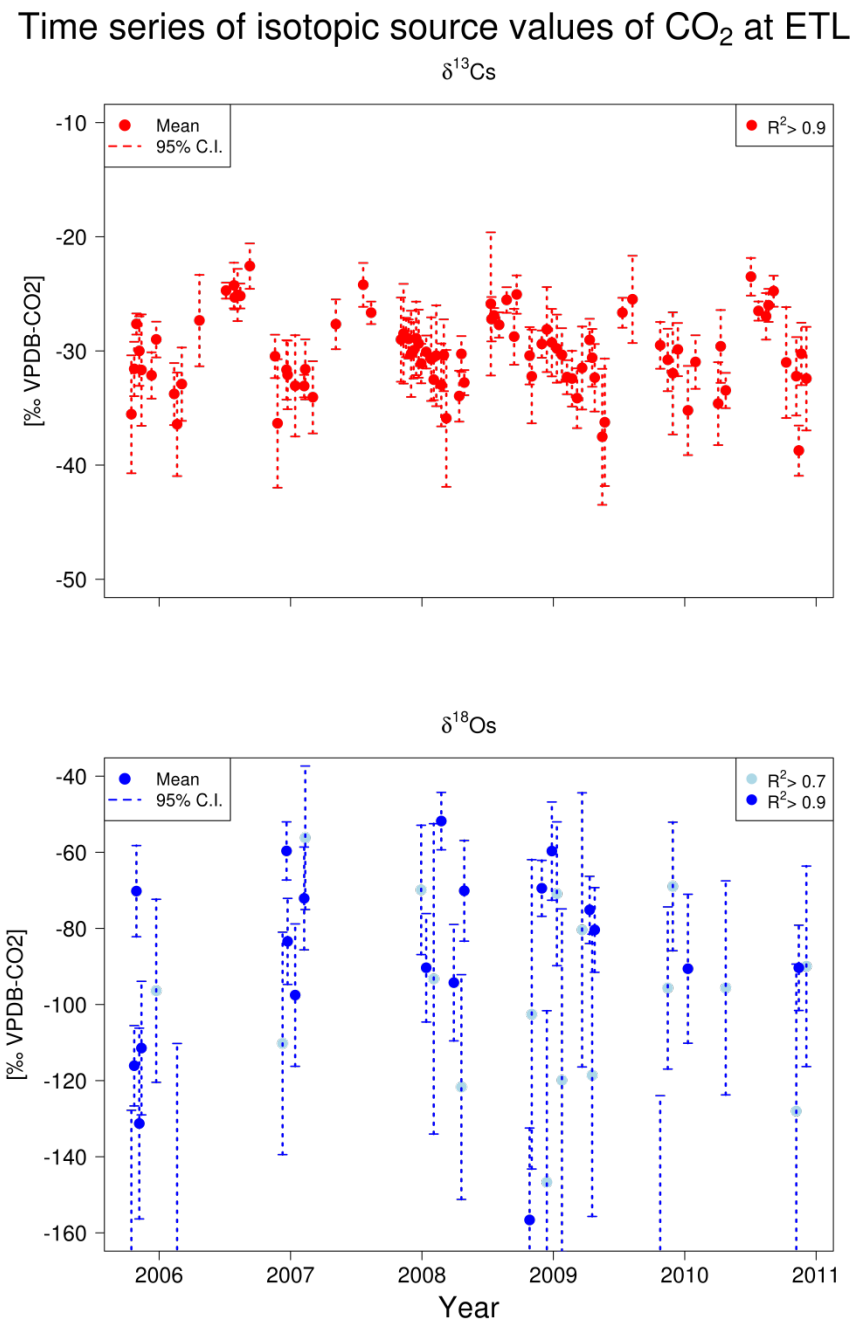

Figure 5 Isotopic source values of CO_2 as determined by the Keeling plot method (Eq.4) for a) $\delta^{13}Cs$ and b) $\delta^{18}Os$. Solid dots indicate best estimates for y-intercepts derived with Ordinary Lease Square linear regressions, and grey vertical lines show the 95% confidence interval calculated with standard error of the regression.

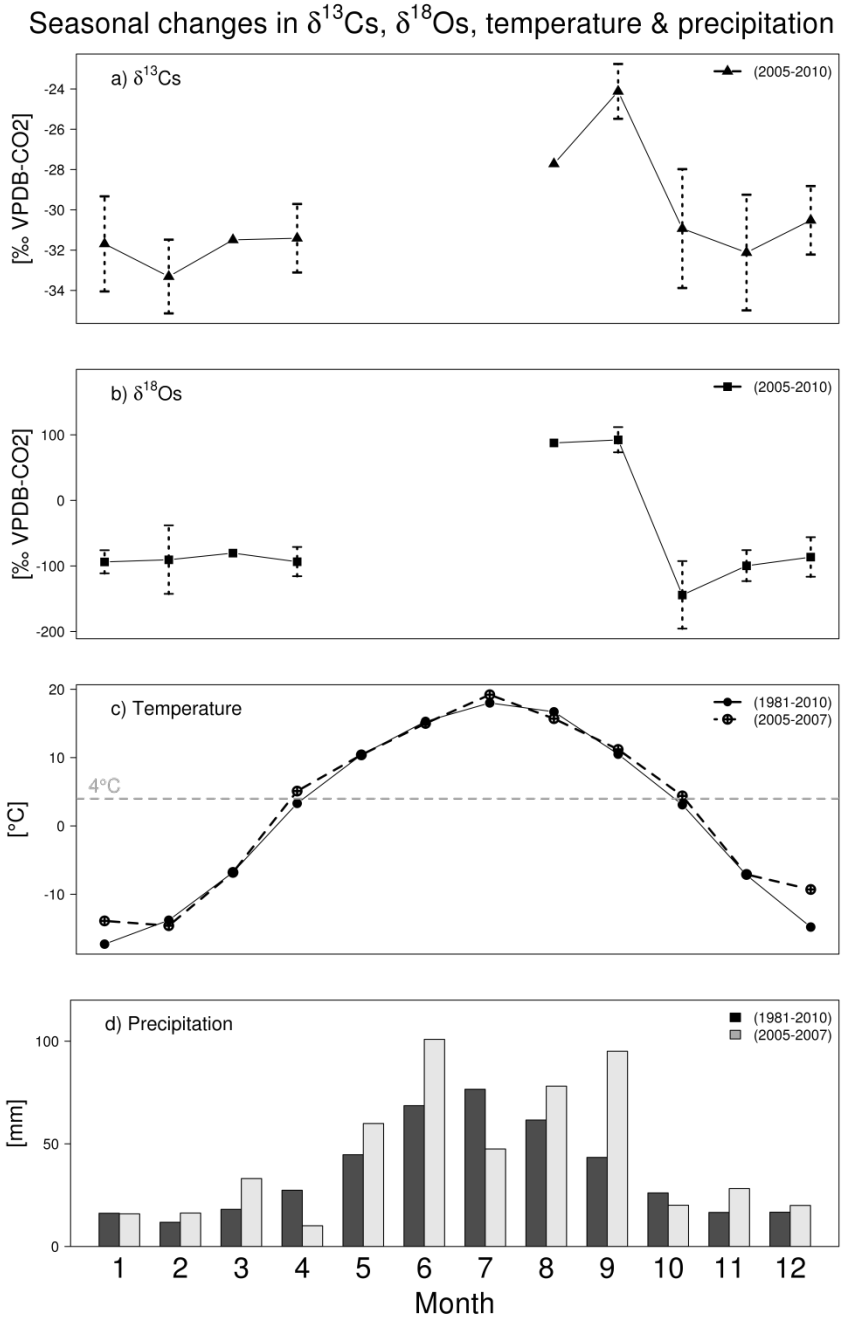

Figure 6 Seasonal changes in source values of $\delta^{13}C$ and $\delta^{18}O$ in relation to ambient natural variables of air temperatures and precipitation amounts measured at the nearest meteorological station at Prince Albert (see Figure 1 for the approximate location). The most recent value of Climate Normals data of air temperatures and precipitation amounts are also presented as a reference. Years this study focuses on were relatively warmer and wetter than usual.

correlation in samples (i.e., $R^2 > 0.90$) are found in cold months when presence of liquid water on near ground surfaces is minimal due to the cold temperatures (Figure 6).

Seasonally speaking, δ^{13}Cs ranges approximately from -29 ‰ to -38 ‰ during cold months and -23 ‰ to -32 ‰ for the rest of sampling period for this study. The δ^{13}Cs values around -30 ‰ typically represent CO_2 originating from fossil fuel consumptions, and less depleted values in summer are likely due to influences from biospheric respiration [*Keeling et al.*, 1984; *Pataki et al.*, 2003a]. The apparent seasonal cycle with more depleted values in winter and less negative values during summer suggests different combination of contributing sources of CO_2 to the atmosphere is measured at ETL. Increased uses of fossil fuels during winter induce the build-up of CO_2 with more negative δ^{13}Cs values, and active biosphere during growing seasons takes up CO_2 from the atmosphere for productions and respires CO_2 in return, which has less depleted δ^{13}Cs values. We constructed additional Keeling plot using nighttime CO_2 and its δ^{13}C sampled at 22 meter of the tower in order to derive δ^{13}Cs for ecosystem respiration. The derived mean value is found at -26 ‰ which indeed matches most of summertime δ^{13}Cs values shown in Figure 5.

According to direct measurement data collected in Salt Lake City, USA, natural gas combustion emits CO_2 with δ^{13}Cs values at about -37 ‰, and CO_2 from gasoline combustions has less depleted δ^{13}Cs values at about -28 ‰, which closely overlaps with the end-member value for the ecosystem respiration [*Pataki et al.*, 2003a; *Pataki et al.*, 2006]. The δ^{13}Cs values for winter seasons in Figure 5, hence, can be interpreted as CO_2 from emissions from conventional fossil fuels if δ^{18}Os values also indicate the fossil fuel sources.

The seasonal variations of δ^{18}Os are challenging to detect because of a fewer number of available data, lower correlations, and larger uncertainty ranges for each δ^{18}Os value as shown in Figure 5. The δ^{18}Os values derived with data that has stronger correlations ($R^2 > 0.90$) are exclusively found in cold months, and the range of derived source values for the oxygen isotope ratio span from

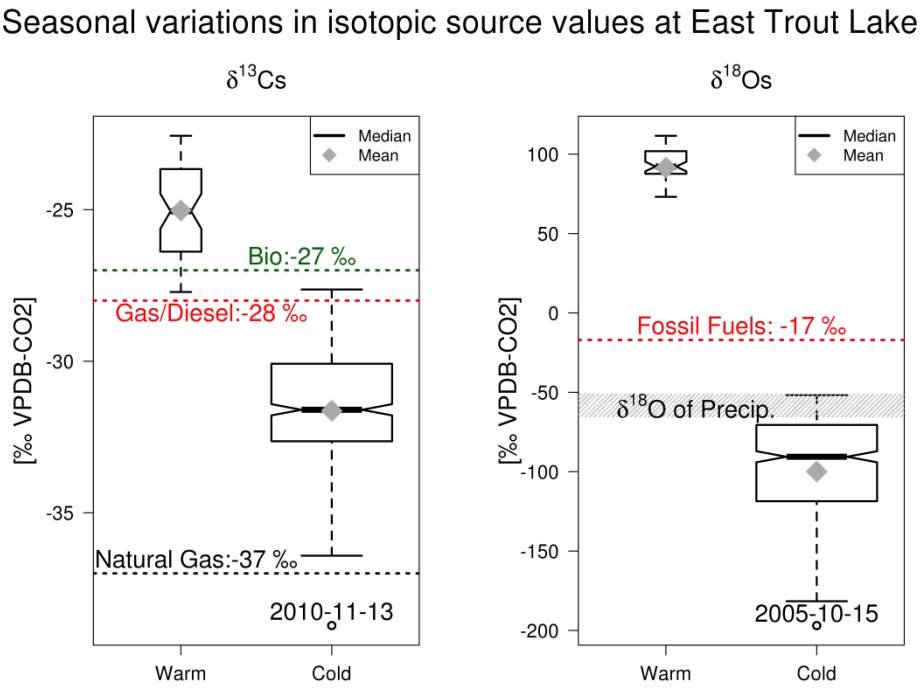

Figure 7 Seasonal differences in distributions of isotope source values of $\delta^{13}C$ (left) and $\delta^{18}O$ (right) measured at ETL. Differences in the size of boxplot represent the number of population in the samples that are considered; for example, because 'Cold' months have more number of highly reliable measurements (determined by R^2), boxplots that represent these months are relatively bigger in the size. During cold months, atmospheric CO_2 measured at ETL are likely influenced by source contributions from major fossil fuel types such as gasoline, diesel, or natural gas as indicated by $\delta^{13}Cs$. On the other hand, $\delta^{18}Os$ values fall far more depleted or enriched what is expected to be observed as influences from local precipitation. During warm months, it is speculated that unexpected natural events such as lightning might have influenced the atmospheric samples that are relatively so small to be deterministic. During cold months when relatively larger number of highly reliable measurements is sampled, we speculate that the significantly depleted oxygen isotope source values in atmospheric CO_2 are likely due to a multiple distillation process, possibly of anthropogenic origins.

about -105 ‰ to -57 ‰ VPDB-CO2. This range of the derived source values for CO_2 measured at ETL marked by disagrees both with the $\delta^{18}Os$ values for CO_2 emitted from fossil fuels in Canada (around –17 ‰ VPDB-CO2, unpublished data from *L. Huang*) and with common ranges of oxygen isotope compositions in different fossil fuel types reported in *Pataki et al.* [2006]. In addition, the

mean value of the δ^{18}Os at about -78 ‰ VPDB-CO2 is much more depleted than CO_2 that would have equilibrated with the oxygen isotope in local meteoric water discussed in Section 3.1. The CO_2 hydrated with meteoric water should have δ^{18}Os values to reflect oxygen isotope ratios in precipitation resented in Figure 4 [*Miller et al.*, 1999; *Flanagan et al.*, 1999; *Mortazavi et al.*, 2004].

As a first order attempt to propose a plausible explanation for the observed source values of δ^{18}O, we implemented different approaches from Keeling plot methods. The result summarized in the Table 1 suggests that the much more depleted δ^{18}Os values cannot be an artifact of mathematical formulations or of linear regressions.

We hypothesize that the source water underwent distillation processes that severely depleted ^{18}O in water vapor before it condensed in ambient air, then atmospheric CO_2 experienced hydration by the isotopically altered water. This hypothesis appears bold, nonetheless, is a technical analogue to transpiration processes taking place in plant stomata or Rayleigh processes in natural systems such as clouds [*Hoefs*, 2009]. The fractionation of oxygen isotopes in water during the steam-condensation processes can be modeled with the Rayleigh equation:

Equation 6

$$\frac{R_V}{R_{V0}} = f^{\alpha-1}$$

where R_{V0} is the isotope ratio of initial bulk composition, and R_V is the instantaneous ratio of remaining vapor. The fractionation factor α for the oxygen isotopes between water and water vapor is dependent on temperature and is obtained from experimentally determined values in literature [*Merlivat et al.*, 1963; *Majoube*, 1971]. Assuming hypothetical distillations utilize local meteoric water as inputs and the source water experienced extreme distillation at temperature gradients ranging from near the critical temperature of 350 ºC to the temperature of 40 ºC, the oxygen isotope ratio in

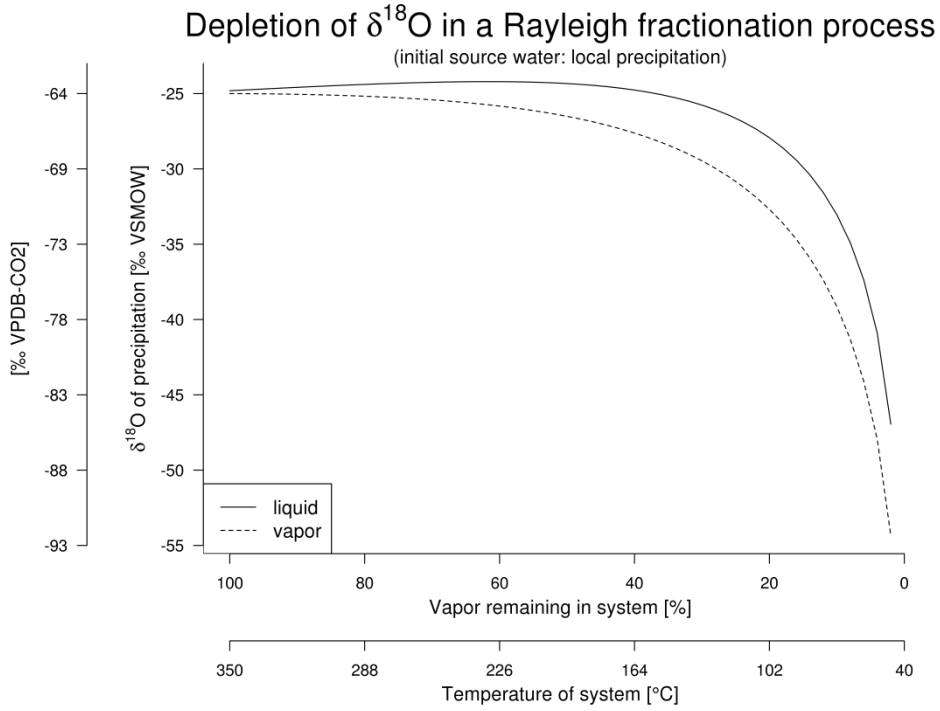

Figure 8 Derivation of $\delta^{18}O$ values due to hypothetical distillation of water. Using the winter time $\delta^{18}O$ values as source water and boiling it to near critical temperature of 350 degree Celsius, then completely condensing vapor into liquid, $\delta^{18}O$ values in liquid-phase water at the end of condensation processes reaches to about -55 ‰ VSMOW. The $\delta^{18}O$ value in water vapor near the end of the process is found more depleted by about 10 ‰ than liquid water. This Rayleigh model shows a possible course of isotopic depletion of $\delta^{18}O$ of H_2O in a closed system. If multiple distillation processes were assumed, the $\delta^{18}O$ values in the end products (i.e., vapor or liquid) would be much more depleted. It is contemplated that processed water had a time to be in equilibrium with atmospheric CO_2

the liquid-phase water at the end of the process can reach at about -55 ‰ while water vapor gets more depleted by about 10 ‰, as illustrated in Figure 6. If atmospheric CO_2 is hydrated with the water condensed from this hypothetical steam, it provides a plausible explanation to some of the less depleted $\delta^{18}Os$ values shown in Figure 5. We emphasize again that this modeling of water isotopes during the hypothetical distillation assumes ideal conditions for Rayleigh processes, in that fractionation depends solely on temperature changes; thus, when a change in fractionation occurs,

calculated $\delta^{18}O$ values will consequently be affected. For example, if some portion of the used water re-enters into boilers for increased efficiency of water consumption and any other portion finds its way out to the natural environment, the oxygen isotope source values would become even more depleted than the value calculated with conditions assumed for the Rayleigh model to produce Figure 6.

Industrial-scale uses of boilers to supply steam and hot water to merchandise productions, for example, are known to involve multiple distillation processes. A couple anthropogenic activities can be listed as significantly potential sources of the much more depleted $\delta^{18}O$ of water that made contact with atmospheric CO_2 on its way of atmospheric movements. For instance, pulp processing depends on continuous water supplies from local wells and surface water systems, and it involves distillation of water for purification purposes as well as material preparation and pulp washing. Another example of anthropogenic distillation of water includes oil sands development that are known to be water intensive where the extracting of bitumen primarily depend on industrial scale steam generators producing hot water and steam gases. Hot water is used to recover bitumen oils during mining, and steam is used mostly in drilling (in-situ) operations such as Steam-Assisted Gravity Drainage [*Shah et al.*, 2010; *Canadian Association of Petroleum Producers*, 2012; Appendix E]. Canada's oil sands industry is clustered around 800 km upwind direction from ETL, and the reported fresh water usage by oil sands producers in 2011 was approximately 158 million m^3 [*Canadian Association of Petroleum Producers*, 2012]. The reported amount of water usage sums up consumption of water for mining and drilling activities that directly involve hot water or steam, which is less than the volume of the total process water that actually ends up in tailing [*Alberta Environment and Sustainable Resources Development*, 2013]. Nonetheless, based on publically available data, the yearly water usage that goes through phase changes during oil sands operations equals nearly to that of 175 Olympic-size swimming pools every day for a year, the amount of water is considered to be

significant enough to leave imprints on the isotopic ratios of fresh water in regional hydrometeorologic cycles. It is reported that oil sands producers recycle about 90% of water that they have utilized [*Alberta Environment and Sustainable Resource Development*, 2013].

2.4 Conclusions

In this study, the $\delta^{13}C$ and $\delta^{18}O$ of atmospheric CO_2 measured at a Canadian Greenhouse Gas Monitoring station in a boreal forest are described in terms of the observed seasonal characteristics over the sampling period. Also, we utilized the Keeling plot methods to study contributing sources of atmospheric CO_2 observed at the remote site in relation to changes in its stable isotope ratios. The results from the extensive atmospheric measurement of CO_2 with isotopic analysis for samples collected at ETL confirms that CO_2 cycles observed at the site change in concert with what is expected from the global trend of accumulating CO_2 as well as regional contributions of the greenhouse gas. Key findings of this study can be summarized as following:

1) CO_2 mixing ratios measured on a weekly basis since October 2005 until December 2010 indicate that seasonal variations of the greenhouse gas exist in concert with the trend of larger spatial scales, and fluctuations of the mixing ratio of CO_2 near the surface during winter seasons are noticeable.
2) Observed $\delta^{13}C$ values almost mirrors seasonal variations of CO_2 concentration, while $\delta^{18}O$ values were scattered to a wider range likely due to its coupling with regional hydrologic cycles.
3) The traditional Keeling plot method combined with the Ordinary Least Square regression provides the best fitting of the given dataset for derivation of isotopic source values.
4) Vertical profiles of measurements for CO_2, $\delta^{13}C$ and $\delta^{18}O$, along with isotope source values (namely $\delta^{13}Cs$ and $\delta^{18}Os$) suggest that active vegetation takes up atmospheric CO_2 during

growing seasons, and fossil fuel influences drive increase in CO_2 concentration during winter seasons.

5) Extremely depleted δ^{18}Os values are derived, which is an intriguing feature by itself. These values imply water that hydrated atmospheric CO_2 observed at the remote boreal site may have undergone significant distillation processes by manufacturing-scale boilers, for example, being used for steam generation processes during industrial operations.

These findings can serve as a starting point for comprehensive monitoring and modeling studies for improving current understanding on carbon and water cycles in northern ecosystems where higher degree of vulnerability from the projected global changes are to impact the region substantially [*Fischlin et al.*, 2007]. As ecosystems and species in boreal regions are likely to undertake a wide range of disturbances associated with climate changes and increasing human activities, interests in studying changes of structure and functioning of the cold region ecosystems will further develop. The method described here can potentially provide critical information in this aspect. As demonstrated in this study, atmospheric CO_2 and its isotope measurements can well be utilized in studies to trace movements of carbon stocks in terrestrial ecosystems in relation with shifts in hydrologic regimes.

2.4.1 Outlook

Keeling plots in this study are constructed using a set of profile data collected at multiple heights above the ground, and air samples in each profile collected below and above the atmospheric boundary layer (ABL) are used in equal weighting for deriving isotopic source values. This treatment of equal weighting between below and above ABL is based on a conception that a profile represents a hypothetical blob of air. Such conceptualization might seem puzzling as the top of ABL acts like a bounding surface that limits free shuffling of fluids above and below it, raising a question to some regarding the well-mixedness assumption of mixing models. However, we learn that atmospheric

constituents mingle over time and space, so its elements become ultimately homogenized, while the total mass of a system is conserved. As long as the mass is conserved, the Keeling plot approaches can be effective to balance the mass and trace the degree of mixing of CO_2 in the atmosphere. Highly correlating CO_2 with its isotopic values within a profile assures that the samples can represent a uniform mixture in terms of the relationship between CO_2 and its stable isotope ratios. This study adopt to utilize a vertical profile measurement, the degree of mixing imprinted with the stable isotope ratios of CO_2 at different heights from a profile may differ, but each profile that shows strong correlations can be utilized to derive its source values.

Profiles having R^2 values less than 0.70 are excluded from the Keeling plot analysis. This strict exclusion significantly reduces the number of available samples in particular for evaluating the seasonal cycle of δ^{18}Os which is closely linked to hydrologic cycles. In order to extend the findings presented in our study to assist future studies in improving confidence in current knowledge on the carbon budgets in the northern eco-regions where many of fundamental elements of biological-climatological-hydrological system are poorly quantified, where appropriate, results from the Keeling plot approaches presented here are anticipated to be evaluated with alternative methods. Potential alternative approaches to derive more temporally continuous seasonal cycle of δ^{18}Os include as following: another configuration of Keeling plot method that allows explicitly prescribing background condition of oxygen isotope ratios in derivation of isotopic source values [*Ballantyne et al.*, 2010]; utilizing numerical simulations, for example, similar to previous studies by *Ciais et al.*, [1997]; directly modeling isotope fluxes from sources as well as spatial extent of mixing processes as observed at a given measurement location in the atmosphere. The third approach has potential to result in outcomes as valuable as contributions from previously implemented research methods because the hybrid modeling approach attempts to assess not only sensitivity of Keeling plot results by imposing robust backgrounds but spatial representativeness of source values derived with Keeling

plot approaches. Thus,a seeking the third approach has a high potential to lay out a way forward to scaling-up existing measurement results for applications to ecosystem or continental scale studies.

Chapter 3
Quantification of source influences on CO_2 variations

Rapidly increasing concentrations of greenhouse gases (GHG) in the atmosphere is the dominant factor in the warming of the climate in recent decades [*Solomon et al.*, 2007]. Various studies on atmospheric CO_2 have played a key role in assessing spatial and temporal variation of greenhouse gas emissions over global scales. In addition to ground-based measurements that provide long term CO_2 records [*Conway et al.*, 1994; *Keeling et al.*, 1995], in recent years satellite measurements of CO_2 have enhanced capabilities [*Hungershoefer et al.*, 2010]. Since the response of the global carbon cycle to fossil fuel emissions will determine the relationship between anthropogenic perturbations and atmospheric concentrations in the context of Kyoto-like treaties, such monitoring and flux constraints have substantial policy importance. Despite recent achievements in measurement techniques, however, the current level of scientific understanding to CO_2 cycles in the atmosphere is distant from the level to assist robust decision making, particularly for monitoring greenhouse gas budges in regional scales for which mitigation strategies to changing climate are developed and implemented.

Data assimilation and inverse modeling of atmospheric CO_2 observations have emerged as a particularly useful means to better quantify regional scale CO_2 sources and sinks. In this context, sophisticated data assimilation systems are currently being developed at major research centers. For example, in the United States, NASA initiated in 2010 the Carbon Monitoring Study (http://carbon.nasa.gov/) while NOAA in parallel has been improving the Carbon Tracker model (http://www.esrl.noaa.gov/gmd/ccgg/carbontracker/), a system that tracks the uptake and release of carbon dioxide at the Earth's surface. In the European Union, the Monitoring Atmospheric Composition and Climate project (http://www.gmes-atmosphere.eu/) has been developing to provide data for monitoring present conditions and forecasting the distribution of key atmospheric constituents for a few days ahead. In Canada, Environment Canada (EC) has been constructing a

carbon assimilation system (EC-CAS) that will provide flux estimates in near-real time to quantify carbon fluxes and to help Canadian stakeholders make more informed decisions regarding management of carbon sources and sinks.

To ensure that the EC-CAS system remains at the forefront of the carbon assimilation field, while the assimilation system is being developed and tested, this study has leveraged on-going work with the STILT model at University of Waterloo to obtain immediate insights into the utility of the existing measurement data that can be assimilated by the system and to guide the development of EC-CAS. In particular, this chapter attempts to understand the atmospheric impacts of the oil sands operations as observed by the long-term measurements of multiple trace gases available at a Canadian Greenhouse Monitoring Network site. In this regards, a novel approach is demonstrated to provide top-down constraints on emission estimates of greenhouse gases from oil sands operations, based on a receptor-oriented modeling approach.

3.1 Methods: a receptor-oriented modeling approach

3.1.1 The receptor at East Trout Lake

Atmospheric trace gas measurements using instruments with calibration standards traceable to international requirements are available at the receptor: the East Trout Lake site (54.35°N, 104.98°W; ETL). ETL is located in the northern boreal forest of Saskatchewan (Figure 1), and the measurement site has been serving as one of the Canadian Greenhouse Gas Measurement Program since its establishment in October 2005 [*Shashkov et al.*, 2007]. Precise measurements of greenhouse gas species took place on a weekly basis by stationed automatic flask samplers which receive airflows from inlets installed at two different heights (22 meter and 100 meter above ground level) on a 105 meter tall tower [*Huang and Worthy*, 2003]. The greenhouse gas species analyzed from each flask samples include CH_4, N_2O, CO, CO_2 and its stable isotopologues (i.e., ^{13}C of CO_2 and ^{18}O of CO_2).

The air samples are filled in two-liter flasks twice a sampling day at 09 and 21 UTC (03 and 15 Local Time) by an automated sampler in the ground station, subject to instrument maintenance needs and weather conditions. These flasks are then shipped to an Environment Canada's laboratory in Toronto, Canada for intended analysis of the greenhouse gas species and the stable isotopes [*Huang and Worthy*, 2005]. The same GHG species, but not the stable isotopes of CO_2, are measured continuously in-situ using a non-dispersive infrared method [*Worthy et al.*, 1998], and these gas measurements for the same species are used to complement one another as well as to serve as a cross-check on data quality. Isotopic measurements of CO_2 by Environment Canada are meticulously carried out and thus are comparable with independent measurements from leading isotope laboratories around the world [*Huang et al.*, 2013].

The measurement efforts are integrated with the climate process research and carbon and water cycles, as well as aerosol studies at the Canadian Aerosol Baseline Measurement Program. Thanks to the comprehensive observation program run at the ETL site, total of 110 Volatile Organic Compound (VOC) species are also analyzed from separate canister samples that are collected weekly at the ETL station [*Wang and Austin*, 2006].

Vertical profiles of measurements for the same greenhouse gas species and several halocarbon species are accomplished by aircraft sampling administrated by NOAA's Earth System Research Laboratory [*Tans et al., 1996; Montzka et al., 1993*]. NOAA's ESRL takes aircraft sampling of the same greenhouse gas species over ETL through collaborative efforts with Environment Canada since October 2005. The flights have been configured to collect air sample at multiple altitudes, which can be combined to line up with the tower measurements as a vertical profile. The air samples are filled in a programmable flask package (PFP; http://www.esrl.noaa.gov/gmd/ccgg/aircraft/packages.html) that consists of 12-pack 0.7-liter flasks. Each of these flasks collects air samples at a different altitude during a flight routine where the

Table 2 Measurements data available at the receptor site, East Trout Lake. Major greenhouse gases are routinely sampled and analyzed in concert with multiple research units and institutes to produce high quality data.

Species	Sampling frequency	Sampling records
Carbon dioxide (CO_2)	Hourly in-situ	2003 – present
Methane (CH_4)	Hourly in-situ	2002 – present
Carbon Monoxide (CO)	Hourly in-situ	2002 – present
Nitrous oxide (N_2O)	Hourly in-situ	2002 – present
Sulphur hexafluoride (SF_6)	Hourly in-situ	2002 – present
CO_2, CH_4, CO, N_2O, SF_6, and H_2	Weekly flask	2005 – present*
^{13}C and ^{18}O in CO_2	Weekly flask	2005 – present*
Volatile Organic Compounds (VOC)	Weekly canister	2007 – present

* Note: ground sampling (22 and 100 meter above surface) by Environment Canada at a tall tower ceased at the end of calendar year 2010, but aircraft measurements by NOAA are ongoing.

aircraft flies to change its navigating altitudes from about 600 meter to 7800 meter above sea level. The 12-pack flask packages are then sent to NOAA ESRL's Global Monitoring Division in Boulder, Colorado for analyses of numerous gas species, as well as being sent to the stable isotopes laboratory at the Institute of Arctic and Alpine Research in University of Colorado at Boulder for CO_2 and its stable isotope analyses.

As a result of the measurement design described above, the ETL site may provide up to 14 vertical samples of atmospheric constituents covering ~7 km above ground level each sampling day. While presenting various aspects in other chemical compositions of the observed atmosphere,

Table 3 Volatile organic compounds considered for correlation with CO_2. The VOC tracers are chosen based on findings presented in *Simpson et al.* [2010] and *Simpson et al.* [2013].

Compound		Chemical characteristics	Lifetime*
Benzene	Aromatics	Increased chemical stability	~ 10 day
Toluene			~ 3 day
Propane	Alkane	Open-chain hydrocarbons C_nH_{2n+2} as methane	~ 11 day
Heptane			~ 2 day
Butane			~ 5 day
Methylcyclohexane			~ 2 day

*based on loss from reaction with constant OH,
assuming 12-h daytime OH radical concentration of 2.0x10 mol·cm^{-3}

we focus for brevity's sake the data analysis on samples of CH_4, CO, CO_2, and several VOC species (i.e., propane (C_3H_8), methylcyclohexane (C_7H_{14}), heptane (C_7H_{16}), butane (C_4H_{10}), benzene (C_6H_6), toluene (CH_3), and acetylene (C_2H_2). These hydrocarbon species are identified by earlier studies as petro-chemical (e.g., oil sands mining or upgrading) tracers exhibiting high concentration enhancements adjacent to the oil sands facilities in Alberta, Canada [*Simpson et al.*, 2010; *Simpson et al.*, 2012; *Simpson et al.*, 2013]. More detailed accounts on variability of CO_2 and its stable isotope ratios are provided elsewhere (*see* Chapter 2). The atmospheric N_2O, another important greenhouse gas species, is not considered here for its primary loss takes place in the stratosphere, whereas CO_2, CO, and CH_4 have sinks in the lower troposphere where atmosphere-land interactions play significant roles. The approximate life-times of major species of VOC considered in this study are summarized in Table 3.

3.1.2 The transport modeling using STILT

The transport model that will be used in this study is the Stochastic Time-Inverted Lagrangian Transport model (STILT, [*Lin et al.*, 2003]).

An air parcel integrates surface fluxes during transport pathway. Thus, atmospheric transport can link scalar sources and sinks with concentration changes in a location. This principle has been successfully utilized to develop inverse models to estimate carbon fluxes. The first major carbon inversion paper at regional scale was provided by *Gerbig et al.* [2003] using a receptor-oriented approach, also using the STILT model. The paper underlined several potentials that future improvements in regional inverse modeling can present to science community, such as advances in representing biosphere-atmosphere gas exchanges in computer models and convective transport modeling. Several other studies [*Peylin et al.*, 2005; *Peters et al.*, 2007; *Deng et al.*, 2007] contributed to further sophistication of Lagrangian approaches with focus on various spatial scales. The research framework of this study has drawn upon techniques and suggestions from those previous inversion studies. The aim of the regional scale transport modeling of current research is to investigate and quantify emission sources of the atmospheric CO_2 measured at ETL.

The Lagrangian particle dispersion modeling approach to derive information on influence of upwind source on tracer concentration changes at receptor has multiple advantages. Firstly, Lagrangian atmospheric models track the air parcels in the moving references, and meteorological fields including winds can be interpolated down to the exact location of a measurement. Because Lagrangian models are known to have minimal numerical diffusion and better at preserving tracer gradients at smaller spatial scales than can Eulerian counterparts [*Lin et al.*, 2011; *Hegarty et al.*, 2013], less atmospheric transport errors are anticipated with the Lagrangian framework. In addition, numerically stable Lagrangian integration allows bigger time steps. This results in efficiently constrained concentration gradients of tracers over the time and space during numerical simulations.

Secondly, by running Lagrangian models backward in time, researchers can establish back-trajectories that reveal the source regions of the observed atmospheric species [*Hegarty et al.*, 2013].

Most Lagrangian models such as the STILT model extract footprint information from assimilated meteorological data. The footprint is similar to the adjoint of an Eulerian transport model: each footprint element is equivalent to the sensitivity of the concentration at a given receptor location with respect to a unit change in surface fluxes. The fact that the model runs backward in time also results in computational efficiency, because a single model run can extract spatially and temporally resolved footprints for emissions at numerous time steps before arrival at the receptor [*Gerbig et al.,* 2003].

Thirdly, the representation of influence with particle distributions minimizes representation errors, since the volume of the atmosphere represented by the particles at the time of the measurement is infinitesimal [*Lin and Gerbig,* 2005]. An ensemble of particles released at a receptor simulates transports of air parcels backward in time. In STILT, modeling turbulent transport is accomplished through the ensemble of stochastically transported particles, which more closely approximates the nature of air parcel movements than typical diffusion coefficients.

3.1.2.1 Model descriptions: initialization and background CO_2

The STILT model was driven by North American Regional Reanalysis (NARR) meteorology [*Mesinger et al.*, 2006], which has been developed and applied toward regional scale tracer modeling purposes [*Lin et al.*, 2003; *Kort et al.*, 2008; *Wen et al.*, 2012]. Using the reliable meteorological inputs, STILT ran backward in time with 3,000 particles released from the receptor at ETL. The ensemble of particles represents air parcels that STILT transports by mean winds and sub-grid turbulences provided from the regional scale meteorology modeling system. Since density of particles deployed over a certain spatial scale is directly related to the sensitivity of receptor to source influences, an infinite number of particles would be ideal for the best possible simulation result.

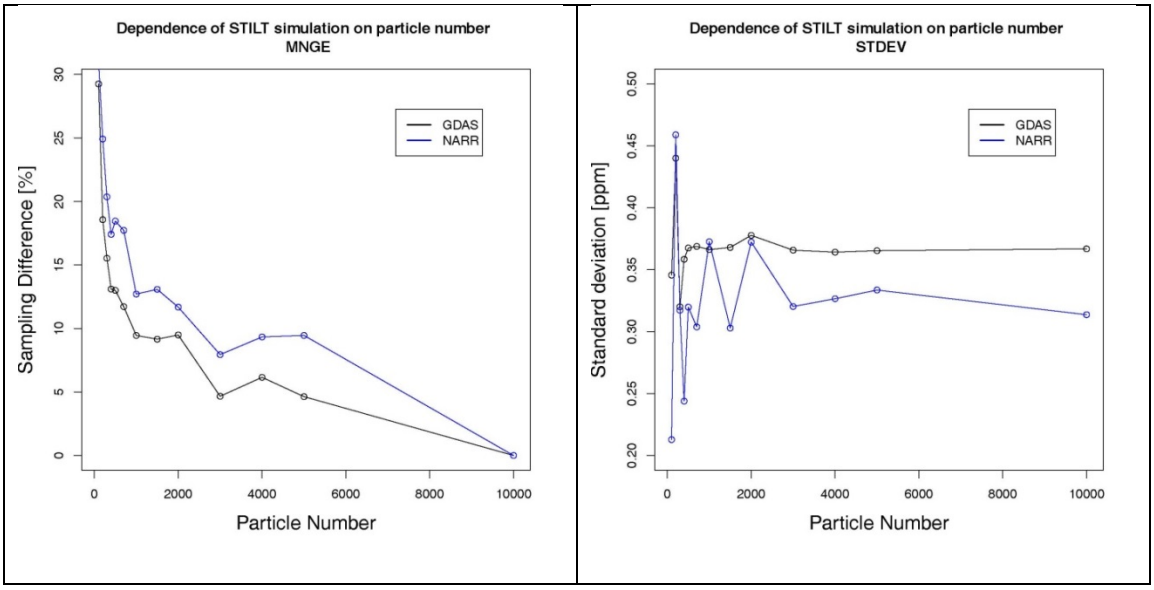

Figure 9 Sensitivity of the number of particles used in transport simulations to CO_2 mixing ratios. The metrics includes Mean Normalized Gross Error (MNGE, left) and Standard Deviation (STDEV, right). Assuming 10,000 particles represent ideally perfect transport, both the MNGE and STDEV converge to their relative minimal errors when 3,000 particles were used. Because using larger number particles costs more to computing, it is commonly recommended to weigh benefits and costs of the number of particles to be employed for a Lagrangian study. An ensemble of 3,000 particles is used to ensure reliability of simulated transport properties for species at optimal computing cost. The meteorology from North American Regional Reanalysis model is used to derive trajectories from STILT runs that are analyzed in this study.

However, considering the computing cost, sensitivity test results suggest that the particle number of 100 transported for 5 days can be an optimal choice for regional scale greenhouse gas modeling purposes [*Kort et al.*, 2008], and 3,000 particles simulated almost 'true' transport condition for chemically active tracers [*Wen et al.*, 2012].

Here in this study, since we are also dealing with several VOC, which display more localized emissions, we adopt 3,000 particles based on the sensitivity test results (Figure 9). This particle number has proven to be reasonable in simulating transport chemically active atmospheric tracers, as found by *Wen et al.*, [2012]. Chemical modules built in STILT to simulate reactions affecting

concentrations of "active" tracers during atmospheric transports are not enabled for this study. This means that VOC being considered in this study are effectively passive and simulated in the same way as CO_2 (refer to Table 3).

The distribution of CO_2 in the atmosphere is governed by processes that affect sources and sinks at the earth's surface, and by atmospheric transport. The NOAA Carbon Tracker model [*Peters et al.*, 2007] predicts distributions of atmospheric CO_2 mole-fractions at 3° longitude by 2° latitude global grid [*NOAA/ESRL*, 2011]. This model provides CO_2 mole-fractions over North America at the improved spatial resolution of 1° longitude by 1° latitude. The STILT model takes CO_2 mixing ratios from the Carbon Tracker grids that correspond to the particle locations at the end of its 5-day back-trajectories. This mixing ratios serve as background CO_2 that the air parcel initially have had before it travels over the source region. With initial concentration of tracers (C_{0p}) at the starting points of the trajectory (i.e., the end point of back-trajectory), integration of particles that carries information about C_{0p} and incremental CO_2 due to source emissions to the moving air parcel (ΔC_p) produces an ensemble of tracer concentrations for each time-step. Hence, researchers are able to estimate total concentration (C_p) at the receptor by using the relations expressed in Equation 7.

Equation 7

$$C(\mathbf{x}_r, t_r) = \frac{1}{N_{tot}} \sum_{p=1}^{N_{tot}} C_p(\mathbf{x}_r, t_r) = \frac{1}{N_{tot}} \sum_{p=1}^{N_{tot}} \left[\Delta C_p(\mathbf{x}_r, t_r) + C_{0p}(\mathbf{x}_r, t_r) \right]$$

For the receptor at ETL, the contributing source area to the observed variations of trace gas mixing ratios is determined by calculating the footprint. The footprint represents sensitivity of tracer mixing ratio to unit changes of surface fluxes, in the unit of [$ppm/(\mu mol \cdot m^{-2} \cdot sec^{-1})$]. Footprint values are calculated with numerous factors. For tracers as CO_2 that has significant sources and sinks near the surface, the planetary boundary layer (PBL) height is particularly important as it initially

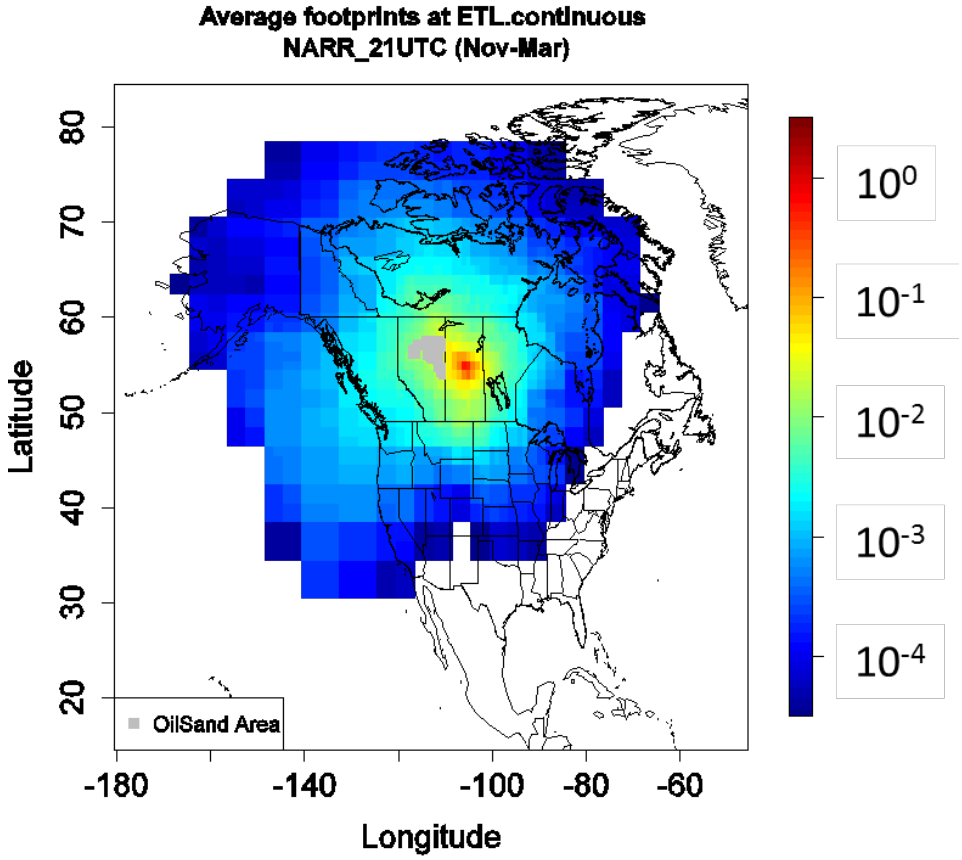

Figure 10 Potential source influences for trace species observed at the receptor site. The East Trout Lake measurement site appears at a 'hot spot' as presented with high "footprint" values. Having the unit of [*ppm*/(*μmol*·m^{-2}·sec^{-1})], footprint values quantify changes in concentration of a tracer modulated by unit changes in fluxes. Obviously, closer to the source area receives stronger influences from source regions, and mixing in the boundary layer is also an important function of footprint. ETL site is well located to monitor airflows coming from a wide range of source regions including the oil sands administration region depicted in grey polygon near the center of high footprint area.

determines the extent to which tracers emitted from surface get diluted by being transported upward. The residence time particles spent in PBL is also valuable parameter to determine the footprint [*Lin et al.*, 2003]. Since influence decays according to distances, fluxes closer to the receptor would influence concentrations more than fluxes from afar would. Thus, the sensitivity near the receptor

should be calculated at enhanced resolutions. In current study, the PBL heights during the course of atmospheric transport from the background to the receptor location are extracted from the meteorological inputs of NARR by the STILT model. Underlying uncertainties in different PBL schemes of the meteorological models and their impacts on transport modeling over North America are discussed by a few previous studies [*Lin and Gerbig*, 2005; *Kretschmer et al*, 2012] , and interested readers are invited to literature and references there in. As a result of combined influences from geographic distances, PBL dynamics and sampling sensitivities by particles released, values of the footprint vary significantly near the receptor, and the dynamic grid resolution changes to about 1 degree as the distance to ETL gets further (Figure 10). Distance to the oil sands area is less than 1,000 km away from the receptor at ETL, and the receptor oriented modeling framework provides varying degree of emission sensitivities relevant to oil sands emissions as shown with footprint values depicted in Figure 10.

3.2 Tracing oil sands signals observed at the receptor site

Alberta's oil sands are an important component of anthropogenic carbon emissions in Canada. With numerous in-situ production wells and refinement plants concentrated in the area, a typical oil sands operation will be a significant source of trace gases to the atmosphere (e.g., carbon dioxide, methane, particulate matter, and volatile organic compounds, and *etc*). Oil sands areas can be spatially well defined, but the land surface of the oil sands mining area is heterogeneous, and the physical properties (e.g., temperature, moisture, or land cover compositions) that influence the overlying atmosphere will be distinct from the surrounding. However, for simplicity the oil sands area will be considered to have nominal surface area sources and to be located in relatively open and homogeneous terrain.

3.2.1 Inventory estimates of CO_2 emission from the oil sands operations

Given the reported GHG emissions per year and the area of oil sands mining operations in the province of Alberta, the surface flux of CO_2 from the oil sands can be approximately 50 $\mu mol \cdot m^{-2} \cdot s^{-1}$. Typical CO_2 flux in an evergreen needle leaf forest is found at less than about 1 $\mu mol \cdot m^{-2} \cdot s^{-1}$ during winter and about – (4 ~ 7) $\mu mol \cdot m^{-2} \cdot s^{-1}$ during growing seasons on a daily basis [*Chen et al*., 2008]. Hence the oil sands flux estimated from inventory data appears to be a strong enough signal to be detected from atmospheric measurements although the value derived with the back-of-the-envelope approach is a rough estimate. Actual traceability of the signal depends on the locations and distance between the source and a receptor. For estimating the oil sands components of the emission, it is desirable to avoid growing seasons when plants take up large amounts of CO_2 from the atmosphere. As such, variation of the atmospheric CO_2 concentration due to vegetation is treated as noise to be removed in this study. To minimize contributions from photosynthesis, a boreal winter (November through the following year March) of the years 2005 ~ 2010 is selected as a study target period. The winter here is defined by months when monthly mean air temperature by Canadian Climate Normals fall below freezing (refer to Figure 6).

3.2.2 Signals at the measurement site of East Trout Lake

Midday mixing ratios of multiple tracers observed at 100 meter above the surface are presented in Figure 11. From the observation results, we first examine seasonal and inter-annual variability of the tracers between 2005 and 2010. The variability here is determined by perturbations that are sustained longer than timescales used in *Langenfelds et al.* [2002]. Low-pass smoothing curves of 4 months are applied used to determine seasonal variability (smoothed curve in Figure 11), and 1.8 years are used for inter-annual variability (trend curve in Figure 11). Prominent seasonal variations are depicted by smoothed curves for CO_2, CO, CH_4, and two other hydrocarbon species. For example, low mixing ratio of CO_2 corresponds to relatively higher CH_4 burden during summer months. This suggests that

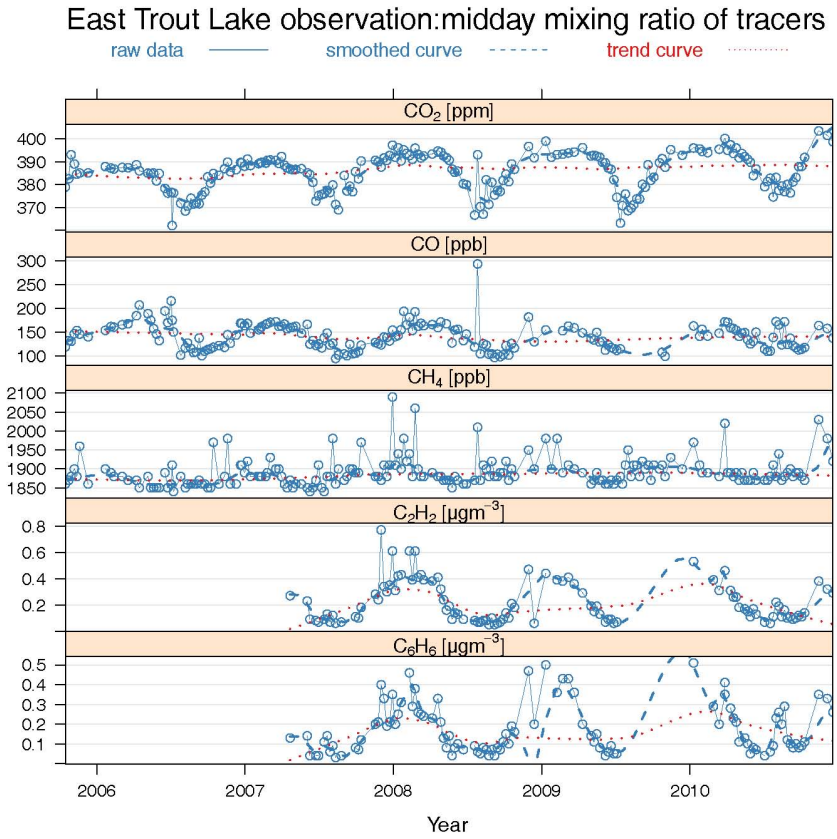

Figure 11 Mid-day mixing ratios of the selected tracers reveal interannual (trend curves; red dotted-lines) and seasonal (smoothed curves; blue dashed-lines) variations. The mixing ratio of atmospheric CO_2 measured at 100 meter above the surface level of ETL site displays an increasing trend as shown with a positive slope of the inter-annual trend curve (red dotted line). This accumulation of CO_2 in the atmosphere is in large part a manifestiation of a global trend shown with the zonal average curve in Figure 2. However, it is highly unlikely that CO_2 measurements at the remote boreal site (ETL) mostly reflect global background atmosphere considering a relatively high concentration of pollutants such as acetylene (C_2H_2)and benzene (C_6H_6) are also detected. In addition, STILT footprint suggests that air parcels arriving at ETL integrate a wide range of source areas including densely populated cities and industrial areas.

vegetation uptake of CO_2 by productive forests and methane emissions by warm wetlands modulate the opposite fluxes of the atmospheric constituents.

The atmospheric CO_2 concentration measured at ETL reveals dynamic seasonal variations. As shown in Figure 2 as well as in Figure 11, the peak value of individual CO_2 during the entire time

period is measured at 403.56 ppm in November 2010, the lowest being at 365.08 ppm in July 2008. Lower concentration values are found in summer months when vegetation near the measurement site is actively sequestering CO_2 for biological production while higher values are in winter when the vegetation is mostly dormant, resulting in the greenhouse gas to accumulate in the atmosphere. Indeed, the daily mean CO_2 concentrations represented as dots in Figure 11 indicate clear increases in CO_2 concentrations, predominantly through the winter seasons.

Methane has been accumulating in concert with other tracer species with differing magnitudes of inter-annual fluctuations in mixing ratio values, as shown in trend curves represented by dotted, red lines in Figure 11. The annual growth rate calculated for methane during the 5 year period is 5.62 $ppb \cdot yr^{-1}$, comparable to the value from an independent study using satellite measurements for the northern hemisphere [*Schneising et al.*, 2011]. These authors observed methane growth rates of 7.5 ± 1.5 $ppb \cdot yr^{-1}$ since 2007, based on zonal averages of satellite measurements for northern hemispheric latitudes including the tropics where the leverage to the observed growth rate is relatively greater. A similar magnitude of methane growth rate is also reported in another independent study by *Dlugokencky et al*. [2009] where observed increases CH_4 in high latitudes are contributed to anomalous warming episodes in Arctic wetlands during year 2007. The growth rate for CO at ETL stayed near zero for the same measurement period. The CO_2 mixing ratio on the other hand has been increasing, particularly notable during winter months. The trend curve representing CO_2 inter-annual growth rates depicts noticeable accumulation of the greenhouse gas over the course of measurement period. The growth rate of CO_2 at ETL during 2005 to 2010 is about 1.60 $ppm \cdot yr^{-1}$. The CO_2 growth rate observed at a northern hemispheric background site (Mauna Loa) during the same period is around 2.07 $ppm \cdot yr^{-1}$ [*Dlugokencky ant Tans,* 2013; *Ballantyne et al.*, 2012]. The relatively slow growth rate of CO_2 observed at ETL can be explained by stagnant low CO_2 mixing ratio during

summer months, which amounts to significance of terrestrial uptakes by the boreal forests in the global CO_2 budget [*Ballantyne et al.*, 2012].

Is the accumulation of CO_2 and CH_4 observed at ETL revealing the global trend or is it more responding to changes in regional scale fluxes? In order to answer this question we investigate correlations between multiple trace gases, based on the fact that certain VOC species tends to represent localized emission processes. For example, since presence of benzene (C_6H_6) is indicative of exhaust gases in local sources, examining its relationship with CO_2 provides for discerning if given CO_2 originated from the local exhausts. Given the sources and sinks of atmospheric methane described in preceding paragraphs, it seems logical to start with an examination on relationships between mixing ratios of CH_4, CO, and CO_2 in terms of whether their seasonality agrees to common processes. All the available data from aircraft samples as well as ground measurements are used to examine relationships between methane and the other two greenhouse gases. The inter-relationship between CH_4:CO_2:CO is projected in a simple linear repression method, and the result of regression analysis is plotted in Figure 12. Grey dots in the figure indicate individual observations made at altitudes below 2 km a.g.l., and star marks data from winter months only. Winter months are defined here as November through next year March when monthly mean air temperature of the site falls below freezing, according to Canadian Climate Normals 2010. Using the CO_2 and CO mixing ratio, the predictability of CH_4 mixing ratio can be established as shown by the plane represented by grey mesh in Figure 12. Solid vertical lines in red colors indicate positive residuals from actual data points to the regression plane, and dashed blue lines indicate negative residuals.

The predictability for CH_4 mixing ratio provided by the regression with linear combination of CO_2 and CO suggests the three greenhouse gases are influenced by common processes in their path of lifecycles in the atmosphere. Despite that the residuals are considerably large, two groups of clustering in different parts of the regression plane seems deserving of attention. The two realm of

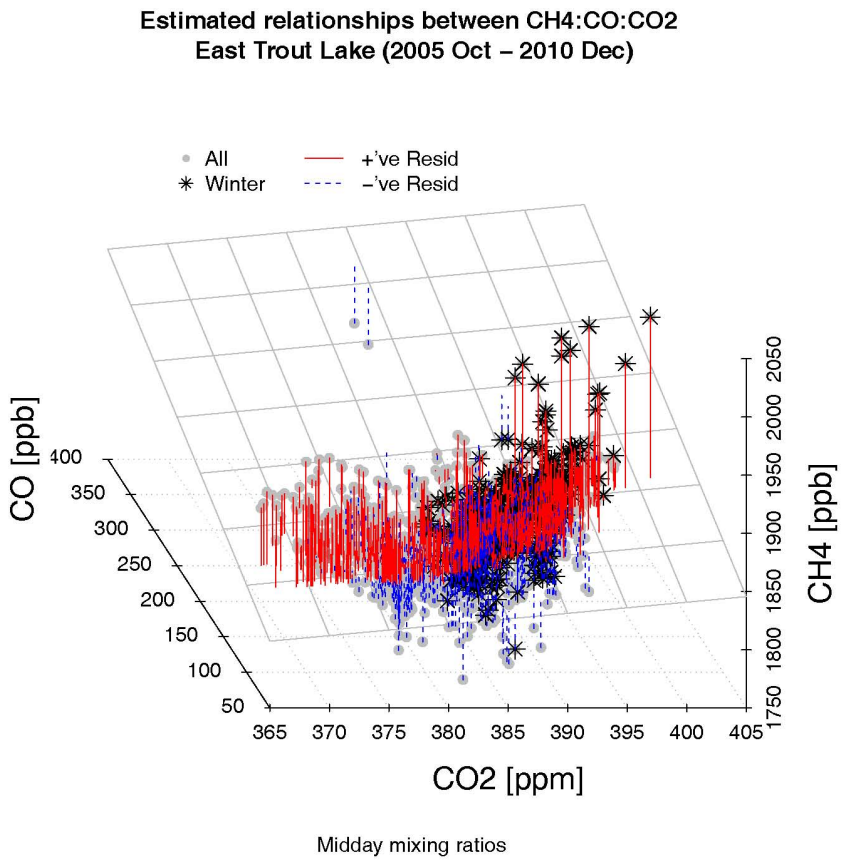

Figure 12 Mixing ratios of CO_2, CO, and CH_4 and their inter-relationships are depicted by regression analysis. The inter-relationship between the three tracers is projected in a simple linear repression plane, and the result of regression analysis is plotted as a grey mesh in Figure 12. Grey dots indicate individual observations made at altitudes below 2 km a.g.l., and star marks data from winter months only. Winter months are defined here as November through next year March when monthly mean air temperature of the site falls below freezing, according to Canadian Climate Normals 2010. Using the CO_2 and CO mixing ratio, the predictability of CH_4 mixing ratio can be established as shown by the regression plane represented by grey mesh in Figure 12. Solid vertical lines in red indicate positive residuals from actual data points to the regression plane, and dashed blue lines indicate negative residuals.

clustering appears in high-CH_4-low-CO_2 during summer when CO is lower and higher-CH_4-high-CO_2 during winter when CO is higher. If high methane episodes derive mainly from natural processes higher mixing ratio is expected during summer when emissions from natural sources are larger. On

Table 4 Molar ratios between species. VOC species measured at ETL shows oil and gas emissions signals that are reported in a previous study in the US. Measurement data at ETL for acetylene, benzene, and CO have very similar molar ratios to shale gas emissions from Colorado, USA. Oil sands emissions tends to more enriched in methane signals [*Simpson et al*., 2010], while many VOC species are simultaneously used for many different processes, making its emission signals discernable from other petroleum industry processes.

Species (y/x)	**Slope** (n=230)	**cf.**
C_3H_8/CH_4	13.66	0.095
$*C_6H_6/C_3H_8$	0.03	17.9
$*C_6H_6/CO$	1.57	1.82
$*C_2H_2/CO$	4.65	4.32
$*C_6H_6/*C_2H_2$	0.27	0.37
CH_4/CO	0.49	--
C_6H_6/CH_4	0.78	--

* denotes units in [ppt]; [ppb] used elsewhere.
cf. values are taken from Table 3 of *Pétron et al*. [2012]

the contrary, the methane mixing ratio observed in the lower troposphere shows higher values during winter months. In addition, low OH during cold seasons should affect other species such as CO, so neither the positive correlations between CH_4 and CO nor are increasing correlation coefficients for higher CH_4 during winter months (Figure 12) expected in a predominantly natural near the measurement site of ETL.

Based on its correlation with other tracers presented in Figure 12 as well as Tables 4 and Table 5, methane appears to have distinctive sources related to oil sands production facilities that support recovery efforts such as hydro-heating and thermal conversion. The correlation with the hydrocarbon species increases, when the oil sands influence represented by footprint is larger than the

Table 5 Correlation between CO_2 and different species. When oil sands influences are stronger than the median values ("big-Foot"), the linear correlation between CO_2 and other tracers, except N_2O and C_3H_8, increases

Species	Correlation coefficient (r)		
	All trajectories (all Footprint)	Selected trajectories (big-Foot)	% changes in correlation coefficient
CO	0.363	0.477	31.4
CH_4	0.586	0.643	9.7
N_2O	0.636	0.586	-7.8
SF_6	0.699	0.803	14.8
C_6H_6 (Benzene)	0.530	0.779	46.9
CH_3 (Toluene)	0.382	0.898	135.0
C_3H_8 (Propane)	0.704	0.658	-6.5
C_7H_{16} (Heptane)	0.653	0.791	21.1
C_4H_{10} (Butane)	0.789	0.878	11.2
C_7H_{14} (Methylcyclohexane)	0.798	0.919	15.1

median value (refer to 'big-Foot' columns in Table 5). The primary sources of propane are natural gas processing, petroleum refining, and gasoline exhausts. The correlation with propane changes little between different seasons. Acetylene is produced by partial combustion of methane, and the butanes are associated with evaporation of fossil fuels rather than combustive fossil fuel emissions. Thus the correlation between butane indicates leakages while acetylene correlation suggests combustions of natural gas. The correlation with acetylene decreases during winter months while correlation with butane increases. Presence of benzene and toluene are detected in highly polluted atmospheres such as near petroleum refineries, and rarely found at remote background sites.

Thus, correlations between CO:C_2H_2 and CO:C_6H_6 indicate the air parcels arriving at ETL have integrated emissions from petroleum industries. Also, increases in the correlation coefficients

under stronger oil sands influences suggest the oil sands region is likely one of the major emission sources of CO_2 measured at ETL.

3.3 Quantification of source influences

The transport history of air parcels arriving in East Trout Lake is determined using the STILT model with meteorological fields output from North American Regional Reanalysis data (NARR). The STILT simulation can be used to interpret source regions of the atmospheric tracers at a receptor. The East Trout Lake site is indeed at the downwind site relative to the oil sands (Figure 1 and Figure 10). Combination of particle locations and residence time of particles provides information that computes sensitivity areas which produces concentration changes of the tracers at the end of the trajectory. To determine the trajectories of air parcels arriving to the altitude of East Trout Lake measurement tower, 3,000 particles are released at 21UTC which translate to 3 pm local time and tracked for 5 days backward in time. The sensitivity of source areas that influenced CO_2 concentration changes at East Trout Lake are simulated through integration of 5 day footprint analysis. From the averaged footprint area presented in Figure 10, it seems that the oil sands are non-negligible contributor to variations of tracer concentration at the receptor location although the footprint is in general widely distributed.

3.3.1 Simulated CO_2 mixing ratio at the receptor

Simulating the CO_2 mixing ratio is accomplished by integrating background CO_2 and emissions that enhances the mixing ratio of CO_2 in air parcels that are transported to the receptor site. Background CO_2 mixing ratio is provided by Carbon Tracker 2010 when 3-D locations of background air are established by ensemble of particles that STILT simulates. In addition, NOAA ESRL's aircraft-based empirical boundary CO_2 for North America and GEOS-Chem model are used as supplementary information in order to test reliability of the background provided by Carbon Tracker and to bench mark the important of future EC-CAS products as potentially improved background CO_2 fields over

Canadian boreal ecosystems as well as over North America. Advection of air parcels is represented by trajectories and source influences to the advecting air is computed with the footprint the Largrangian model outputs (See 3.1.2 for details). The fossil fuel CO_2 contributions are obtained with emission inventories. With changes in trajectory, footprint provides useful information to determine transports of the trace gases in relation with how the source influences vary with time. Multiplication of sensitivity areas by emission fluxes results in concentration changes (ΔC_p) at each particle location. The fossil fuel CO_2 emission inventories that can be used include emission grids available through the Carbon Tracker which also provides 1 by 1 degree longitude and latitude fossil fuel flux as a NOAA's contribution to North American Carbon Program, or Emission Database of Global Atmospheric Research run by European Commission (EDGAR, http://themasites.pbl.nl/en/themasites/edgar/index.html).

Recently*, Oda and Maksyutov* [2011] developed a global annual fossil fuel CO_2 emission inventory with 1 km horizontal resolution for the last two decades. They used point source database and night-lights to construct the *a priori* to be used for flux inversion studies using GOSAT measurements, which this study utilizes. The Open-source Data Inventory of Anthropogenic CO_2 Emission (ODIAC) provides emissions at a selection of spatial resolutions with a seasonal cycle represented. In order to account for variability of per capita emissions in Canada, we apply 1º x 1º spatial scaling map to ODIAC emissions (Figure 13). The spatial scale factors contribute to reduction of systematic errors related to emissions from combustions and point sources [*Nassar et al.*, 2013].

The simulated CO_2 captures general trends of CO_2 mixing ratio observed at ETL (R^2=0.75; bias=-2.6 ppm), although the negative bias are particularly pronounced during times of relatively higher CO_2 mixing ratio, for example, around 400 ppm the discrepancy between observed and

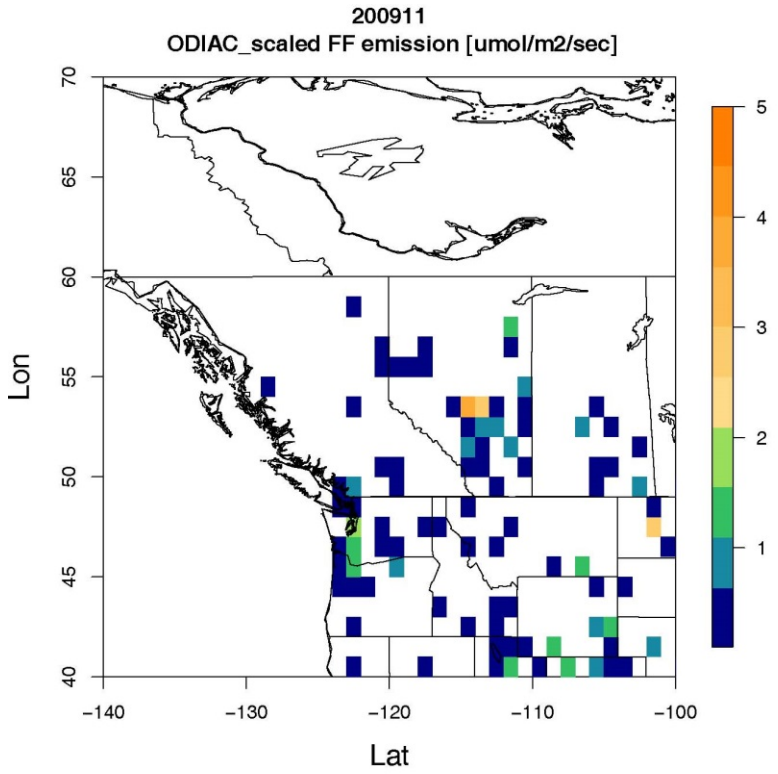

Figure 13 An example of ODIAC emission grid used in this study. This particular example shows fossil fuel emissions accounted for in the dataset in November of 2009. As ODIAC product is based on satellite measurement of night lights, it highlights urbanized areas and point sources such as power plants and mines. Temporal scaling factors are applied to ODIAC emissions, which effectively reduces biases in ODIAC emissions [*Nassar et al.*, 2013]. There are certain level of oil sands emissions depicted by ODIAC. To avoid "double-counting" of emission estimates, we mask out ODIAC emissions from oil sands grids.

simulated are larger than the average (Figure 14). Underestimation of CO_2 mixing ratio by the model suggests that there are sources that are missing in ODIAC fossil fuel emissions.

3.3.2 Simulating the excess-CO_2 and its uncertainties

Net changes in CO_2 (excess-CO_2) at the receptor defines the dCO_2, which is computed by subtracting out boundary values (initial location of trajectory) from the measured CO_2 mixing ratio. Most of excess-CO_2 values represented by grey circles in Figure 15 during winter time are positive,

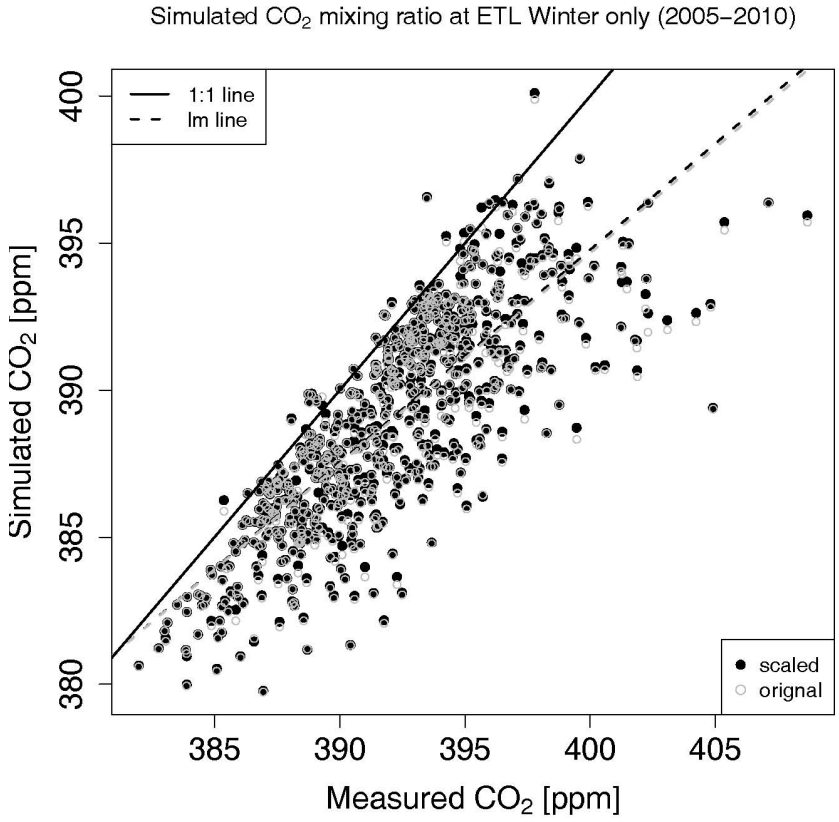

Figure 14 Simulated versus observed CO_2 mixing ratio at ETL. Simulated CO_2 is computed by integrating background CO_2 and emitted CO_2 over the course of trajectory. Emitted source contributions from ODIAC during trajectories are computed using the footprint function. Applying the scaling factors to ODIAC emissions reduces biases. The simulated CO_2 captures general trends of CO_2 mixing ratio observed at ETL, although the negative bias tend to exacerbates in the relatively higher CO_2 mixing ratio regimes, for example, around 400 ppm. Underestimation of CO_2 mixing ratio suggests that there are sources that are missing in ODIAC fossil fuel emissions.

meaning emissions elevate the atmospheric CO_2 at the ETL site above the boundary condition. However, with fossil fuel emissions by ODIAC ($ffCO_2$ represented by blue triangles in Figure 15), even after applying scaling factors to the emission inventory, the inventory explains only approximately 13% of total excess-CO_2 (dCO_2) observed at the receptor site.

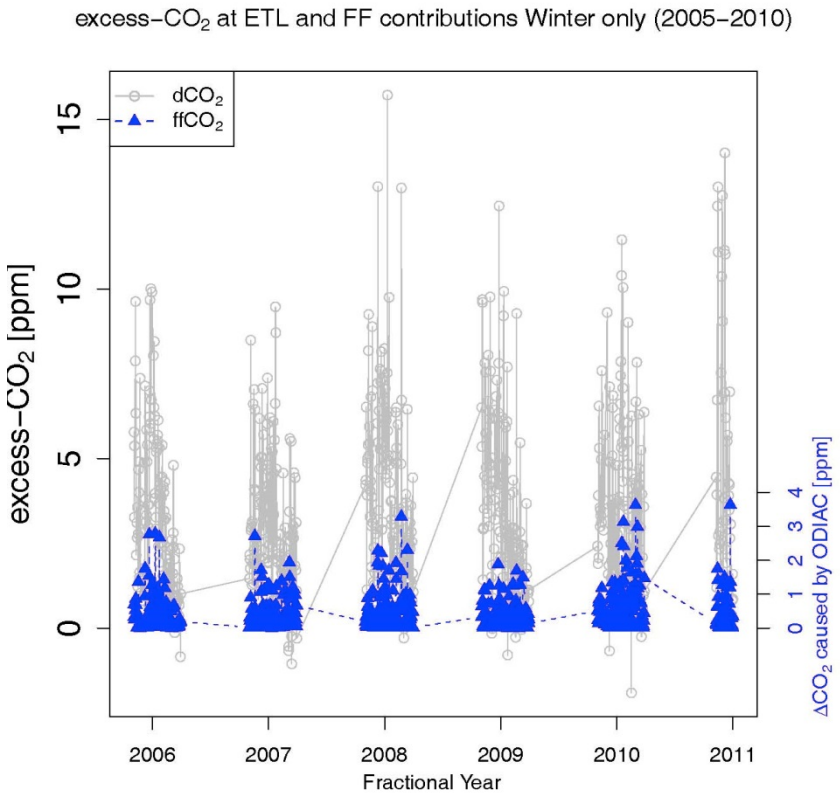

Figure 15 The net changes in CO_2 (excess-CO_2, dCO_2) observed at ETL. dCO_2 is calculated by subtracting background CO_2 provided by Carbon Tracker from the observed CO_2 mixing ratio at ETL. ΔCO_2 is a portion of excess-CO_2 caused by a particular source, for example, by ODIAC. ΔCO_2 caused by ODIAC represents fossil fuel emissions added to the air parcels over the course of trajectories. The scaling factors are applied to ODIAC emissions. Traditional fossil fuel emissions comprise about 13% of total CO_2 excess during the winter months.

We examined possible uncertainties in the boundary conditions adopted in current framework. Along with Carbon Tracker's CO_2 fields, additional background CO_2 values are introduced from an independent GEOS-Chem simulation carried out at the University of Toronto and from NOAA ESRL's empirical CO_2 background available for North American coast lines [*A. Andrews*, personal communication]. While Carbon Tracker provides 4-D (three spatial dimensions plus time-varying) CO_2 fields at 1º x 1º lon/lat which is fully available to entire time period of our

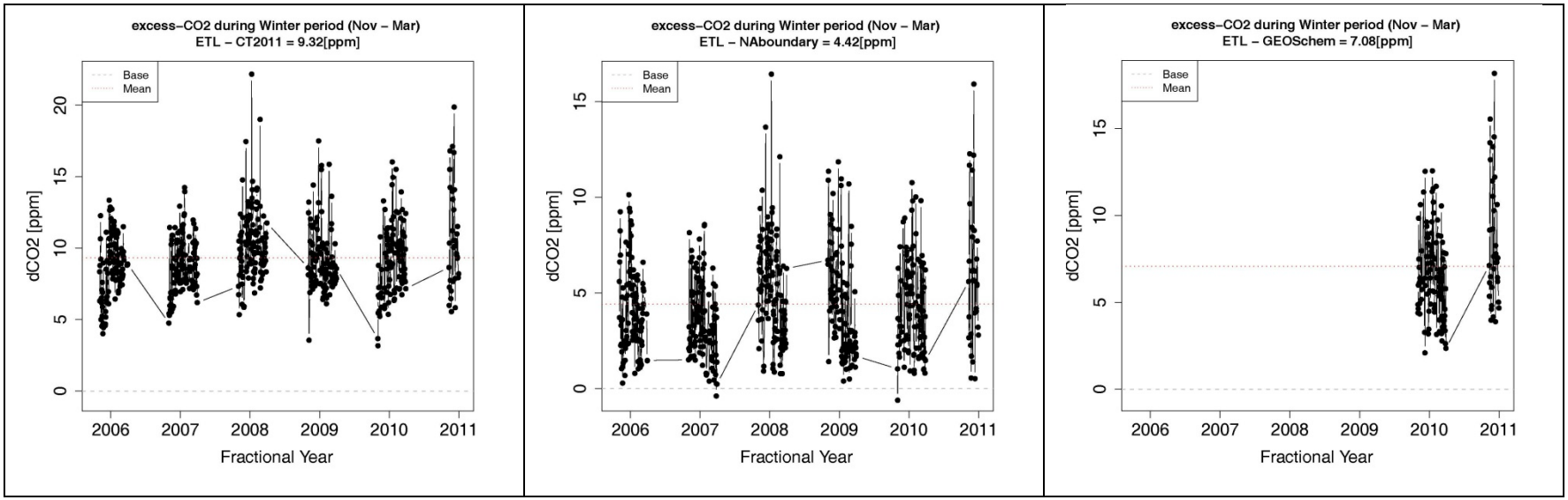

Figure 16 Discrepancies in simulated dCO_2 values depending on background values. Background CO_2 data can be obtained from NOAA's Carbon Tracker model (left), NOAA's measurement-based empirical data (center), or independent modeling with GEOS-Chem model (right). NOAA's data including Carbon Tracker model data and the empirical data are publically available for downloads, and GEOS-Chem model data was obtained through collaboration with University of Toronto through EC-CAS. Carbon Tracker tends to provide lower CO_2 mixing ratios at the background locations, thus resulting in larger dCO_2 values. Carbon Tracker provides data comes with relatively high spatio-temporal resolution in the available dataset that are easily accessible makes it as a reasonable choice of background data for carbon cycle studies. Its extensive number of user community is expected to provide an additional scrutiny to data quality.

interest, GEOS-Chem model supplies 4-D CO_2 fields at 5º x 4º lon/lat for limited time period from July 2009 until the end of calendar year 2010 when GOSAT provides effective constraints on model simulations at a coarse horizontal grids. The North American empirical dataset derive from NOAA ESRL's profile measurements and provides tracer concentrations that are linearly interpolated at Pacific and Atlantic coast lines of the continent, but not between the coast lines.

Significant discrepancies in dCO_2 arise when different background product are adopted as shown in Figure 16. Over the 5 year time period, Carbon Tracker suggests mean enhancement of CO_2 is about 9.3 ppm from the background while NOAA's empirical data results in about 4.4 ppm enhancements. When GEOS-Chem simulation results are used for backgrounds, its mean ΔCO_2 differs by more than 2 ppm in comparison to when using Carbon Tracker or NOAA's empirical products. It is difficult to determine in this study which background condition between the three products is more realistic and better represents the "true" values as the background conditions examined here derive from independent study designs and objectives. However, it seems intriguing to find such discrepancies in dCO_2 caused by different background conditions.

The endpoints of trajectories are the same, but the CO_2 concentrations at which the background locations are imposed may vary between three products. NOAA ESRL's measurement-based product is limited to specific longitudes and latitudes that approximate coastlines of the North American continent while Carbon Tracker and GEOS-Chem provide 3-D spatial gradient of CO_2 over the continent. This would lead to differences in the spatial extent dCO_2 represent. Also, the spatial resolutions at which models provide background CO_2 differ significantly. The difference in the spatial resolution at which CO_2 concentrations are provided affects the ensemble mean of CO_2 as determined by Equation 7. There also exists a temporal difference. The GEOS-Chem background CO_2 is available for only a single year, whereas background conditions from Carbon Tracker and NOAA ESRL's empirical product is available for 5 years.

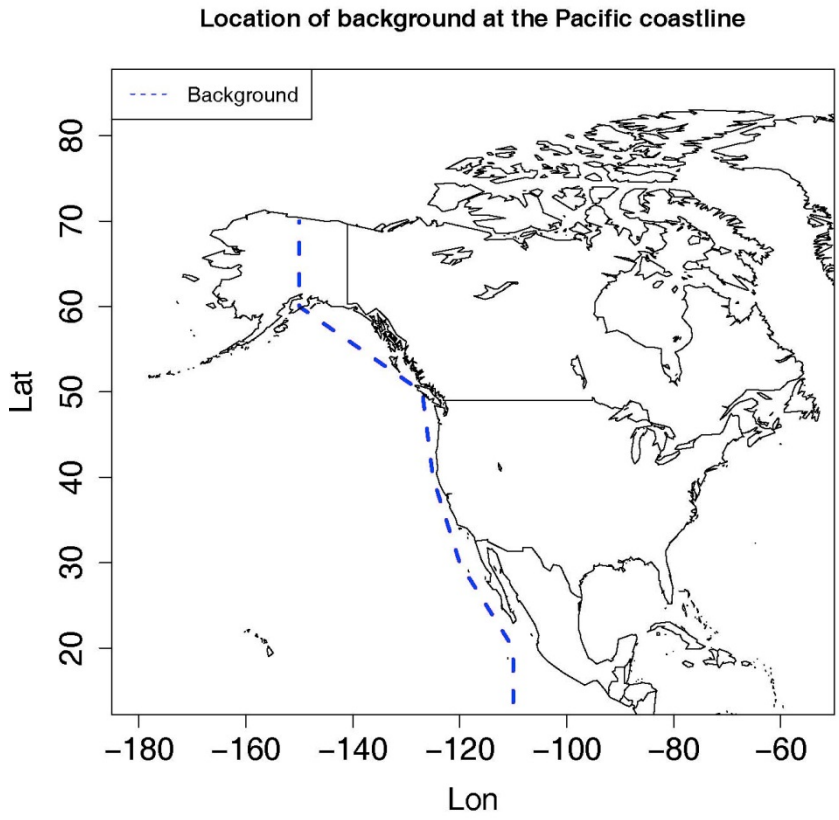

Figure 17 The location of background where CO_2 mixing ratio is initialized in STILT transport modeling is shown with a blue dashed line that is roughly parallel to Pacific coastline of North America. The boundary represents grids that NOAA ESRL's empirical product provides CO_2 background data for. The NOAA's empirical background data is constant to time and offers vertical profiles of CO_2 mixing ratio for the specified latitude and longitude of the background, thus it provides a 'curtain' of CO_2 mixing ratio at the locations represented by the blue dashed line.

To minimize possible systematic differences between the various backgrounds, we focus on the winter season of 2009/2010 when background information is available from all three products. In addition, we also limit the location of background to longitudes and latitudes that approximate the Pacific coastlines of North America (Figure 17). The differences in background CO_2 concentration at the same Pacific coastlines for the selected one winter season presented in Figure 18 seem to add

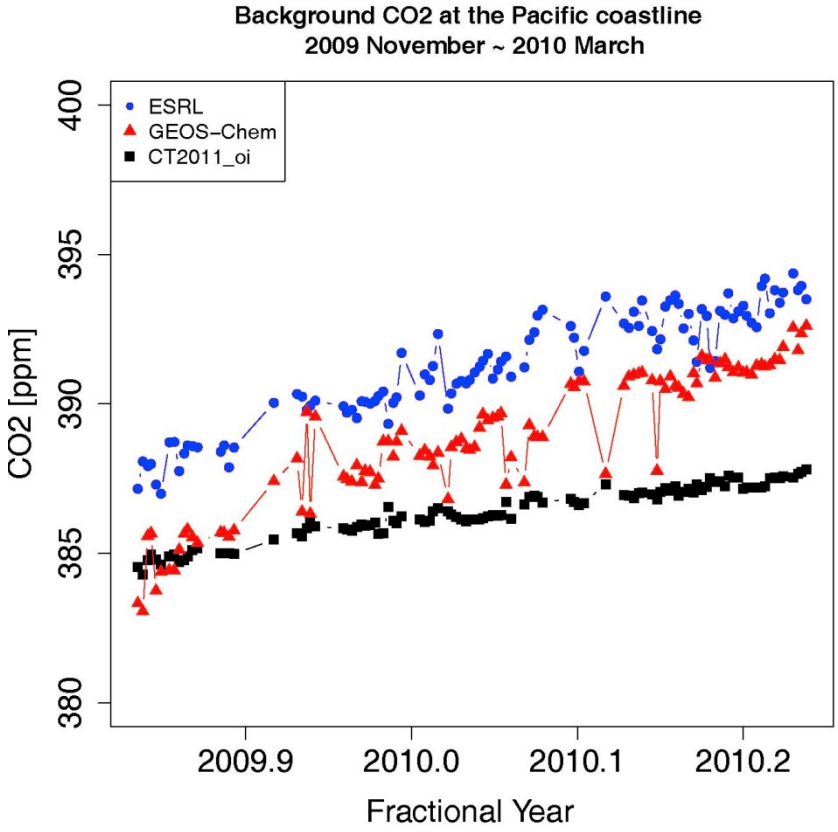

Figure 18 Background CO_2 compared at the same longitudes and latitudes. Variability of background CO_2 generally better agrees between NOAA ESRL's empirical product and GEOS-Chem model results. Background CO_2 concentration at the locations represented by Carbon Tracker are found generally lower than the background by the other two.

valuable comparisons between the background products. Firstly, NOAA ESRL's measurement product and GEOS-Chem generally better agree in terms of variability in background CO_2. Secondly, Carbon Tracker almost always provide relatively lower CO_2 mixing ratio than the background from the other two products, except for GEOS-Chem near the beginning of the season. The average difference in background CO_2 between Carbon Tracker and NOAA ESRL's empirical product is about 5ppm during the selected winter months.

Table 6 Altitudes at the boundary defined by the North American empirical curtain CO_2 mixing ratio, where particles are initialized to take CO_2 background.

Above Sea Level (m)	500	1500	2500	3500	4500	5500	6500
Particles initialized (%)*	31.7	37.4	19.1	7.6	2.5	1.1	0.6

* values represents the number of particles in % among the total particles intersecting the boundary "curtain" that approximates the Pacific coastline of North America.

It is also important to locate altitudes where the Lagrangian particles are initialized, since for example, NOAA ESRL's product is optimized for altitudes below 2 km. The altitudes where the particles are initialized to take boundary information are summarized in Table 6. Approximately 90 % of background CO_2 takes initial information at altitudes below 2.5 km asl, and the vast majority of advected CO_2 is influenced by the atmospheric boundary layer processes as about 70 % of particles spent time below 1.5 km asl at the background before they are being advected over the source regions in-land to arrive at the receptor after 5 days. Assuming the measurement uncertainties at the receptor location is less than 0.1 ppm, the discrepancy in simulated dCO_2 values between Carbon Tracker, NOAA's measurement based products, and GEOS-Chem can cause significant errors in quantification of source contributions as the dCO_2 values are principally derived by differences in CO_2 mixing ratio between the background and the receptor. Given 1ppm uncertainty is present at the background CO_2 mixing ratio, the resulting estimate of oil sands emissions, based on footprint and transport simulations by STILT model, changes by 31.7%.

3.3.3 Partitioning of excess-CO_2 into contributing sources

The relative proportion of each source to the mixture can be deduced through isotope end-member values. When isotopic source values (a.k.a. 'signatures' or 'fingerprints') of each contributing source and the mixture are determined for multiple samples, the fractional contributions of each source to the

mixture are calculated for the point measurements. For instance, $^{13}C/^{12}C$ ratio can be used to trace CO_2 to reveal photosynthetic uptake, plant and soil respiration, and fossil fuels. Also, $^{18}O/^{16}O$ records phase changes of water vapor in processes taking place over various scales, such as evaporation, condensation, biomass burning, or consumption of fossil fuels. These isotopic fingerprints from the two isotopes provide a unique niche in evaluating biological and anthropogenic contributions to CO_2 mixing ratio.

In general, calculations use either a mean isotopic signature for the mixture or perform a separate calculation for each sample of the mixture and report confidence intervals for fractional contributions of sources based on replications. A good example of the second approach is provided in *Pataki et al.* [2003a; 2003b], and confidence intervals tend to represent variability of isotopic signature of the mixture rather than including variability of isotope composition of individual sources. In this study, a mean isotope signature of the mixture is utilized to calculate a fraction of each source in an attempt to propagate errors into uncertainties about the estimation of source proportions, following *Veldkamp and Weitz* [1994] and *Philips and Gregg* [2001].

Given well-mixed atmosphere, the measured values are represented by sum of CO_2 advected from background and CO_2 emitted from local sources:

Equation 8

$$c_T = c_B + c_S$$

Then, subtracting background values from measured mixing ratio results in c_S that represents excess-CO_2 caused by contributions from sources. The transport history of air parcels arriving in ETL can explicitly reveal geographic locations where it has traveled, and CO_2 mixing ratio at a remote location can serve as background. Trajectories to locate backgrounds are modeled through an atmospheric

transport modeling framework [*Gerbig et al.*, 2003] using Stochastic Time Inverted Lagrangian Transport model [*Lin et al.*, 2003], driven by meteorology from North American Regional Reanalysis [*Mesinger et al.*, 2005] for 5 days backward in time from each measurement. CO_2 mixing ratio at the background locations are then determined from corresponding 3 dimensional coordinates that Carbon Tracker [*Peters et al.*, 2007] provides at a high resolution for North America.

To quantify the fractions of source contributions (i.e., '*f*') from three identified sources (i.e., respiration, fossil fuels, and oil sands) using two stable isotope values (i.e., δ^{13}C and δ^{18}O) measured at the receptor, following set of mass balance equation is used.

Equation 9

$$
\begin{aligned}
&f_R + f_{FF} + f_{OS} = 1, \\
&\delta^{13}C_R f_R + \delta^{13}C_{FF} f_{FF} + \delta^{13}C_{OS} f_{OS} = \delta^{13}C_S, \\
&\delta^{18}O_R f_R + \delta^{18}O_{FF} f_{FF} + \delta^{18}O_{OS} f_{OS} = \delta^{18}O_S,
\end{aligned}
$$

where subscript $_R$, $_{FF,\ OS}$ and $_S$ stands for respiration, fossil fuels, oil sands, and source respectively. Further, $f_R=c_R/c_S$, $f_{FF}=c_{FF}/c_S$, $f_{OS}=c_{OS}/c_S$, and they are assumed to remain overall constant during the sampling period of year 2005 to year 2010 for which $\delta^{13}C_S$ and $\delta^{18}O_S$ are determined with the Keeling method. We focus on proportion of CO_2 source contribution from the oil sands area. It seems prudent to assume that the oil sands would have a distinct isotopic source signature than that of conventional fossil fuels because of its petro-chemical properties [*CAPP*, 2012]. Measurement results also suggest that flares from oil sands facilities emit unique tracers that are distinguishable from other fossil fuel emissions [*Simpson et al.*, 2010; *Simpson et al.*, 2013]. Conventional fossil fuels are considered as a group to include gasoline, natural gas, and coals. $\delta^{13}C_{FF}$ and $\delta^{18}O_{FF}$ are obtained from a mean value using actual measurements in various locations in Canada [unpublished data from *H. Lin*, personal communication]. The nighttime CO_2 mixing ratio measured at 22 meter tower and its $\delta^{13}C$ can be

utilized to derive carbon isotope source values of the ecosystem respiration $\delta^{13}C_R$, and derived mean value is found at -26‰ for the dataset. The derivation of oxygen isotope source value for ecosystem respiration ($\delta^{18}O_R$) requires use of a model [*Craig and Gordon*, 1965; *West et al.*, 2008]. Descriptions for the Craig-Gordon model to calculate evaporative enrichments of the oxygen isotope during respiration in vegetation canopy are provided in Appendix C and Appendix D, and technical details can also be found in references therein. Oil sands end-member values of $\delta^{13}C_{OS}$ and $\delta^{18}O_{OS}$ are based on literature reviews and empirical assumptions.

While errors from measurements or models are relatively standard and well documented, uncertainties in $\delta^{13}C_S$ and $\delta^{18}O_S$ are subject to errors in the different Keeling plot approaches and will propagate through analytical solutions to Equation 9. Significance tests were performed in each linear regression (Type I method) to the Keeling plots using Equation 4 in order to constrain upper and lower bounds of a derived source value at confidence intervals of 95%.

Table 7 Isotopic values (mean values and uncertainties) used for the linear mixing model expressed in Equation 9.

<table>
<tr><th rowspan="2">Parameters (mean±stdev)</th><th colspan="2">Values [‰ VPDB-CO2]</th><th colspan="2" rowspan="2">Source of uncertainty</th></tr>
<tr><th>Mean</th><th>Uncertainty</th></tr>
<tr><td>$\overline{\delta C_{FF}} \pm \sigma^2_{\delta C_{FF}}$</td><td>-28</td><td rowspan="2">1</td><td colspan="2" rowspan="2">measurement errors for Canadian fossil fuels</td></tr>
<tr><td>$\overline{\delta O_{FF}} \pm \sigma^2_{\delta O_{FF}}$</td><td>-17</td></tr>
<tr><td>$\overline{\delta C_{OS}} \pm \sigma^2_{\delta C_{OS}}$</td><td>-40</td><td>1</td><td colspan="2">theoretical guess</td></tr>
<tr><td>$\overline{\delta O_R} \pm \sigma^2_{\delta O_R}$</td><td>-37</td><td>4.5</td><td rowspan="4">standard deviations or confidence intervals at 95%</td><td>the C-G model</td></tr>
<tr><td>$\overline{\delta C_S} \pm \sigma^2_{\delta C_S}$</td><td>-29</td><td>3.1</td><td rowspan="3">the Keeling plot</td></tr>
<tr><td>$\overline{\delta O_S} \pm \sigma^2_{\delta O_S}$</td><td>-78</td><td>15.8</td></tr>
<tr><td>$\overline{\delta C_R} \pm \sigma^2_{\delta C_R}$</td><td>-26</td><td>0.5</td></tr>
<tr><td>$\overline{\delta O_{OS}} \pm \sigma^2_{\delta O_{OS}}$</td><td>-80</td><td>2.7</td><td colspan="2">temperature variance</td></tr>
</table>

The STILT simulation provided a solution toward finding three unknown proportions of each sources independent of stable isotopes mixing models; namely, $\Delta CO_{2\_ODIAC}/dCO_2 \equiv f_{FF} \approx 0.13$. With this additional constraint from available through the receptor oriented modeling framework, the isotopic mass balance suggests that 38% of access-CO_2 observed at East Trout Lake is due to oil sands sources; $f_{OS} \approx 0.38$. The remaining fraction of 49% comes from respirations.

The uncertainties in f_{OS} is approximated by propagating parameter uncertainties through the first order Taylor approximation for the solution to the linear mixing model [*Taylor*, 1997]. Uncertainties in a function q that has variable of x and y for example is calculated by the sum of the uncertainties in x and y. This is general rule that applies to different types of functions of q, whether q being $x+y$, xy, or x/y. With x and y measured with uncertainties of δx and δy and the measured values being used to compute the function $q(x,y)$, if the uncertainties in x and y are independent and random, the uncertainties in q is $\delta q = \sqrt{\left(\frac{\partial q}{\partial x}\delta x\right)^2 + \left(\frac{\partial q}{\partial y}\delta y\right)^2}$. In any case, it is never larger than the ordinary sum and for uncertainties of f_{OS}

Equation 10

$$\sigma_{f_{OS}} \leq \left|\frac{\partial f_{OS}}{\partial \delta^{13}C_R}\right|\sigma_{\delta^{13}C_R} + \left|\frac{\partial f_{OS}}{\partial \delta^{13}C_{FF}}\right|\sigma_{\delta^{13}C_{FF}} + \cdots + \left|\frac{\partial f_{OS}}{\partial \delta^{18}O_S}\right|\sigma_{\delta^{18}O_S}$$

The result of error propagation indicates that uncertainty of f_{OS} is ≤ 0.15, meaning f_{OS} evaluated at the mean is 38 % of total excess-CO_2 and its uncertainties are found at ± 15%.

3.4 Conclusions

Given that uncertainties in background CO_2 linearly propagate to estimations of regional scale emission, discrepancies of dCO_2 between different background CO_2 products found in this study have significant implications. For example, when 1 ppm error results in uncertainties of more than 30%,

discrepancy of 5 ppm that exist between Carbon Tracker and the NOAA's measurement-based product can significantly complicate interpretation of results as final results would differ by more than 150 % depending on which background was used to compute the emission estimates.

By assimilating reliable measurements, EC-CAS has the potential to provide improved boundary conditions to regional scale emission estimations for Canadian stakeholders to make informed decisions toward intended managements of carbon sources and sinks, while contributing to broader scientific communities.

3.4.1 Outlook

Precise observations of the mixing ratio and the isotopic compositions of atmospheric CO_2 have been used to partition a measured change in concentration into different contributing surface fluxes, for example in this study by terrestrial versus oceanic or natural versus anthropogenic origins. The isotopic mass balance provides the foundation for partitioning of sources and sinks, which relies on the fundamental assumption that the background parameters for mixing models such as the Keeling plot method are known. Treatments of background parameters are found usually in two ways, either by employing a meticulous experimental design to ensure constant background conditions, or by prescribing reasonable references as background conditions (Appendix F). Although theories behind mixing model approaches are well understood, these kinds of treatments of backgrounds for mixing model parameters still require caution in various practical applications. This is mainly because both i) constant background values for any given mixing in the atmosphere can rarely be established due to dynamic nature of the mixing medium, and ii) variability of CO_2 and its isotopic composition are strongly influenced not only by atmospheric transport and mixing but also by changes in surface fluxes, which can themselves be highly variable.

One of the researches to be conducted in order to address is on the treatment of background parameters of isotope mixing models. Outcomes of such investigation will include assessment of

appropriate spatio-temporal scopes of mixing models by comparisons between traditional approaches and simulation results. This will constitute a key step to further developments of integrating spatial aspects to Keeling plot-like methods and significantly contribute to the broader scientific community concerned with regional-scale cycles of atmospheric tracers, including CO_2 and its stable isotope components.

Examining and propagating uncertainties in modeling transports can be quantified and propagated through STILT runs, following the method described in *Lin and Gerbig* [2005]. Expected results of the transport error propagation will help quantify uncertainties in ΔCO_{2_ODIAC}. Also, Inverting f_{OS} into oil sands emissions and examine the outcome from the inversion against inventory emission reports will provide an additional top-down constraints on independent inventories such as Canada's National Inventory Report.

Chapter 4
Summary

The CO_2 mixing ratio and $\delta^{13}C$ and $\delta^{18}O$ measured at ETL were used to examine variability and derive isotopic sources of the atmospheric CO_2. The traditional Keeling plot method combined with "Type I" regression provides the best fitting for the given dataset. The correlations between CO_2 mixing ratio and its isotopic components are stronger during winter especially for oxygen isotopes, indicating its linkage to vigorous hydrologic cycles during growing season of warmer months.

Seasonal ranges of δ^{13}Cs of the atmospheric CO_2 measured at ETL span from about -22‰ in summer to about -36‰ in winter. More negative values during winter seasons are expected because of increased influences from burning fossil fuels. The apparent seasonal cycle of CO_2 mixing ratio and its strong anti-correlation to δ^{13}C reveals that depleted (more negative) values in the wintertime corresponding to increased combustion of fossil fuels, and enriched (less negative) values in the warmer months which is from mixed influences by either gasoline combustion or ecosystem respiration.

Extraordinary end-member values for atmospheric $\delta^{18}O$ of CO_2 were derived, and it is speculated that the extraordinary negative values could have originated from large scale industrial distillation-condensation processes potentially the SAGD operations used by in-situ oil sands mining activities taking place near ETL.

The excess-CO_2 (dCO_2) values that are calculated by subtracting the corresponding CO_2 mixing ratio determined for a background of CO_2 measured at ETL should constitute contributions from local sources. Contributions by fossil fuel sources to dCO_2 are calculated by simulating the transport of CO_2 fluxes using the STILT model with the improved ODIAC emission grids, and the

simulation result suggests that fossil fuel emissions that the ODIAC emission accounts for have added on average 13% to the calculated dCO_2.

A linear mixing model analysis based in mass balance of stable isotopes of CO_2 was performed to partition the determined sources into respective proportions. The best estimate for oil sands contribution to excess-CO_2 is found at 38% with uncertainties as large as 15%. Appropriate isotope source values accompanying approximate uncertainties for different samples including fossil fuel types can further expand findings of current study to a comprehensive source portioning of CO_2 mixing ratio into vegetation vs. soil as well as different fossil fuel types.

Bibliography

Alam, J. M., and J. C. Lin, 2008, Toward a fully Lagrangian atmospheric modeling system, *Mon. Weather Rev., 136*(12), 4653–4667, doi:10.1175/2008MWR2515.1.

Andres, R. J., G. Marland, T. Boden, and S. Bischof, 2000, Carbon dioxide emissions from fossil fuel consumption and cement manufacture, 1751– 1991, and an estimate of their isotopic composition and latitudinal distribution, in *The Carbon Cycle*, edited by T. M. L. Wigley and D. S. Schimel, pp. 53– 62, Cambridge Univ. Press, New York, USA.

Alberta Environment and Sustainable Resource Development (AESRD), esrd.alberta.ca; Oil Sands Information Portal (OSIP), osip.alberta.ca; Government of Alberta-Alberta's Oil sands, oilsands.alberta.ca; accessed online on July 12th, 2013.

Bakwin, P.S., P.P. Tans, J.W.C. White, and R.J. Andres, 1998, Determination of the isotopic ($^{13}C/^{12}C$) discrimination by terrestrial biology from a global network of observations, *Global Biogeochem.Cycles*, 12(3), 555-562, doi: 10.1029/98GB02265.

Ballantyne, A.P., J.B. Miller, and P.P. Tans, 2010, Apparent seasonal cycle in isotopic discrimination of carbon in the atmosphere and biosphere due to vapor pressure deficit, *Global Biogeochem. Cycles*, 24, GB3018, doi:10.1029/2009GB003623.

Ballantyne, A. P., C. B. Alden, J. B. Miller, P. P. Tans, and J. W. C. White (2012), Increase in observed net carbon dioxide uptake by land and oceans during the past 50 years, *Nature*, 488, 70-73, doi:10.1038/nature11299.

Bindlish, R., T. Jackson, A. Gasiewski, and co-authors, 2006, Soil moisture mapping and AMSR-E validation using the PSR in SMEX02, *Remote Sensing of Environment*, 103, 127–139, doi:10.1016/j.rse.2005.02.003

Birks, S.J., T.W.D. Edwards, J.J. Gibson, and co-authors, 2003, *Canadian Network for Isotopes in Precipitation*, University of Waterloo/Meteorological Service of Canada.

Birks, S.J., and J.J. Gibson, 2009, Isotope Hydrology Research in Canada, 2003-2007, *Canadian Water Resources Journal*, 34(2), 163–176.

Blanken, P.D., and T. A. Black. 2004. The canopy conductance of a boreal aspen forest, PrinceAlbert National Park, Canada. *Hydrol. Process.*, 18;1561–1578, DOI: 10.1002/hyp.1406

Bonan, G. 2008. *Ecological Climatology: concepts and applications* 2nd ED, Cambridge University Press, UK.

Bousquet, P., P. Ciais, P. Peylin, and co-authors, 1999, Inverse modeling of annual atmospheric CO_2 sources and sinks: 1. Method and control inversion, *J. Geophys. Res.*, 104(D21), 26161– 26178.

Bowling, D.R., S.P. Burns, T.J. Conway, R.K. Monson, and J.W.C. White, 2005, Extensive observations of CO_2 carbon isotope content in and above a high-elevation subalpine forest, *Global Biogeochem. Cycles*, 19, GB3023, doi:10.1029/2004GB002394.

Bowling, D.R., D.E. Pataki, J. Randerson, 2008, Carbon isotopes in terrestrial ecosystem pools and CO_2 fluxes (Tansley Review), *New Phytologist*, 178:24-40, doi: 10.1111/j.1469-8137.2007.02342.x

Brand, W.A., L. Huang, H. Mukai, A. Chivulescu, J.M. Richter, and M. Rothe, 2009, How well do we know VPDB? Variability of $\delta^{13}C$ and $\delta^{18}O$ in CO_2 generated from NBS19-calcite, *Rapid Commun. Mass Spectrom.*, 23, 915–926, doi: 10.1002/rcm.3940.

Brankov E., Rao S.T. and Porter P.S., 1997, A Trajectory-clustering-correlation methodology for examining the long-range transport of air pollutants. *Atmos. Environ.,* 32(9), 1525-1534.

Brenninkmeijer, CAM, P. Kraft, and W.G. Mook, 1983, Oxygen isotope fractionation between CO_2 and H_2O. *Isotope Geosc.,* 1, 181–190.

Brutsaert, W.H. 1975. The roughness length for water vapor, sensible heat and other scalars. *J. Atm. Sci*. 32:2028-2031.

Butler, R., 1991, *Thermal recovery of oil and bitumen*, Prentice-Hall, N.J., USA.

Canadian Association of Petroleum Producers (CAPP), 2012, *The facts on oil sands: upstream dialog*, also accessible online at www.capp.ca/upstreamdialogue.

Chen, B., J.M. Chen, G. Mo, and co-authors, 2008, Comparison of regional carbon flux estimates from CO_2 concentration measurements and remote sensing based footprint integration, *Global Biogeochem. Cycles*, 22, GB2012, doi:10.1029/2007GB003024

Chen, B., N.C. Coops, D. Fu, H.A. Margolis, and co-authors. 2011. Assessing eddy-covariance flux tower location bias across the Fluxnet-Canada Research Network based on remote sensing and footprint modelling. *Agricultural and Forest Meteorology*, 151: 87–100. doi:10.1016/j.agrformet.2010.09.005

Christi, M. J., G. L. Stephens, 2004, Retrieving profiles of atmospheric CO_2 in clear sky and in the presence of thin cloud using spectroscopy from the near and thermal infrared: A preliminary case study, *J. Geophys. Res*., 109, D04316, doi:10.1029/2003JD004058.

Cerling, T.E., D.K. Solomon, J. Quade, and J.R. Bowman, 1991, On the isotopic composition of carbon in soil carbon dioxide, *Geochimica et Cosmochimica Acta*, 55(11), 3403-3405.

Ciais, P., P. P. Tans, J. W. C. White, M. Trolier, and co-authors, 1995, Partitioning of ocean and land uptake of CO_2 as inferred by $\delta^{13}C$ measurements from the NOAA Climate Monitoring and Diagnostics Laboratory global air sampling network, *J. Geophys. Res*., *100,* 5051-5070, 1995.

Ciais, P., P.P. Tans, A.S. Denning, R.J. Francey, M. Trolier, H.A.J. Meijer, J.W.C. White, J.A. Berry, D.A. Randall, G.J. Collatz, P.J. Sellers, P. Monfray, and M. Heimann, 1997, A three-dimensional

synthesis study of $\delta^{18}O$ in atmospheric CO_2:2.Simulations with the TM2 transport model, *J. Geophys. Res.*, 102(D5), 5873-5883, doi: 10.1029/96JD02361.

Conway, T. J., P. P. Tans, L. S. Waterman, and co-authors, 1994, Evidence for interannual variability of the carbon cycle from the National Oceanic and Atmospheric Administration/Climate Monitoring and Diagnostics Laboratory Global Air ampling Network, *J. Geophys. Res.*, 99(D11), 22,831– 22, 855.

Covey, W. 1959. *Testing a hypothesis concerning the quantitative dependence of evapotranspiration on availability of moisture. Soil Physics*, A&M College of Taxas, M.S. Thesis, 58 pp.

Craig, H., 1961, Isotopic variations in meteoric waters, *Science*, 133, 1702-1703.

Craig, H., and L. I. Gordon, 1965, Deuterium and oxygen 18 variations in the ocean and marine atmosphere, in *Stable Isotopes in Oceanographic Studies and Paleotemperatures*, edited by E. Tongiorigi, pp. 9–130, Lab. di Geol. Nucl., Cons. Naz. Delle Ric., Pisa, Italy.

Criss, R.E., 1999, Isotopic exchange and equilibrium fractionation. In: *Principles of stable isotope distribution*, Oxford University Press, New York, NY, USA.

Crawford, J., S. Chambers, D. Cohen, and co-authors, 2007, Receptor modelling using Positive Matrix Factorisation, back trajectories and Radon-222, *Atmos. Environ.,* 41, 6823-6837.

Dansgaard, W., 1964, Stable isotopes in precipitation, *Tellus*, 16, 436-468.

Deng, F., J. M. Chen, C.-W. Yuen, and co-authors, 2007, Global monthly CO_2 flux inversion with focus over North America, *Tellus, 59B*, 179-190.

Derber J.C., D.F. Parrish, and S.J. Lord, 1991, The new global operational analysis system at the National Meteorological Center, *Weather and Forecasting*, 6, 538-547.

Dlugokencky, E. J., L. Bruhwiler, J. W. C. White, L. K. Emmons, P. C. Novelli, S. A. Montzka, K. A. Masarie, P. M. Lang, A. M. Crotwell, J. B. Miller, and L. V. Gatti, 2009, Observational

constraints on recent increases in the atmospheric CH_4 burden, *Geophys. Res. Lett*., 36(L18803), doi:10.1029/2009GL039780.

Dlugokencky, E. J., E. G. Nisbet, R. Fisher, and D. Lowry, 2011, Global atmospheric methane: budget, changes and dangers, *Phil. Trans. R. Soc. A* , 369, doi: 10.1098/rsta.2010.0341.

Dlugokencky, E. J., and P. Tans (2013), Trends in atmospheric carbon dioxide, NOAA Earth System Research Laboraty (www.esrl.noaa.gov/gmd/ccgg/trends/), accessed in November 2013.

Draxler, R. R., and J. L. Heffter (Eds.), 1989, *Across North America Tracer Experiment (ANATEX),* vol. I, *Description, Ground-Level Sampling at Primary sites, and Meteorology, NOAA Tech.Memo., ERL ARL-167,* 83 pp.

Edwards, T.W.D., B.B. Wolfe, J.J. Gibson, and D. Hammarlund, 2004, Use of water isotope tracers in high latitude hydrology and paleohydrology. In: *Long-Term Environmental Change in Arctic and Antarctic Lakes*, [R. Pienitz, M.S.V. Douglas and J.P. Smol (eds.)], Kluwer Academic Publishers, Dordrecht, The Netherlands.

Ehleringer, J.R., and C.S. Cook, 1998, Carbon and oxygen isotope ratios of ecosystem respiration along an Oregon conifer transect: preliminary observations based on small-flask sampling, *Tree Physiology*, 18, 513-519.

Enting, I.G., 2002, *Inverse problems in atmospheric constituent transport*, Cambridge University Press, New York, 389 pp.

Farquhar, G.D., J.R. Ehleringer, and K.T. Hubic, 1989, Carbon isotope discrimination and photosynthesis, *Annu. Rev. Plant Physiol. Plant Mol. Bioi.*, 40, 503-537.

Fischlin, A., G.F. Midgley, J.T. Price, R. Leemans, B. Gopal, C. Turley, M.D.A. Rounsevell, O.P. Dube, J. Tarazona, A.A. Velichko, 2007, Ecosystems, their properties, goods, and services. In: *Climate Change 2007: Impacts, Adaptation and Vulnerability*. *Contribution of Working Group II*

to the Fourth Assessment Report of the Intergovernmental Panel on Climate Change, [Parry, M.L., O.F. Canziani, J.P. Palutikof, P.J. van der Linden and C.E. Hanson (eds.)], Cambridge University Press, Cambridge, UK.

Farquhr, G., J. Lloyd, 1993, Carbon and oxygen isotope effects in the exchange of carbon dioxide between terrestrial plants and the atmosphere. In: *Stable isotopes and plant carbon-water relations*, [Ehleringer, J.R., A. Hall, G. Farquhr (eds.)], Academic Press, San Diego, CA, USA.

Flanagan, L. B., and J. R. Ehleringer, 1998, Ecosystem-atmosphere CO_2 exchange: Interpreting signals of change using stable isotope ratios, *Trends Ecol. Evol.*, 13(1), 10– 14.

Flanagan, L. B., J. R. Brooks, G. T. Varney, and J. R. Ehleringer, 1997, Discrimination against C18O16O during photosynthesis and the oxygen isotope ratio of respired CO_2 in boreal forest ecosystems, *Global Biogeochem. Cycles*, 11(1), 83–98.

Flanagan, L.B., T. Cai, T.A. Black, A.G. Barr, J.H. McCaughey, H.A. Margolis, 2012, Measuring and modeling ecosystem photosynthesis and the carbon isotope composition of ecosystem-respired CO_2 in three boreal coniferous forests. *Agric. For. Meteorol.*, 153, 165-176, doi:10.1016/j.agrformet.2011.03.001

Forster, P., V. Ramaswamy, P. Artaxo, and co-authors, 2007, Changes in Atmospheric Constituents and in Radiative Forcing. *In: Climate Change 2007: The Physical Science Basis. Contribution of Working Group I to the Fourth Assessment Report of the Intergovernmental Panel on Climate Change* [Solomon, S., D. Qin, M. Manning, Z. Chen, M. Marquis, K.B. Averyt, M.Tignor and H.L. Miller (eds.)]. Cambridge University Press, Cambridge, United Kingdom and New York, NY, USA.

Francey, R., and P.P. Tans, 1987, Latitudinal variation in oxygen-18 of atmospheric CO_2, *Nature*, 327,495–497.

Frey, R.A, S.A. Ackerman, Y. Liu, and co-authors, 2008, Cloud detection with MODIS. Part I: Improvements in the MODIS cloud mask for collection 5, *J. Atmos. and Oceanic Technology*, 25, 1057-1072, doi: 10.1175/2008JTECHA1052.1

Fritz, P. and J.C. Fontes, 1980, *Handbook of environmental isotope Geochemistry*, Elsevier, Amsterdam, The Netherland.

Gat, J.R. and R. Gonfiantini, 1981, *Stable isotope hydrology: deuterium and oxygen-18 in the water cycle*, Vienna, Austria.

Gat, J.R., 1996, Oxygen and hydrogen isotopes in the hydrologic cycle, *Annu. Rev. Earth Planet Sci.*, 24. 228-262

Gat, J.R., W.G. Mook, and H.A.J. Meijer, 2001, *Environmental isotopes in the hydrologic cycle*: Volume II Atmospheric water, edited by W.G. Mook, Paris, France.

Gerbig, C., J. C. Lin, S. C. Wofsy, and co-authors, 2003, Toward constraining regional-scale fluxes of CO_2 with atmospheric observations over a continent: 2. Analysis of COBRA data using a receptor-oriented framework, *J. Geophys. Res.*, 108(D24), 4756, doi:10.1029/2002JD003770.

Gerbig, C., S.K. Korner, J.C. Lin, 2008, Vertical mixing in atmospheric tracer transport models: error characterization and propagation, *Atmos. Chem. Phys*., 8, 591–602

Gibson, J.J., T.W.D. Edwards, S.J. Birks, N.A. St.Amour, W.M. Buhay, P. McEachern, B.B. Wolfe, and D.L. Peters, 2005, Progress in isotope tracer hydrology in Canada, *Hydrological Processes,* 19, 303-327.

Gosselin, P, S.E. Hrudey, M.A Naeth, and co-authors, 2010, Environmental and Health Impacts of Canada's Oil Sands Industry: The Expert Panel Report, *The Royal Society of Canada*.

Gosselin, P, S.E. Hrudey, M.A Naeth, and co-authors, Environmental and Health Impacts of Canada's Oil Sands Industry: Executive Summary, *The Royal Society of Canada Expert Panel*, 2010, p. 11.

Gurney, K. R., Law, R. M., Denning, A. S., and co-authors, 2002, Towards robust regional estimates of CO_2 sources and sinks using atmospheric transport models, *Nature*, 415, 626–630.

Harris, P.P., C. Huntingford, P.M. Cox, and co-authors, 2004, Effect of soil moisture on canopy conductance of Amazonian rainforest., *Agricultural and Forest Meteorology*, 122:215–227, doi:10.1016/j.agrformet.2003.09.006

Hegarty, J., R. R. Draxler, A. F. Stein, and co-authors, 2013, Evaluation of Lagrangian Particle Dispersion Models with Measurements from Controlled Tracer Releases. *J. Appl. Meteor. Climatol.*, 52, 2623–2637, doi: http://dx.doi.org/10.1175/JAMC-D-13-0125.1

Higuchi, K., D. Worthy, D. Chan, and A. Shashkov, 2003, Regional source/sink impact on the diurnal, seasonal and inter-annual variations in atmospheric CO_2 at a boreal forest site in Canada, *Tellus*, 55B, 115–125.

Hoefs, J., 2009, *Stable isotope Geochemistry 6^{ed}*, Springer, Berlin, Germany.

Hopke, P.K., Li C.L., Ciszek W. and Landsberger S., 1995, The use of bootstrapping to estimate conditional probability fields for source locations of airborne pollutants. *Chemometrics and Intelligent Laboratory Systems* 30, 69-79.

Huang, L. and D. Worthy 2003, Flask Sampling Strategy by MSC for Atmospheric Observations of Greenhouse Gases and CO_2 Isotopes over Canada: Status& Plan, in: *Report of the 12th WMO/IAEA Meeting of Experts on CO_2 Concentration and Related Tracer Measurement Techniques*, September 2003, GAW publication 161, Toronto, 94–100, 2005.

Huang, L., and D. Worthy, 2005, Flask Sampling Strategy by MSC for atmospheric observations of greenhouse gases and CO_2 isotopes over Canada: status and plan, Report of the *12th WMO/IAEA meeting of experts on CO_2 concentration and related tracer measurement techniques*, Toronto, September 2003, GAW publication 161: 94-100.

Huang, L., A. Chivulescu, E. Ernst, and co-authors, 2013, Maintaining consistent traceability in high precision isotope measurements of CO_2: verifying atmospheric trends of $\delta^{13}C$, *Atmos. Meas. Tech.*, 6, 1685–1705, doi:10.5194/amt-6-1685-2013.

Hungershoefer, K., F.M. Breon, P. Peylin, and co-authors, 2010, Evaluation of various observing systems for the global monitoring of CO_2 surface fluxes, *Atmos. Chem. Phys.*, 10, 10503–10520, doi:10.5194/acp-10-10503-2010

Imasu, R., Y. Hayashi, A. Inagoya, and co-authors, 2010, Retrieval of minor constituents from thermal infrared spectra observed by GOSAT TANSO-FTS sensor, *Proc. of SPIE*, Vol. 7857, 785708, doi: 10.1117/12.870684.

Jarvis, P.G., and K.G. McNaughton, 1986, Stomatal control of transpiration. *Advances in Ecological Research*, 15:1-49.

Jensen, M.E., R.D. Burman, and R.G. Allen (Ed)., 1990, Evaporation and irrigation water requirements, *ASCE manuals and Reports on Engineering Practice No. 70*, American Society of Civil Engineers, New York, USA.

Kayler, Z.E., L. Ganio, M. Hauck, T.G. Pypker, and co-authors, 2009, Bias and uncertainty of $\delta^{13}CO_2$ isotopic mixing models, *Oecologia*, DOI 10.1007/s00442-009-1531-6

Keeling, C. D., 1958, The concentration and isotopic abundances of atmospheric carbon dioxide in rural areas, *Geochim. Cosmochim. Acta*, 13, 322–334.

Keeling, C. D., 1961, The concentration and isotopic abundance of carbon dioxide in rural and marine air, *Geochim. Cosmochim. Acta*, 24, 277–298.

Keeling, C. D., R. B. Bacastow, A. F. Carter, and co-authors, 1989, A three-dimensional model of atmospheric CO_2 transport based on observed winds, 1, Analysis of observational data, in Aspects

of Climate Variability in the Pacific and the Western Americas, *Geophys. Monogr. Ser.*, vol. 55, edited by D. H. Peterson, pp. 165– 236, AGU, Washington, D. C..

Keeling, C. D., and T. P. Whorf, 1994, Atmospheric CO_2 records from sites in the SIO air sampling network, in *Trends '93: A Compendium of Data on Global Change*, Oak Ridge Natl. Lab. Rep., ORNL, CDIAC-65, pp. 16–26, Oak Ridge Natl. Lab., Oak Ridge, Tenn.

Keeling, C. D., T. P. Whorf, M.Wahlen and J. van der Plicht, 1995, Interannual extremes in the rate of rise of atmospheric carbon dioxide since 1980, *Nature*, *375*, 666-670.

Kim, M.G., L. Huang, J. C. Lin, T. W. D. Edwards, C. Sweeney, P. P. Tans, J. W. C. White, B. H. Vaughn, 2013, Variability of isotopic values of CO_2 measured at a Canadian Greenhouse Gas Measurement Program site, unpublished manuscript.

Kljun, N., T.A. Black, T.J. Griffis, and co-authors, 2006, Response of net ecosystem productivity of three boreal forest stands to drought, *Ecosystems*, 9, 1128– 1144, doi:10.1007/S10021-005-0082-X.

Kretschmer, R., Gerbig, C., Karstens, U., and Koch, F.-T., 2012, Error characterization of CO_2 vertical mixing in the atmospheric transport model WRF-VPRM, *Atmos. Chem. Phys*., 12, 2441-2458, doi:10.5194/acp-12-2441-2012.

Kroopnick, P., and H. Craig, 1972, Atmospheric oxygen: Isotopic composition and solubility fractionation, *Science*, 175, 54– 55.

Kort, E. A., J. Eluszkiewicz, B. B. Stephens, J. B. Miller, C. Gerbig, T. Nehrkorn, B. C. Daube, J. O. Kaplan, S. Houweling, and S. C. Wofsy, 2008, Emissions of CH_4 and N_2O over the United States and Canada based on a receptor oriented modeling framework and COBRA-NA atmospheric observations, *Geophys. Res. Lett.*, 35(L18808), doi:10.1029/2008GL034031.

Kuze, A., H. Suto, M. Nakajima, and co-author, 2009, Thermal and near infrared sensor for carbon observation Fourier-transform spectrometer on the Greenhouse Gases Observing Satellite for greenhouse gases monitoring, *Applied Optics*, 48(35), 9716-6733.

Laws, E., 1997, *Mathematical Methods for Oceanographers*, John Wiley, New York, USA.

Langenfelds, R. L., R. J. Francey, B. C. Pak, L. P. Steele, J. Lloyd, C. M. Trudinger, and C. E. Allison, 2002, Interannual growth rate variations of atmospheric CO2 and its d13C, H2, CH4, and CO between 1992 and 1999 linked to biomass burning, *Global Biogeochem. Cycles*, 16(3), 1048, doi:10.1029/2001GB001466.

Legg, B.J., and M.R. Raupach, 1982, Markov-chain simulations of particles dispersion in inhomogeneous flows: The mean drift velocity induced by a gradient in Eulerian velocity variance, *Boundary Layer Meteorol.*, 24, 3-13.

Legendre, P., and L. Legendre, 1998, *Numerical ecology* 2nd Ed., No. 20 in Development in Environmental Modelling, Elsevier, Amsterdam, The Netherland.

Lin, J.C, D. Brunner, C. Gerbig, 2011, Studying atmospheric transport through Lagrangian models, *EOS*, 92(21), 177-178.

Lin, J. C., and C. Gerbig, 2005, Accounting for the effect of transport errors on tracer inversions, *Geophys. Res. Lett.*, 32, L01802, doi:10.1029/2004GL021127.

Lin, J. C., C. Gerbig, S. C. Wofsy, and co-authors, 2003, A near-field tool for simulating the upstream influence of atmospheric observations: The Stochastic Time-Inverted Lagrangian Transport (STILT) model, *J. Geophys. Res.*, 108(D16), 4493, doi:10.1029/2002JD003161.

Lloyd, J., and G.D. Farquhar, 1994, ^{13}C discrimination during CO_2 assimilation by the terrestrial biosphere, *Oecologia*, 99, 201–215.

Lu, X. and Q. Zhuang 2010, Evaluating evapotranspiration and water-use efficiency of terrestrial ecosystems in the conterminous United States using MODIS and AmeriFlux data, *Journal of Remote Sensing*, 114, 1924-1939, doi:10.1016/j.rse.2010.04.001

Mahadevan, P., T. Koike, X. Li, and co-author, 2003, A simplified land data assimilation scheme and its application to soil moisture experiments in 2002 (SMEX02), *Water Resour. Res.*, 39(12), 1341, doi:10.1029/2003WR002124

Mahadevan, P., S. C. Wofsy, D. M. Matross, and co-authors, 2008, A satellite-based biosphere parameterization for net ecosystem CO_2 exchange: Vegetation Photosynthesis and Respiration Model (VPRM), *Global Biogeochem. Cycles*, 22, GB2005, doi:10.1029/2006GB002735.

Majoube, M., 1971, Fractionnement en oxygène 18 et en deuterium entre l'eau et sa vapeur*, J. Chim. Phy.*, 10, 1423-1436.

Maksyutov, S., N. Kadygrov, Y. Nakatsuka, and co-authors, 2008, Projected impacts of the GOSAT observations on regional CO_2 flux estimations as a function of total retrieval error, *Journal of the Remote Sensing Society of Japan*, 28(2), 190-197.

Merlivat, L., R. Botter, and G. Nief, 1963, Fractionnement isotopique au cours de la distillation de l'eau, *J. Chim. Phys*., 60, 56-59. As sited in *Principles of Stable isotope distribution*, Criss, R.B., 1999, Oxford Press, New York.

Mesinger, F., et al., 2006, North American Regional Reanalysis, *Bull. Amer. Meteor. Soc.*, 87, 343–360, doi:10.1175/BAMS-87-3-343.

Meteorological Service of Canada, 2013, *The 1981 to 2010 Canadian Climate Normals*, available at ftp://ftp.tor.ec.gc.ca/Pub/Normals/English/. Accessed on September 4th, 2013.

Miller, J.B., D. Yakir, J.W.C. White, and P.P. Tans, 1999, Measurements of $^{18}O/^{16}O$ in the soil-atmosphere CO_2 flux, *Global Biogeoch. Cycles*, 13, 761–774, doi: 10.1029/1999GB900028.

Miller, J. B., and P. P. Tans, 2003, Calculating isotopic fractionation from atmospheric measurements at various scales, *Tellus (B)*, 55, 207–214.

Mills, G.A., and H.C. Urey, 1940, The kinetics of isotopic exchange between carbon dioxide, bicarbonate ion, carbonate ion and water, *J. Am. Chem. Soc.*, 62, 1019–1026.

Miyamoto, Y., M. Inoue, I. Morino, O. Uchino, T. Yokota, T. Machida, Y. Sawa, H. Matsueda, C. Sweeney, P. P. Tans, A. E. Andrews, and P. K. Patra, 2013, Atmospheric column-averaged mole fractions of carbon dioxide at 53 aircraft measurement sites, *Atmos. Chem. Phys.*, 13, 5265–5275, doi:10.5194/acp-13-5265-2013.

Monteith, J. L., 1965, Evaporation and the environment. 205-234. In The state and movement of water in living organisms, *XIXth Symposisum. Soc. For Exp. Biol.*, Swansea, Cambridge University Press.

Monteth, J. L., 1981, Evaporation and surface temperature, *Q.J.Roy. Meteorol.Soc.* 107:1-27.

Mortazavi, B., J.L. Prater, and J.P. Chanton,2004, A field-based method for simultaneous measurements of the $\delta^{18}O$ and $\delta^{13}C$ of soil CO_2 efflux, *Biogeosciences*, 1, 1-9, doi:10.5194/bg-1-1-2004.

Montzka, S. A., R. C. Myers, J. H. Butler, J.W. Elkins, and S.O. Cummings, 1993, Global tropospheric distribution and calibration scale of HCFC-22, *Geophys. Res. Lett.*, 20, 703-706.

Murray, F.W., 1967, On the computation of saturation vapor pressure, *J.Appl.Meteorol*. 6: 203-204.

National Energy Borard, 2006, *Canada's Oil Sand: opportunities and challenges to 2015*, An energy market assessment, p. 38.

National Inventory Report, 2011, *Greenhouse gas sources and sinks in Canada 1990-2009*, The Canadian Government`s Submission to the UN Framework Convention on Climate Change, Executive Summary, p. 20.

Nassar, R., L. Napier-Linton, K. R. Gurney, R. J. Andres, T. Oda, F. R. Vogel, and F. Deng, 2013, Improving the temporal and spatial distribution of CO2 emissions from global fossil fuel emission data sets, *J. Geophys. Res*.,118, 917–933, doi:10.1029/2012JD018196.

Nehrkorn, T., J. Eluszkiewicz, S.C. Wofsy, and co-authors, 2010, Coupled weather research and forecasting–stochastic time-inverted lagrangian transport (WRF–STILT) model, *Meteorol. Atmos. Phys.*, 107, 51–64, DOI 10.1007/s00703-010-0068-x

Oda, T., and S. Maksyutov, 2011, A very high-resolution (1km×1 km) global fossil fuel CO_2 emission inventory derived using a point source database and satellite observations of nighttime lights, *Atmos. Chem. Phys.*, 11, 543–556, doi:10.5194/acp-11-543-2011

Pataki, D.E., R. Oren, G. Katul and J. Sigmon, 1998, Canopy conductance of *Pinus taeda, Liquidambar styraciflua* and *Quercus phellos* under varying atmospheric and soil water conditions. *Tree Physiology*, 18:307-315.

Pataki, D. E., J. R. Ehleringer, L. B. Flanagan, and co-authors, 2003, The application and interpretation of Keeling plots in terrestrial carbon cycle research, *Global Biogeochem. Cycles*, 17(1), 1022, doi:10.1029/2001GB001850.

Pataki, D. E., D. R. Bowling, and J. R. Ehleringer, 2003b, Seasonal cycle of carbon dioxide and its isotopic composition in an urban atmosphere: Anthropogenic and biogenic effects, *J. Geophys. Res.*, 108(D23), 4735, doi:10.1029/2003JD003865.

Pataki, D. E., R.J., Alig, A.S. Fung, and co-authors, 2006, Urban ecosystems and the North American carbon cycle, *Global Change Biology*, 12, doi: 10.1111/j.1365-2486.2006.01242.

Patra, P., S. Maksyutov, and T. Nakazawa, 2005, Analysis of atmospheric CO_2 growth rates at Mauna Loa using CO_2 fluxes derived from an inverse model, *Tellus*, 57B, 357–365.

Pendall, E., D.G. Williams, S.W. Leavitt, 2005, Comparison of measured and modeled variations in piñon pine leaf water isotopic enrichment across a summer moisture gradient, *Oecologia*, 145(4), 605-618, doi: 10.1007/s00442-005-0164-7.

Penman, H. L., 1948, Natural evaporation from open water, bare soil and grass. *Proceedings of the Royal Society of London*, 193A, 120-45.

Penman, H. L., 1953, The physical basis of irrigation control. *Rep. 13th Int. Hort. Congr.*, 2:913-914.

Penman, H. L., 1956, Estimating evaporation. *Trans.Am.Geophy.Union*, 37:43-50.

Penman, H. L., 1963, Vegetation and hydrology. *Tech. Comm. No. 53*, commonwealth Bureau of Soils, Harpenden, England. 125pp.

Peters, W., A. Jacobson, R. Sweeney, and co-authors, 2007, An atmospheric perspective on North American carbon dioxide exchange: CarbonTracker, *P. Natl. Acad. Sci. USA*, 104, 18925–18930.

Pétron, G., et al., 2012, Hydrocarbon emissions characterization in the Colorado Front Range: A pilot study, *J. Geophys. Res.*, 117(D04304), doi:10.1029/2011JD016360.

Peylin, P., P.J. Rayner, P. Bousquet, and co-authors, 2005, Daily CO_2 flux estimates over Europe from continuous atmospheric measurements: 1, inverse methodology, *Atmos. Chem. Phys.*, 5, 3173–3186.

Phillips, D.L, and J.W. Gregg, 2001, Uncertainty in source partitioning unsing stable isotopes, *Oecologia*, 127, 171-179.

Pielke, R.A. Sr., 2002, *Mesoscale meteorological modeling 2ed*, Academic Press, CA, USA.

Plate, E.J, 1971, Aerodynamic characteristics of atmospheric boundary layers, U.S Atomic Energy Comm., *Critical review Series*, TIC-25465. 190pp.

Platt, U. and J. Stutz, 2008, Differential Absorption Spectroscopy. In: U. Platt and J. Stutz, *Differential Optical Absorption Spectroscopy, Physics of Earth and Space Environments*, pp. 135–174, doi: 10.1007/978-3-540-75776-4 6

Raupach, M.R., and J.J. Finnigan, 1988, Single-layer models of evaporation from plant canopies are incorrect but useful, whereas multilayer models are correct but useless: Discuss. Aust. J. Plant Physiol.15:706-716.

Puckett, K., and D. Worthy, 2010, QA/SAC Switzerland: Global Atmosphere Watch station information system, http://gaw.empa.ch/gawsis/reports.asp; Candian Greenhouse Gas Measurement Program, http://www.ec.gc.ca/mges-ghgm/.

Randerson, J.T., C.J. Still, J.J. Balle´, I.Y. Fung, S.C. Doney, P.P. Tans, T.J. Conway, J.W.C. White, B. Vaughn, N. Suits, and A.S. Denning, 2002, Carbon isotope discrimination of arctic and boreal biomes inferred from remote atmospheric measurements and a biosphere-atmosphere model, *Global Biogeochem. Cycles*, 16(3), doi:10.1029/2001GB001435.

Rayner, P.J., I. G. Enting, R. J. Francey, and co-author, 1999, Reconstructing the recent carbon cycle from atmospheric CO_2, d13C and O_2/N_2 observations, *Tellus*, 51B, 213-232.

Rayner, P. J., M. R. Raupach, M. Paget, P. Peylin, and E. Koffi, 2010, A new global gridded data set of CO_2 emissions from fossil fuel combustion: Methodology and evaluation, *J. Geophys. Res.*, 115, D19306, doi:10.1029/2009JD013439

Ryall, D. B., R. G. Derwent, A. J. Manning, and co-authors, 2001, Estimating source regions of European emissions of trace gases from observations at Mace Head, *Atmos. Environ., 35*(14), 2507–2523, doi:10.1016/ S1352-2310(00)00433-7.

Rodgers, C. D., 2000*, Inverse methods for atmospheric sounding: theory and practice*, World Scientific, Singapore, 238 pp.

Román, M., C.B. Schaaf, C.E. Woodcock, and co-authors, 2009, The MODIS (Collection V005) BRDF/albedo product: Assessment of spatial representativeness over forested landscapes, *Journal of Remote Sensing*, 113, 2476-2498, doi:10.1016/j.rse.2009.07.009

Schneising,O.,M. Buchwitz, M. Reuter,J. Heymann,H. Bovensmann, and J. J. Burrows, 2011, Long-term analysis of carbon dioxide and methane column-averaged mole fractions retrieved from SCIAMACHY, *Atmos. Chem. Phys.*, 11, 2863-2880, doi:10.5194/acp-11-2863-2011.

Sheppard, S.M., 1981, Stable isotope geochemistry of fluids, *Physics and Chemistry of the Earth*, 13-14, 419-445.

Shah, A., R. Fishwick, J. Wood, G. Leeke, S. Rigby, and M. Greaves, 2010, A review of novel techniques for heavy oil and bitumen extraction and upgrading, *Energy Environ. Sci.*, 3, 700–714, doi: 10.1039/b918960b

Shashkov, A., K. Higuchi, D. Chan, 2007, Aircraft vertical profiling of variation of CO_2 over a Canadian Boreal Forest Site: a role of advection in the changes in the atmospheric boundary layer CO_2 content, *Tellus,* 59B, 234–24, DOI: 10.1111/j.1600-0889.2006.00237.x.

Simpson, I. J., N. J. Blake, B. Barletta, G. S. Diskin, H. E. Fuelberg, K Gorham, L. G. Huey, S. Meinardi, F. S. Rowland, S. A. Vay, A Weinheimer, M. Yang, and D. R. Blake (2010), Characterization of trace gases measured over Alberta oil sands mining operations: 76 speciated C_2–C_{10} volatile organic compounds (VOCs), CO_2, CH_4, CO, NO, NO_2, NO_y, O_3 and SO_2, *Atmos. Chem. Phys.*, 10, 11931-11954, doi:10.5194/acp-10-11931-2010.

Simpson, I. J., M. P. S. Andersen, S. Meinardi, L. Bruhwiler, N. J. Blake, D. Helmig4, F. S. Rowland, and D. R. Blake, 2012, Long-term decline of global atmospheric ethane concentrations and implications for methane, *Nature*, 448, 490-494, doi:10.1038/nature11342

Simpson, I. J., J. E. Marrero, S. Batterman, S. Meinardi, B. Barletta, and D. R. Blake, 2013, Air quality in the industrial heartland of Alberta, Canada and potential impacts on human health, *Atmos. Environ.*, *81*, 702–709, doi:10.1016/j.atmosenv.2013.09.017.

Sokal, R. R., and F. J. Rohlf, 1995, *Biometry*, W. H. Freeman, New York, USA.

Solomon, S., D. Qin, M. Manning, R.B. Alley, and co-authors, 2007, Technical Summary. In: *Climate Change 2007: The Physical Science Basis. Contribution of Working Group I to the Fourth Assessment Report of the Intergovernmental Panel on Climate Change* [Solomon, S., D. Qin, M. Manning, Z. Chen, M. Marquis, K.B. Averyt, M. Tignor and H.L. Miller (eds.)], Cambridge University Press, NY, USA.

Stephens, B. B., Gurney, K. R., Tans, P. P., and co-authors, 2007, Weak northern and strong tropical land carbon uptake from vertical profiles of atmospheric CO_2, *Science*, 316, 1732–1735.

Sternberg, L. da S.L., 1997, Interpretation of recycling indexes, *Aust. J. Plant Physiol.*, 24, 395–398.

Stohl, A., 1998, Computation, accuracy and applications of trajectories—A review and bibliography, *Atmos. Environ., 32*(6), 947–966, doi:10.1016/S1352-2310(97)00457-3.

Stull, R. 1988. *An introduction to boundary layer meteorology*, Kluwer Academic Press, The Netherlands.

Taylor, John, 1997, *An introduction to error analysis*, 2nd Ed., University Science Books, USA.

Tans, P. P., 1981, 13C/12C of industrial CO_2, in *Carbon Cycle Modelling*, edited by B. Bolin, John Wiley, Hoboken, N. J., USA.

Tans, P.P., J. A. Berry, and R.F. Keeling, 1993, Oceanic $^{13}C/^{12}C$ observations: A new window on oceanic CO_2 uptake, *Global Biogeochem. Cycles*, 7, 353-368, doi:10.1029/93GB00053.

Tans, P. P., et al., 1996, Carbon Cycle (Group Report), Climate Monitoring and Diagnostics Laboratory, No. 23, In: *Summary Report 1994-1995*, [Hoffman, D. J., J. T. Peterson and R. M. Rosson (eds)]. US Department of Commerce, Boulder, CO, USA.

Tetens, O. 1930. Uber einige meteorologiche Begriffe. Z. Geohpys., 6:297-309. (in German)

Thomson, D.J., W.L. Physick, and R.H. Maryon, 1997, Treatment of interfaces in random walk dispersion models, *J. Appl. Meteor.*, 36, 1284-1295.

Trolier, M., J. W. C. White, P. P. Tans, K. A. Masarie, and P. A. Gemery, 1996, Monitoring the isotopicc omposition of atmospheric CO_2: Measurements from the NOAA global air samplingn etwork, *J. Geophys. Res.*, 101, 25897-25916.

Uliasz, M., 1996, Regional modeling of air pollution transport in the southwestern United States. *Environmental Modelling: Computer Methods and Software for Simulating Environmental Pollution and Its Adverse Effects,* P. Zannetti, Ed., Computational Mechanics, 145–181.

Veldkamp, E., and Weitz, A.M., 1994, Uncertainty analysis of $\delta^{13}C$ method in soil organic matter studies, *Soil Biol. Biochem*.., 26, 153-160.

Wang, D. K., and C. C. Austin, 2006, Determination of complex mixtures of volatile organic compounds in ambient air: canister methodology, *Anal. Bioanal. Chem.*, 386, 1099–1120, doi: 10.1007/s00216-006-0466-6

Wen, D., J.C. Lin, F. Meng, and co-authors, 2011, Quantitative assessment of upstream source influence on total gaseous mercury observation in Ontario, Canada, *Atmos. Chem. Phys.*, 11, 1405-1415.

Wen, D**.,** J. C. Lin**,** D. B. Millet, A. F. Stein, and R. R. Draxler, 2012, A backward-time Lagrangian air quality model, *Atmos. Environ.*, 54, 373-386, doi:10.1016/j.atmosenv.2012.02.042.

West, J.B., A. Sobek, and J.R. Ehleringer, 2008, A simplified GIS approach to modeling global leaf water isoscapes, *PLoS ONE*, 3(6), doi:10.1371/journal.pone.0002447.

Widory, D. and M. Javoy, 2003, The carbon isotope composition of atmospheric CO_2 in Paris, *Earth and Planetary Science Letters*, 215, 289~298.

Wilson, T.B. and T.P. Meyers, 2007, Determining vegetation indices from solar and photosynthetically active radiation fluxes, *Agricultural and Forest Meteorology*, 144, 160–179, doi:10.1016/j.agrformet.2007.04.001.

Worthy, D. E. J., I. Levin, N. B. A. Trivett, J. F. Hopper, and M. K. Ernst, 1998, Seven years of continuous methane observations at a remote boreal site in Ontario, Canada, *J. Geophys. Res.*, 103, D13, 15995-16007.

Yakir, D., and L. L. Sternberg, 2000, The use of stable isotopes to study ecosystem gas exchange, *Oecologia*, 123, 297–311.

Yakir, D., and X. F. Wang, 1996, Fluxes of CO_2 and water between terrestrial vegetation and the atmosphere estimated from isotope measurements, *Nature*, 380, 515– 517.

Yurtsever Y., and J.R. Gat, 1981, Atmospheric waters. In: *Stable Isotope Hydrology: Deuterium and Oxygen-18 in the water cycle* [Gat, J.R., and R. Gonfianiti (eds.)], Technical report series NO. 210, IAEA, Vienna.

Zickfeld, K., V. K. Arora, and N. P. Gillett, 2012, Is the climate response to CO_2 emissions path dependent?, *Geophys. Res. Lett.*, 39, L05703, doi:10.1029/2011GL050205.

Zobitz, Z.M., J.P. Keener, H. Schnyder, and D.R. Bowling, 2006, Sensitivity analysis and quantification of uncertainty for isotopic mixing relationships in carbon cycle research, *Agric. For. Meteorol.*, 136, 56-75, doi:10.1016/j.agrformet.2006.01.003

Appendix A

Summary of measurement data

Height [A.G.L.]	# of data points		CO_2 [ppm]		$d^{13}C$ (‰ in VPDB-CO_2)		$d^{18}O$ (‰ in VPDB-CO_2)	
[m]	Warm†	Cold†	Warm†	Cold†	Warm†	Cold†	Warm†	Cold†
6500 <	4	5	380.3±4.9	382.1±6.8	-8.05±0.15	-8.19±0.23	-0.10±0.18	0.22±0.24
5501~6500	0	31	NA	386.5±3.4	NA	-8.35±0.11	NA	0.01±0.31
4501~5500	5	37	381.9±4.6	386.6±4.0	-8.09±0.12	-8.38±0.13	0.00±0.17	-0.07±0.28
3501~4500	7	39	380.3±2.8	386.2±4.4	-8.06±0.06	-8.37±0.15	0.14±0.11	-0.08±0.26
2501~3500	4	45	380.2±4.6	387.1±3.8	-8.02±0.15	-8.39±0.13	-0.17±0.42	-0.12±0.29
1501~2500	12	121	387.0±5.0	388.1±4.2	-7.91±0.22	-8.46±0.15	-0.84±0.83	-0.40±0.44
951~1500	8	69	376.1±4.4	388.9±4.3	-7.82±0.22	-8.51±0.15	-1.25±0.91	-0.64±0.46
851~950	0	9	NA	390.6±3.1	NA	-8.58±0.11	NA	-0.70±0.32
751~850	1	0	377.8	NA	-7.79	NA	-1.93	NA
651~750	3	36	373.4±3.3	390.6±4.6	-7.75±0.20	-8.59±0.15	-1.53±0.46	-0.96±0.57
551~650	0	3	NA	389.7±2.4	NA	-8.59±0.14	NA	-0.89±0.23
451~550	0	2	NA	396.7±6.3	NA	-8.72±0.30	NA	-1.53±0.58
351~450	4	26	374.5±2.8	391.5±4.6	-7.76±0.14	-8.65±0.18	-1.83±0.20	-1.29±0.65
100	4	31	373.9±3.3	392.8±5.3	-7.76±0.15	-8.77±0.22	-1.45±0.36	-1.80±0.91
22	3	21	372.6±3.6	391.7±5.5	-7.74±0.20	-8.74±0.24	-1.30±0.10	-1.73±0.82

† Warm season includes months of May to September, when the monthly mean air temperature is above 4 °C.
October to April of the following year is defined to be Cold season.

Appendix B

Unit conversion for $\delta^{18}O$ of precipitation: from [VSMOW] to [VPDB-CO2]

	$d^{18}O_{prec\text{-}H2O}$ [‰ VSMOW]	$d^{18}O_{pre\text{-}H2O}$ [‰ VPDB]	$\frac{R_{H_2O}}{R_{VSMOW}}$	$\frac{R_{H_2O}}{R_{VPDB}}$	$\frac{R_{H_2O}}{R_{VPDB\text{-}CO_2}}$	$d^{18}O_{pre\text{-}H2O}$ [‰ VPDB-CO_2]	$dD_{pre\text{-}H2O}$ [‰ VSMOW]
January	-26.69	-55.88	0.973308	0.944134	0.934555	-65.45	-206.22
February	-23.46	-52.74	0.976542	0.947271	0.937660	-62.34	-179.31
March	-20.52	-49.88	0.979483	0.950124	0.940485	-59.52	-157.78
April	-14.93	-44.47	0.985069	0.955543	0.945848	-54.15	-111.35
May	-12.12	-41.74	0.987879	0.958268	0.948545	-51.45	-88.61
June	-12.73	-42.33	0.987273	0.957681	0.947964	-52.04	-96.33
July	-12.36	-41.97	0.987643	0.958039	0.948319	-51.68	-96.97
August	-11.69	-41.32	0.988313	0.958690	0.948963	-51.04	-89.55
September	-12.82	-42.42	0.987180	0.957590	0.947875	-52.13	-98.15
October	-16.89	-46.37	0.983108	0.953640	0.943965	-56.04	-128.98
November	-21.30	-50.64	0.978700	0.949365	0.939732	-60.27	-166.42
December	-24.66	-53.91	0.975336	0.946101	0.936502	-63.50	-190.16

1) Isotopic values in precipitation is analysised using data collected at Bratt's Lake, SK (CNIP) data from May 2003 to Nov 2010 and Wynyard, SK (GNIP) data from Aug 1975 to Jul 1982.

2) The δ values are converted to VPDB-CO2 scale using following formua.

$d^{18}O_{samp/VSMOW} = 1.03091 * d^{18}O_{samp/VPDB} + 30.91$

$^{18}R_{vpdb}/^{18}R_{VSMOW}$:1.03090

$^{18}R_{vpdb\text{-}co2}/^{18}R_{vpdb}$:1.01025

Appendix C
Craig-Gordon model

Ecosystem CO_2 exchange also have a significant influence on the oxygen isotope ratio of atmospheric CO_2. Two main oxygen isotope effects occur during photosynthesis. First one involves a diffusion fractionation because of the difference in mass between CO_2 containing ^{18}O and ^{16}O. Second effect is an isotopic exchange reaction occurring to oxygen in CO_2 and oxygen in H_2O. During this exchange reaction, or equilibrium isotope effect, the oxygen isotope ratio of CO_2 becomes enriched in ^{18}O relative to that of plant water. CO_2 isotopically equilibrate water according to:

Equation 11 $$H_2{}^{18}O_{(l)} + CO_{2(g)} \leftrightarrow H^+ + [HCO_2{}^{18}O]^-_{(aq)} \leftrightarrow H_2O_{(l)} + CO^{18}O_{(g)}$$

The temperature-dependent value for the equilibrium fractionation ε_{eq-co2} between the oxygen in the CO_2 and water is $\varepsilon_{eq-co2}(T) = 17604/T - 17.93$, where $d\varepsilon_{eq-co2}/dT = -0.20‰$, so that at 25°C, $\varepsilon_{eq-co2} = 41.11‰$ [*Brenninkmeijer et al.*, 1983]. Water must be in the liquid phase for the hydration reaction to occur. The quantity of water involved in the isotopic equilibrium reaction is many orders of magnitude greater than that of the CO_2 present, so isotopically equilibrated CO_2 will take on the oxygen isotopic ratio of the water in which it is dissolved regardless of its initial $^{18}O/^{16}O$ ratio. The rate constant for the isotopic reaction is two-thirds the ratio of the chemical reaction because of the three oxygen present in the intermediate species [*Mills and Urey*, 1940]. This means that the amount of CO_2 that escapes from the leaf can be approximately 2/3 of the total that diffused in, depending on the amount of CO_2 in the plant cells (chloroplasts) and the resistance to diffusion along the path from the plant cell to the air. The discrimination against $C^{18}O^{16}O$ during photosynthesis acts to enrich

atmospheric CO_2 in ^{18}O. The magnitude of the increase in the $^{18}O/^{16}O$ ratio of atmospheric CO_2 during photosynthetic gas exchange is dependent on factors affecting water balance including tranpriation, groundwater, or precipitation. Clearly, some knowledge of the isotopic composition of the local hydrologic cycle is necessary to interpret isotopic composition of local soil water and precipitation. Ecosystem respiration acts in opposite to photosynthesis by releasing CO_2 depleted in ^{18}O to the atmosphere. The primary factor affecting the oxygen isotopic ratio of respired CO_2 is the equilibrium isotopic effect that occurs between oxygen in CO_2 and oxygen in plant and soil water.

In this study, a steady-state Craig-Gordon model that calculates leaf water $\delta^{18}O$ was implemented based on the formulation in *Craig-Gordon* [1965]. This relatively simplified approach provides one modeling result for the site of enrichment inside the leaf, recognizing diurnal changes of leaf water is not captured. Explicit non-steady-state calculation was not modeled given limited understanding to parameterize large scale biome difference or micrometeorological dynamics. It is noted that the atmospheric measurements were carried out once a week to during mid-day, and the Craig-Gordon model outputs the isotopic composition of leaf water for the same time.

It is first assumed that there is no fractionation from water uptake from soil to root, and that fractionation during movement of water inside plants from root to leaf is negligible. The isotopic composition of water in the leaf then is determined by considering the equilibrium effect (i.e., phase change) and the kinetic effect (i.e., diffusion) of the source water (i.e., precipitation). Equilibrium fractionation (α^*) occurs as a function of temperature change and is described as follows:

$\alpha^* = \frac{R_L}{R_V} = e^{(\frac{a}{T^2} - \frac{b}{T} - c)}$, where e is Euler's number (i.e., exponential), R_L is the liquid water isotope ratio ($^{18}O/^{16}O$), R_V is the water vapor isotope ratio, and T is temperature in degrees Kelvin. For oxygen isotope a= 1137, b =0.4156, c = 0.0020667 [*Majoube*, 1971]. Kinetic fractionation is

described for diffusion from the evaporating surface inside the leaf to the atmosphere, taking into account diffusion through the leaf boundary layer. The kinetic fractionation factor has been estimated as $\alpha_k = 1.032$ for oxygen, and for diffusion through a boundary layer is $\alpha_{kb} = 1.021$.

Equation 12

$$R_e = \alpha\left[\alpha_k R_S\left(\frac{e_i - e_s}{e_i}\right) + \alpha_{kb} R_S\left(\frac{e_s - e_a}{e_i}\right) + R_A\left(\frac{e_a}{e_i}\right)\right],$$

where R_e is the isotope ratio of evaporatively enriched leaf water,

R_S is the isotope ratio of the source water,

R_A is the isotope ratio of the atmospheric water vapor,

e_i is internal leaf vapor pressure,

e_s is the leaf surface vapor pressure,

and e_a is atmospheric vapor pressure.

Leaf surface vapor pressure is estimated using equations canopy bulk-stomatal conductance and transpiration rate [Appendix D]. Predicted leaf water isotope ratios initially converted in delta values (δ) are then expressed as parts per thousand or per mil (%) relative to the isotope standard ‘‘Standard Mean Ocean Water’’ (SMOW). The oxygen isotope values of respired CO_2 is calculated according to the [*Brenninkmeijer et al.*, 1983] and reported in VPDB-CO2 scale in this study.

Appendix D

Estimation of key input variables for the Craig-Gordon Model

A.1) Pennman-Monteith method

The evaporation from a saturated surface is a thermodynamic process in which energy is required to change water from liquid to vapor. *Penman* [1948] equation was originally for evaporation over open water, which describes evaporation as a weighted linear combination of net available energy and the vapor pressure deficit of air. *Penman* [1953] later developed an equation for single leaves that included leaf resistance. The Penman equation has since been extended to include vegetation surface resistance [*Covey*, 1959] and aerodynamic resistance terms [*Monteith*, 1965]. The Penman-Monteith equation [*Monteith*, 1965] combined the thermodynamic and aerodynamic aspects of evaporation into a mathematical equation by substituting the appropriate resistance and is commonly written as

Equation 13

$$\lambda E = \frac{s\left(R_n - G\right) + 86400\,\rho C_p \left(e_*\left[T_a\right] - e_a\right)/r_{aH}}{s + \gamma\left(r_{aW}/r_{aH}\right)}$$

Terms in Equation 13above consist of

net available energy $\left(R_n - G\right)$: R_n is net radiation flux, G is sensible heat flux into the soil in [MJ·m^{-2}·d^{-1}], and 86400 is a day in [second], needed when wind speed is measured in [ms^{-1}],

vapor pressure deficit of air $\left(e_*\left[T_a\right] - e_a\right)$: $e_*[T_a]$ is saturation vapor pressure, e_a is vapor pressure in [kPa], ρ air density in [~1.15 kg·m^{-3}],

C_p specific heat of dry air in [~ 0.001005 MJ·kg^{-1}·°C^{-1}],

r_H aerodynamic resistance of sensible heat in [s·m^{-1}],

r_W aerodynamic resistance of water vapor in [s·m^{-1}],

γ the psychrometric constant in [kPa·°C^{-1}],

s the slope of the saturation vapor pressure-temperature curve [kPa·°C^{-1}],

Latent heat flux increases as net available energy increases and decreases as sensible heat flux increases. For a constant value of net available energy, latent heat flux decreases as surface temperature increases. Evaporation is also an aerodynamic process related to turbulent transport of water vapor away from the surface, where latent heat flux increases as evaporative demand $\left(e_a - e_*\left[T_s\right]\right)$increases.

A.2) Breakdown of terms used in the Pennman-Monteith equation

Saturation vapor pressure is approximated by Clausius-Clapeyron equation:

$$e_*\left[T_a\right] = e_0 \cdot \exp\left[\frac{L}{R_v} \cdot \left(\frac{1}{T_o} - \frac{1}{T_a}\right)\right],$$

where e_0 =0.611 kPa and T_0=273 °K are constant parameter, and R_v = 461 J·K^{-1}·kg^{-1}, over a flat water surface latent heat of vaporization L_v=2.5x10^{6}J·kg^{-1}, thus for liquid water L/R_v= 5423 K; over a flat ice surface latent heat of deposition L_d=2.83x10^{6}J·kg^{-1}, thus for solids L/R_v= 6139 K.

Actual vapor pressure becomes known when RH or T_{dew} is measured:

RH =$e_a/e_*[T_a]$ ·100, thus e_a = (RH/100)·$e_*[T_a]$;

$$T_{dew} = \left[\frac{1}{T_0} - \frac{R_v}{L_v} \cdot \ln\left(\frac{e_a}{e_0}\right)\right]^{-1}, \text{ thus } e_a = e_*[T_{dew}].$$

The psychrometric constant is given by $\gamma = \left(C_p \cdot P\right) / 0.622 L_v$,

where C_p is the specific heat capacity of dry air in [$J \cdot kg^{-1} °C^{-1}$] and P is pressure in [Pa]; typical value is found around 66.5$Pa \cdot °C^{-1}$, but depending on air pressure at a location the value can be ~ 60 $Pa \cdot °C^{-1}$,e.g., 1km asl.

The slope of the saturation vapor pressure versus temperature evaluated at T_a is given by $s = \frac{de_*[T_a]}{dT}$, or by empirical formula of *Tetens* [1930] or *Murray* [1967] at a given temperature

$s = \frac{2503 \exp\left(\frac{17.27 \cdot T_a}{T_a + 237.3}\right)}{(T_a + 237.3)^2}$, where T_a in [°C].

A.3) The "big-leaf" formulation of latent heat

Monteith [1981] extended the Penman-Monteith equation to a canopy of leaves, and this equation is widely used to derive surface or canopy resistance.

$$\lambda E = \frac{s(R_n - G) + 86400 \rho C_p (e_*[T_a] - e_a)/r_{aH}}{s + \gamma (r_c + r_{aW})/r_{aH}}$$

where r_c is canopy or surface resistance and r_{aH} and r_{aW} are aerodynamic resistance for sensible and water vapor respectively. This is a "big-leaf" formation [*Raupach and Finnigan*, 1988] of latent heat flux in which the latent heat exchange with the atmosphere is regulated by two resistances acting in series. A canopy resistance, r_c, governs processes within the plant canopy, and an aerodynamic resistance for water vapor, r_{aW}, governs turbulent process above the canopy. By measuring evapotranspiration from a canopy and if all other terms are known, the Penman-Monteith equation can be solved for canopy or surface resistance [*Pataki et al.*, 1998; *Harris et al.*, 2004; *Blanken and*

Black, 2004]. The resistance r_{aH} and r_{aW} are aerodynamic resistance to heat and moisture, respectively, between the atmosphere at height z and the surface. Given the bulk surface resistance dealing with the transfer from surface to the adjacent height above [*Javis and McNaughton*, 1986], in a equation where $r_{aH} \sim r_{aW}$ reduces to

Equation 14

$$\lambda E = \frac{s(R_n - G) + 86400\,\rho C_p (e_*[T_a] - e_a)/r_{aW}}{s + \gamma(1 + r_c/r_{aW})}$$

, where $r_{aW} = \frac{1}{k^2 u_z}\left[\ln\left(\frac{z_{wind} - d}{z_{0M}}\right)\ln\left(\frac{z_{RH} - d}{z_{0W}}\right)\right]$.

This aerodynamic resistance to water vapor, r_{aW}, takes the inverse of the transport coefficient regardless of whether it is for sensible heat or water vapor. k is the von Karman constant [-0.41], u_z is the wind speed at height z in [m], z_{wind} and z_{RH} are measurement height in [m] for wind speed and relative humidity, respectively.

The displacement length is given by $d \approx (2/3)h_c$ where h_c is the vegetation height in [m].

The roughness parameter for water vapor, z_{0W}, is extremely difficult to determine experimentally, whereas z_{0M} can be approximated by the empirical relationships [*Plate*, 1971; *Brutsaert*, 1975; *Monteith*, 1981]:

$z_{0M} \approx 0.058(h_c)^{1.19}$, for $h_c \geq 2m$; $z_{0M} \approx 0.123(h_c)$, for $h_c \leq 2m$. Then $z_{0W} \approx 0.1 z_{0M}$.

The bulk canopy or surface resistance over daily and monthly time-scale can be estimated as $r_c \approx \frac{r_l}{LAI_{active}}$, where r_l is the bulk stomatal resistance of a well-illuminated leaf [single "big

leaf"~100 sm^{-1}], $LAI_{active} \sim 0.5LAI$ for vegetation, where leaf area index, *LAI*, [m^2 of leaf area per m^2 soil surface] ~ 1.5 ln(h_c) + 5.5 for alfafa, $LAI \sim 24h_c$ for dense vegetation. For boreal woodland global mean *LAI* is about 3.1±2.28.

"LAI varied from 0.5 to 8 m^2 m^{-2} in the 1000 × 1000 km research area and ~3.5 to 4.5 m^2 m^{-2} for the area surrounding these two towers within a 100-km of radius [*Chen et al.*, 2008]." -- East Trout Lake & Candle Lake

For tall forest has low aerodynamic resistance and is coupled to the atmosphere, evapotranspiration approaches to a rate imposed by canopy resistance thereby $\lambda E = \rho C_p \left(e_* \left[T_a\right] - e_a\right) / \left(\gamma \cdot r_c\right)$[*Bonan*, 2008].

A.4) Moisture flux (or evaporation rate) from a latent heat flux

Heat and moisture budgets are coupled, as described in Eq.1. Hence, the latent heat flux ($W \cdot m^{-2}$ or $J \cdot s^{-1} \cdot m^{-2}$) is, by definition, associated with a flux of moisture ($kg_{water} \cdot m^{-1} \cdot s^{-1}$) [*Stull*, 1998].

$Flux_{moist} = \frac{\lambda E}{L_v}$, where latent heat of vaporization L_v=2.5x$10^6$$Jkg^{-1}$.

The moisture flux can also be expressed as an evaporation rate in terms of depth of liquid water that is lost per unit time (e.g., $mm \cdot day^{-1}$) [*Stull*, 1998].

Given a latent heat flux, evaporation rate is given by $Evap = \frac{\lambda E}{\rho_{liq} \cdot L_v} = a \cdot \lambda E$, where a= 3.90X10^{-10} $m^3 \cdot W^{-1} \cdot s^{-1}$ or a= 0.0377($m^2 \cdot W^{-1}$)($mm \cdot day^{-1}$), and ρ_{liq}=1025 $kg_{liq} \cdot m^{-3}$.

Given a latent heat flux of 300 $W \cdot m^{-2}$;

1— moisture flux is [300 ($J \cdot s^{-1} \cdot m^{-2}$)]/[$2.5 \times 10^6 J \cdot kg^{-1}$]=0.120 $g \cdot s^{-1} \cdot m^{-2}$=0.00666 $mol \cdot m^{-2} \cdot s^{-1}$.

- H_2O=18.01528 g/mol, thus 1 g_{water} is equivalent to 0.0555 mole.

2— evaporation rate is [0.0377($m^2 \cdot W^{-1}$)($mm \cdot day^{-1}$)]·[300 ($W \cdot m^{-2}$)]=10.11 $mm \cdot day^{-1}$.

3— *Blanken and Black* [2004, Figure 1 and Figure 2] reported surface conductance of ~ 600 $\mu mol \cdot m^{-2} \cdot s^{-1}$ over Prince Albert National Park (quite near to our site) during July 2004.

A.5) Measurement data available from Fluxnet-Canada

The SK-OJP site that is situated on a mature Jack Pine forest at the province of Saskatchewan, [53.96163 °N, 104.6920 °W; Figure 1 & Table 2 of *Chen et al.*, 2011], is the closest Fluxnet-Canada location from East Trout Lake, SK.

It offers computed values of fluxes (both above canopy flux at the measurement height of 28m agl and storage flux: 0 to 28m) and meteorological variables. The data publicly available for download covers up to year 2009 from 1999.

ftp://daac.ornl.gov/data/fluxnet/fluxnet_canada/data/

PI's (SK-OJP site): Harry McCaughey, Andy Black and Alan Barr

Email address of PI's: mccaughe@post.queensu.ca, andrew.black@ubc.ca, alan.barr@ec.gc.ca

Appendix E

$\delta^{18}O$ source of observed CO_2 and oil sands mining operations

Bituminous sands are a major source of the unconventional oil. To produce oil from the bituminous sands, different approaches are needed to access to the oil sands formation, depending on depth of the deposit from the surface. When the depth is less than 70 meter open pit mining operations is preferred while deposits below 150 meter are accessible through wells. The current bitumen production process from open pit mining is schematically described in Chapter 4 of The Royal Society of Canada expert panel report on Environmental and Health Impacts of Canada's Oil Sands Industry [*Gosselin et al.*, 2010]. After harvesting, oil sands ore is crushed into smaller lumps and transported using conveyors to a separation plant where hot water is added to make the bitumen slurry at temperature of 45 to 60 °C. To maintain the desired temperature of the slurry, water added to the plant should have a temperature close to boiling, and certain portion of hot water would evaporate and condense upon the contact with colder slurry. In contrary to open pit mining, in-situ operations using wells employ various extraction techniques which mostly depend on thermal recovery of bitumen [*Butler*, 1991]. The Cyclic Steam Stimulation (CSS) technique has been in operation for Alberta's oil sands since 1985, and it uses cycles of steam injection through a production well. In CSS, steam at temperature of 350 ~ 400 °C is injected to wells for a time period of weeks or months. Once the heat soaks into oil fields, the hot oil is pumped out of the well before the process is repeated. The Steam Assisted Gravity Drainage (SAGD) technique also makes use of steam and has been deployed in Canada since 1990's when the technology became inexpensive to implement for oil sands mining operations. SAGD uses two wells one at the bottom and the other at the top of formation. Steam is injected at the upper well to melt bitumen so that it flows downward to be pumped out through the lower well.

Neglecting kinetic equilibrium and assuming that the isotopic fractionation of water is caused by simple equilibrium processes that are limited to two-phase closed systems, the fractionation of ^{18}O

can be approximated by a Rayleigh condition. The Rayleigh condition refers to a slow process with immediate removal of the condensate from the vapor after formation. The steam injection processes described in the previous paragraph can be considered closed system involving liquid and vapor in which Rayleigh process takes place. The equilibrium isotope effects between co-existing phases at equilibrium can be described by an exchange reaction through which the isotope fractionation factor α is defined by the ratio of the abundance of the isotopes involved in the exchange reaction [*Gat and Gonfiantini*, 1981]. The equilibrium isotope effect is temperature dependent, and so is α.

For the equilibrium exchange reaction between liquid water and vapor, the exchange process is written as

$$H_2O_L + H_2O_V^* \leftrightarrow H_2O_L^* + H_2O_V$$

, where * stands for the rare isotopic species, and subscript $_L$ and $_V$ for liquid and vapor, respectively. For ^{18}O, exchange reaction constant is obtained by calculating the isotopic ratio:

Equation 15

$$\frac{[H_2{}^{18}O]_L[H_2{}^{16}O]_V}{[H_2{}^{16}O]_L[H_2{}^{18}O]_V} = \frac{{}^{18}R_L}{{}^{18}R_V} = \alpha_e,$$

where ^{18}R is the isotope ratio of oxygen in the water molecules, and square brackets denote the respective concentration of molecules.

The α_e for the liquid-vapor (i.e., liquid relative to vapor) values are expressed in δ notation with the ‰ unit. The fractionation factor α_e is discussed more thoroughly by *Gat et al.* [2001] as well as *Fritz and Fontes* [1980]. The best value for α_e for ^{18}O is given by *Majoube* [1971] as a function of temperature:

Equation 16

$$\ln\alpha_e = \frac{1.137}{T^2}\times 10^3 - \frac{0.4156}{T} - 2.0667\times 10^{-3}$$

The function in Equation 16 above yields α_e of +11.72‰ at 0 °C, decreasing to +9.79‰ at 20 °C. This calculation means the temperature effects on equilibrium of $\Delta\alpha_e/\Delta T$=0.0965‰ per degree Celsius for the 0 to 20 °C interval. If linearly extrapolated with the constant rate of decrease in α_e according to temperature, the fractionation of 33 ~ 38‰ would have been found at high temperatures of 350 ~ 400 °C. Thus, given δ^{18}O-source of CO_2 at -60 ‰ [or about -17‰ VSMOW] accepted as the value from oil sands before steam injection state, the y-intercept values of at around -100 ‰ [or about -60‰ VSMOW] shown in Figure 5 are explainable. As the steam injection repeated, through CSS for instance, to extract more bitumen from the same deposit, depleted ^{18}O in the oil fields will experience another cycle of equilibrium fractionation but with larger α_e since $^{18}R_V$ in (Equation 15) became gradually smaller during the extraction with CSS process. Thus δ^{18}O-source of CO_2 from the oil sands would progressively become more negative in time even though the source region of CO_2 stays in the same geologic formation. The repeated steam injection through a well may be responsible for more negative values shown in Figure 5.

It is possible to speculate that hot water stimulates not only the production of bitumen but the chemical reactions between water and other molecules in the deposit. In addition, high pressure is assumed for water to reach temperature at 400 °C, which in turn further affects isotopic fractionation. However, these two complicated scenarios may be beyond the scope of current study and remain as a separate future work.

Appendix F

Use of vertical profile measurements for the Keeling plot

Assumptions of the Keeling plot method have been partly examined by a number of earlier studies. However, since assumptions are fundamental to interpretation of results produced with the Keeling method, revisiting their robustness to a specific dataset assures Keeling plot analysis in up-scaling its applications to broader measurement settings. Keeling plot method works on a basis that gradient of molar-ratio of CO_2 and its isotopic ratios together records the contributing sources being added to a given mixture, thus requiring background to be known as either a constant or a variable. Assumptions of constant backgrounds that are traditionally accepted as standard for a remote measurement site often present with challenges to experimental designs for data analysis of anthropogenic outflows, since explicit background to the Keeling plot approach may be needed for interpreting potentially complex combination of sources to those measurements.

Additional constraint is required to establish a reliable relationship between background and sources for data obtained from such measurement sites. One realization of the relationship is accomplished by fitting a curve through a time series of long-term measurements. Alternatively, a reference location can serve as a background granted that the atmosphere flown over sources gets "well-mixed" along its way to the measurement site. In Figure A.1, a Thoning curve (in red) was fit through a weekly time-series of measurements made at free-troposphere (in grey) using aircrafts. The red line was taken as background for the ground measurements (in black) made closer to sources at 100 meter above ground level. Namely, the free-tropospheric measurement is used here as the 'reference'. Both of ground and aircraft measurements are coordinated to be aligned as a profile at the same measurement site, and the sampling was completed less than 2 hours. Then, variability for the product of CO_2 and $\delta^{13}C$ (CO_2*$\delta^{13}C$) is examined in Figure A.2 in order to construct a Keeling plot for each month which is presented in Figure A.3. The result shown in Figure A.3 represents monthly

variations of $\delta^{13}C$ sources. The black dots use the retrieved variable backgrounds, and grey assumes a constant background. The coefficient of determination (a.k.a R^2) for a given set of ground measurements during each month is appended in the Figure A.3 as well. The results shown in Figure A.3 suggests that, when utilizing weekly flask samples for higher precision/accuracy data of CO_2 isotopes (which applies to data from most of isotopic CO_2 measurement networks), variable background conditions for given measurements assist in reliable derivation of isotopic source values of CO_2. This statement is supported by the fact that the monthly variation of source values derived

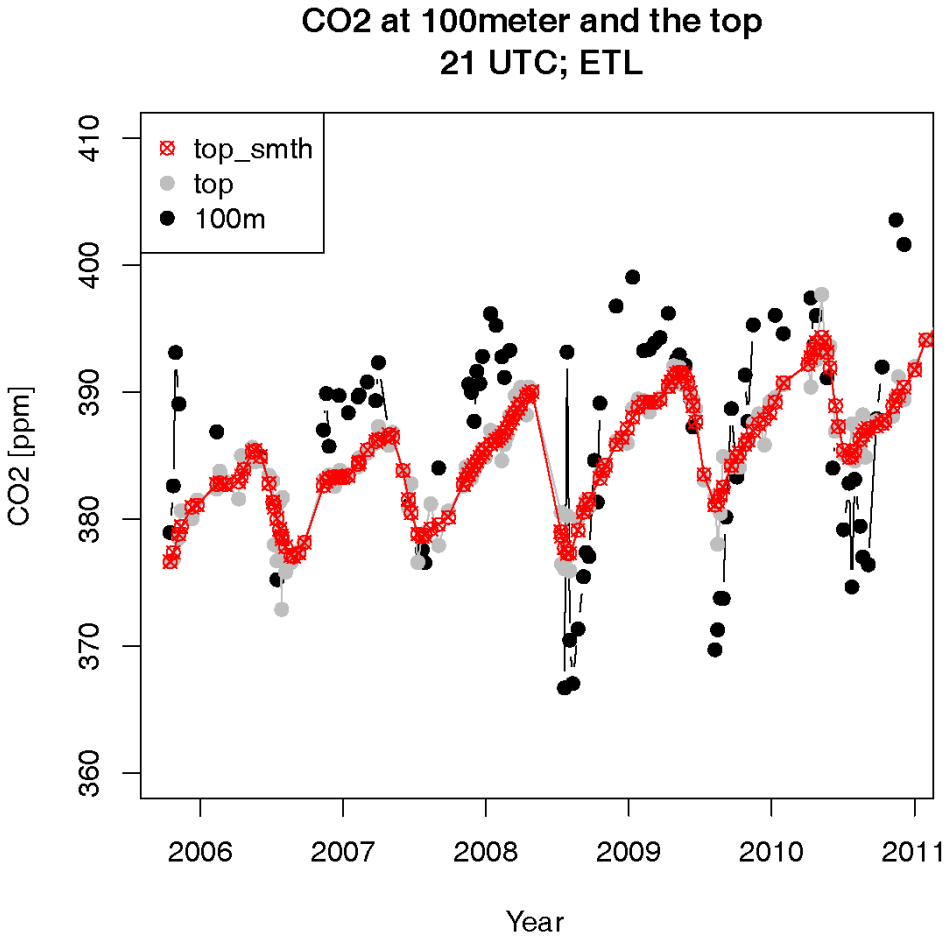

Figure A. 1 Retrieving backgrounds; CO_2 is shown as an example. The measurement is at 100 m agl, and the background is from 7.3 km agl.

with varying backgrounds better depicts climatological transition of contributing sources from biospheric activities during the summer to consumptions of fossil fuels during the winter. One immediate research question emerges from the observation that constructing Keeling plots with a weekly sampling requires variable background conditions; what makes a reliable background for a Keeling plot analysis?

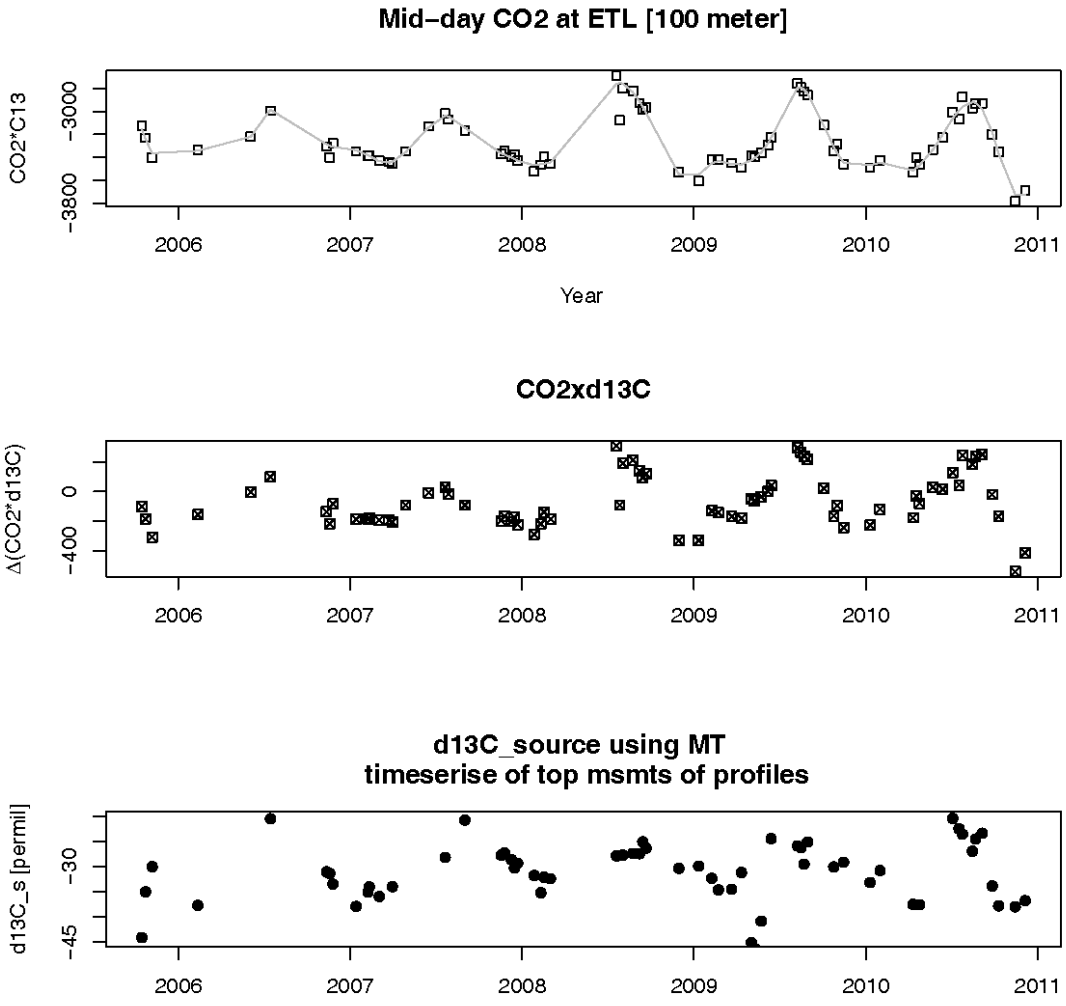

Figure A. 2. Keeling plot analysis with prescribed backgrounds.

Additional comparison of Keeling plot results between when using the free-troposhere (shown in Figure A.1) and when using "self-referenced" (namely when a time-series of ground measurements is de-trended to establish a background to itself; figure not shown) reveals that a reference location such as free-troposphere provides Keeling plots with more reliable variability in background.

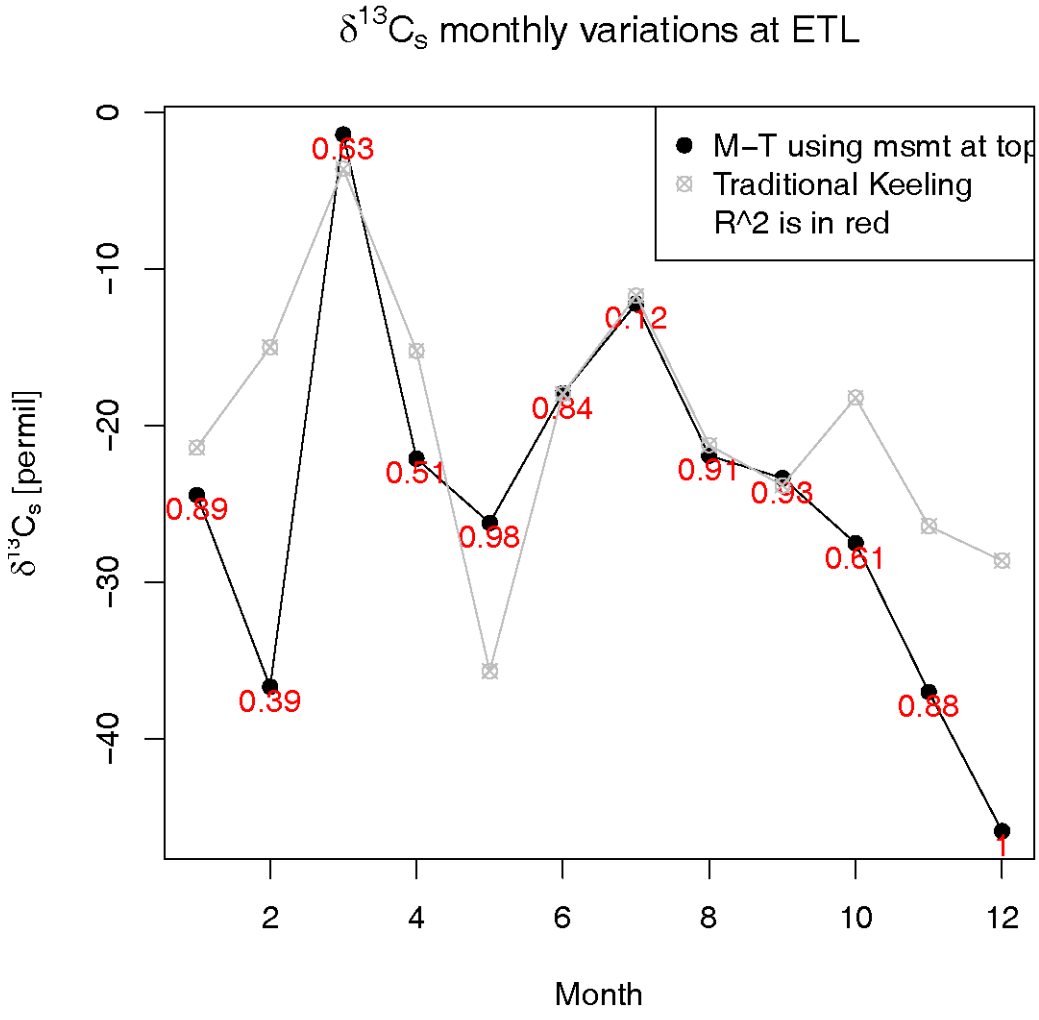

Figure A. 3 Comparing the results of Keeling plots; one with prescribing variable backgrounds, the other assuming a constant background.

The atmosphere sampled by an aircraft at about 7 kilometer above ground level would exhibits a number of physical and chemical properties unlike a counter part that is sampled at the planetary boundary layer, and a number of processes significantly controlling atmospheric CO_2 mixing ratio lie on the surface. Hence it seems almost expected that one questions about validity of introducing free-tropospheric measurements to examining source influences of CO_2 which may be decoupled from the air aloft. Indeed, this particular aspect of analysing atmospheric CO_2 data is extensively addressed by *Ballantyne et al.* [*Global Biogeochem. Cycles*; 2010]. The authors conclude that free-tropospheric measurements should be used when calculating isotopic source values from the boundary layer observations. Drawing on the work by these authors, an investigation was carried out regarding whether a profile measurement can be an appropriate choice to derive a source value. This was implemented out using synthetic model data which simulates vertical profiles of CO_2 and $\delta^{13}C$ at the exact measurement location Figure A.1~A.3 are based at. Typically the atmosphere near the surface is considered decoupled from what lies above, as indicated by steep vertical gradients shown in Figure A.4. However, results using the synthetic model data strongly support that, as long as the atmosphere is well-mixed, regardless of its vertical extents, Keeling plot analysis can be performed using a profile measurement to derive reliable source values. In Figure A.5, calculated values are found less than 0.2 ‰ range of the anticipated source value to be derived at -26 ‰. The well-mixed condition is ensured when a strong correlation between CO_2 and $\delta^{13}C$ is demonstrated (for instance, $R^2 > 0.95$).

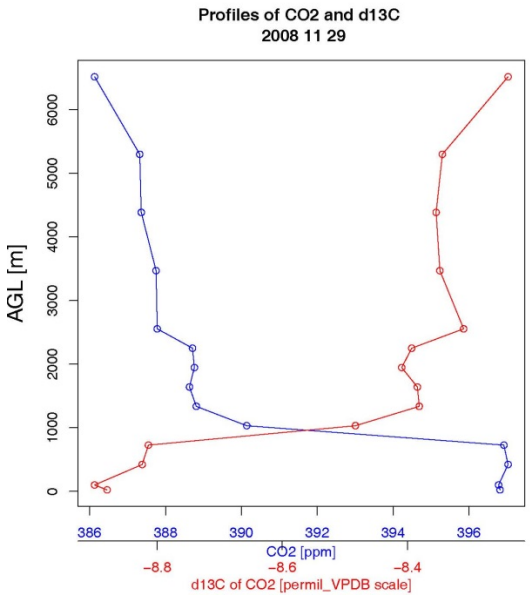

Figure A. 4 A typical profile of CO_2 mixing ratio and $\delta^{13}C$, measured at the ETL site.

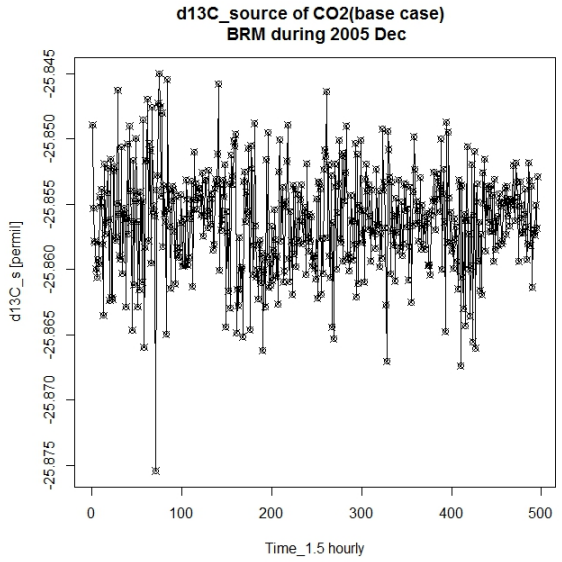

Figure A. 5 Derived source values of $\delta^{13}C$, using simulated profile data. A constant background is assumed to each profile.

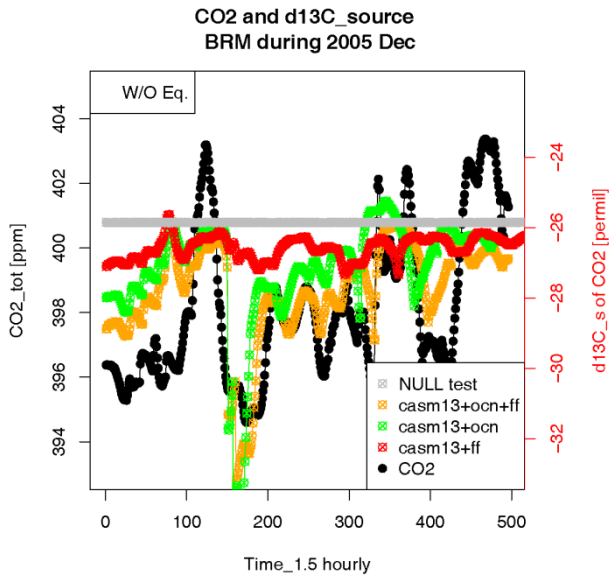

Figure A. 6 Simulating influences of additive atmospheric CO_2 on its isotopic source values. A constant background is assumed for Keeling plot analysis.